Maren Wohltmann geb. Bender

Holocene sea-level changes in Southeast Asia

Dissertation

Zur Erlangung des Doktorgrades der Naturwissenschaften

(Dr. rer. nat.)

Am Fachbereich Geowissenschaften der Universität Bremen

Erster Gutachter: Prof. Dr. Alessio Rovere

Zweiter Gutachter: Prof. Dr. Marta Pappalardo

Vorgelegt von

Maren Wohltmann, geb. Bender

Bremen, Mai 2020

Datum der Verteidigung: 25. Juni 2020

Imagination is more important than knowledge.

Knowledge is limited.

Imagination encircles the world.

Albert Einstein

(in an Interview with the Sunday Evening Post (1929))

I. Abstract

Sea-level changes are dynamic processes and changes in relative sea-level (RSL) are common occurrences in the history of Earth, with different rates over time. Since the beginning of the industrial revolution (ca. 1880 AD) greenhouse gas emissions increased and the related climate change accelerated the modern sea-level rise. This became an increasingly important threat within the last century, in particular for global societies where people are living on low-lying coastlines only a few meters above mean sea level (MSL). The study of Holocene (~11.5 ka BP) sea levels is an important tool to understand the natural processes affecting coastal regions, as paleo RSL positions can help assess long-term vertical land motion and , hence, the risk of local flooding and land loss.

In the Holocene, sea-level rise was initiated by increasing temperatures of the Last Glacial Maximum (LGM) ~21 ka BP. Land-ice melt caused the eustatic sea level to rise, triggering processes related to glacial isostatic adjustments (GIA), such as, for example, ocean syphoning, land leveling and changes in the gravitational attraction and Earth rotation. Due to these processes, water masses migrated from the poles to equatorial regions, affecting many far-field areas that experienced a sea-level highstand. In fact, after ice-melting slowed down and stopped (~6 to 4 ka BP), water masses migrated back to the poles, generating RSL highstand patterns, which can be seen in the geological record above present sea level in many far-field (i.e., located away from the ice sheets) areas.

At these places, different RSL indicators such as coral reefs, salt marshes or beachrocks, were deposited or developed above modern MSL. Today, they provide important benchmarks on local paleo sea-level histories, once post-depositional processes affecting their elevations are taking into account. In general, there are two types of RSL indicators: index points and limiting indicators. Index points are documenting the paleo sea-level position, and marine or terrestrial limiting points, were formed above or below the local tidal ranges. These latter indicate that the paleo RSL was surely above (marine limiting point) or surely below (terrestrial limiting points) the measured elevation of the indicator. According to well-established protocols, all RSL indicators need to have an age, obtained with radiometric dating, coordinates and elevation of the sample. RSL index points also need to have and associated indicative meaning (IM), composed of the indicative range (IR) and the reference water level (RWL). Additional to geological field data, Holocene sea-level studies must include the result of geophysical models that calculate the intensity and timing of GIA, taking into account different ice and earth model combinations.

In this thesis, I worked to refine Holocene sea-level histories in Southeast Asia. First, I present a Holocene sea-level database, compiled from published literature. The database includes 546 data points of the broader region of South and Southeast Asia. Within different sample sets, we highlight that some problems such as data inconsistencies, general lack of data, or insufficient data information from literature complicate the analysis of the general sea-level history for the broader study region. Further, besides GIA, the main driver for the RSL highstand at many regions, we identify the need to better constrain syn- and post-depositional processes causing further departures from Eustasy.
I then present the results of original fieldwork in the Spermonde Archipelago (SW Sulawesi). Here, we surveyed and dated 24 new RSL index points for the mid to Late-Holocene. Our data, based on highly accurate measurements of fossil microatolls, were supposed to help solving data inconsistencies within the rarely studied region. This study shows that the new data support previous results based on fossil microatolls but cannot completely solve local data inconsistencies derived from two older studies, comprising mainly marine and terrestrial limiting indicators. Using our data in combination with a large suite of GIA models, we discuss possible tectonic rates in our study area. In combination with previous studies, our data show the possibility that one populated island is subject to relevant subsidence. This should be evaluated by further studies, and opens up relevant questions regarding the fate of small, low-

lying, heavily populated, tropical islands in face of climate change.

As understanding RSL histories is essential, another approach to gauge the relevance and importance of missing RSL information from our large database was developed within this thesis. We use a statistical analysis to better evaluate how GIA models fit geological field data. The results of this exercise can help to highlight if deviating RSL histories predicted by GIA models and observations are based on major data inconsistencies, a lack of data points or if post-depositional processes could be the reason for conflicts between RSL observations and model predictions in the related regions. Therefore, 16 study areas were compared to 54 GIA models providing positive or negative mismatches between model and data RSL predictions. The results are divided into two analyses, calculating the probability for the mismatch between the entire dataset and all GIA models and between each single index point and the models. The results show, that in three cases the results of both analyses differ significantly with each other, five regions indicate only low probability results implying that GIA is not the only driving factor and post-depositional processes cannot be excluded, and eight regions provide high probability results indicating GIA as the main driver for the paleo RSL positions.

In the following chapter 1, I explain in detail the general importance of paleo sea-level investigations, how they contribute to the prediction of future sea-level variability and, which are the driving processes affecting RSL due to glacial-isostatic adjustments. In chapter 2, I provide the methodologies used for all aspects regarding the compilation of the database, the sampling and dating methods. I also outline why GIA models are important within the context of the thesis. The chapters 3 to 7 present the main results of my work and include manuscripts that are published and in preparation. In the chapter 8, I show that standardization of sea-level data is indispensable for the comparison of different sea-level studies to indicate the RSL history for a broader region and to highlight critical regions that are at risk of flooding. I further show in this chapter, that a statistical probability calculation can be used to better constrain GIA models to sea-level data if GIA was the main driver of RSL rise in Holocene in the study site. In the final chapter 9, I summarize the contributions of this work to science and give an outlook of future work.

II. Zusammenfassung

Meeresspiegeländerungen sind dynamische Prozesse und die langfristige relative Meeresspiegelschwankung (*„relative sea level“*, RSL) ist eine bekannte Erscheinung in der Geschichte unserer Erde, bei dem die Schwankungsraten mit der Zeit variieren. Seit dem Beginn der industriellen Revolution (seit ca. 1880 AD) steigen die Treibhausgasemissionen und der damit verbundene Klimawandel beschleunigte den modernen Meeresspiegelanstieg. Für die globale Gesellschaft, in der Menschen an Küstenlinien nur wenige Meter über dem mittleren Meeresspiegel (*„mean sea level*“, MSL) leben, wurde dies im letzten Jahrhundert zu einer ernstzunehmenden Bedrohung. Deswegen ist die Studie der Holozänen (~11.5 ka BP) Meeresspiegelschwankungen ein wichtiges Instrument um die natürlichen Prozesse, die die Küstenregionen beeinflussen, zu verstehen. Historische RSL können dabei helfen langzeitliche vertikale Landbewegungen und somit das Risiko von Überschwemmungen oder dauerhaftem Landverlust zu beurteilen.

Der Anstieg des Holozänen Meeresspiegels ereignete sich nach dem letzten, glazialen Maximum (LGM, ~21 ka BP) und wurde durch ansteigende Temperaturen ausgelöst. Die Landeisschmelze verursachte das Ansteigen des eustatischen Meeresspiegels und löste so Prozesse aus, die mit glazialisostatischen Anpassungen (Glacial-Isostatic Adjustment, GIA), wie z.B. Wassermassenumverteilung, Landnivellierung, Änderungen der Erdanziehungskraft und Erdrotation, in Zusammenhang gebracht werden. Aufgrund dieser Prozesse bewegten sich die Wassermassen von den Polen zum Äquator, wodurch viele dieser Regionen von dem Meeresspiegelanstieg betroffen waren. Nachdem die Eisschmelze sich verlangsamte und schließlich stoppte (~6 bis 4 ka BP), flossen die Wassermassen wieder zurück zu den Polen und ließen morphologische Muster, die durch den Meeresspiegelhochstand entstanden sind, zurück. Sie können heute in vielen der äquatorialen Region (sogenannte far-field Regionen, die weit Entfernt von den Eisschilden liegen) in den geologischen Überlieferungen wiedererkannt werden.

In diesen Regionen lagerten sich z. B. Korallenriffen, Salzwiesen oder versteinerten Stränden ab, die sich oberhalb des modernen mittleren Meeresspiegels befinden. Sie zeigen wichtige Anhaltspunkte für die ehemalige lokale Meeresspiegelgeschichte auf, sofern ihre Position nach ihrer Ablagerung nicht durch höhenverändernde Prozesse beeinflusst wurde. Allgemein gibt es zwei RSL Indikatoren: Index-Punkte und limitierende Indikatoren. Index-Punkte dokumentieren die Höhe des ehemaligen Meeresspiegels während limitierende Indikatoren (marin und terrestrisch) sich entsprechend unterhalb oder oberhalb des lokalen Tidenhubs bildeten. Dabei zeigen sie, dass der ehemalige RSL sicher oberhalb (marin limitierende Punkte) oder sicher unterhalb (terrestrisch limitierende Punkte) der gemessenen Index-Punkt-Höhe lag. Gemäß gut etablierter Protokolle, müssen all RSL Indikatoren ein radiometrisch datiertes Alter, Koordinaten und eine Höhe besitzen. RSL Indexpunkte müssen außerdem ihr spezifisches „*Indicative Meaning*“ (IM) aufzeigen. Dieses besteht aus dem indikativen Bereich (*„indicative range“*, IR) und der damit verknüpften Wassertiefe (*„Reference Water Level“*, RWL). Zusätzlich zu den geologischen Proben, müssen Holozäne Meeresspiegelstudien die Ergebnisse aus geophysikalischen Modellen beinhalten, die die Intensität und den Zeitpunkt von glazialisostatischen Anpassungsprozessen berechnen und wobei sie verschiedene Eis- und Erdmodellkombinationen mit einbeziehen.

In dieser Doktorarbeit habe ich daran gearbeitet Holozäne Meeresspiegelgeschichten in Südost Asien zu verbessern. Zuerst präsentiere ich eine Datenbank über den Holozänen Meeresspiegel, die aus veröffentlichter Literatur zusammengestellt wurde und 546 Datenpunkte aus der Region Süd- und Südostasiens umfasst. Innerhalb der verschiedenen Datensätze zeigen sich einige Probleme, wie Inkonsistenzen und generelle Datenlücken zwischen den einzelnen Datensätzen oder unzureichende Dateninformationen in der zugehörigen Literatur, die die Analyse der allgemeinen Meeresspiegelgeschichte für die größere Studienregion erschweren. Zusätzlichen, zu den glazialisostatischen Anpassungen, die in vielen Regionen als Hauptgrund für die

II. Zusammenfassung

Meeresspiegelhochstände gesehen werden, haben wir festgestellt, dass es wichtig ist Veränderungen während und nach der Indikatorablagerung, die weitere Abweichungen von der Eustasie verursachen, besser einzugrenzen. Weiterführend zeige ich die Ergebnisse von der Feldarbeit im Spermonde Archipel (SW Sulawesi). Dort haben wir 24 neue, auf sehr akkuraten Messungen von Mikroatollen basierende, relative Meeresspiegel-Indikatorpunkte des Mittleren bis Späten Holozäns datiert, die helfen die Inkonsistenz zwischen den Datensätzen aus der spärlich studierten Region des Spermonde-Archipels in SW Sulawesi zu minimieren. Diese Studie zeigt, dass die neuen Daten die Ergebnisse einer früheren Studie, die ebenfalls auf Mikroatollen basiert, unterstützt aber die Inkonsistenz zu den Daten von zwei älteren Studien, die hauptsächlich limitierende Indikatoren beinhalten, nicht minimieren können. Wir diskutieren anhand unserer Daten und in Kombination mit einer großen Anzahl von GIA Modellen, mögliche tektonische Raten in unserem Untersuchungsgebiet. Zusammen mit früheren Studien, zeigen unsere Daten, dass eine bewohnte Insel möglicherweise absinkt. Dies sollte unbedingt mit weiteren Studien evaluiert werden und eröffnet wichtige Fragen bezüglich des Schicksals von kleinen, tiefliegenden, dicht bewohnten tropischen Inseln hinsichtlich des Klimawandels.

Da es sehr wichtig ist die RSL-Geschichten zu verstehen, wurde in dieser Doktorarbeit ein anderer Ansatz entwickelt um die Relevanz und Wichtigkeit der fehlenden Meeresspiegelinformation aus unserer großen Datenbank zu beurteilen. Es wird eine statistische Analyse genutzt um besser bewerten zu können, wie gut GIA Modelle mit den geologischen Proben übereinstimmen. Die Ergebnisse können dabei helfen aufzuzeigen, ob die RSL Abweichungen zwischen den Vorhersagen der GIA Modelle und denen, die von Index Punkten abgeleitet wurden, auf größere Inkonsistenzen, Datenlücken oder höhenverändernden Prozessen basieren. Für diese Analyse wurden 16 Studienregionen mit 54 GIA Modellen verglichen, wobei die Ergebnisse positive und negative Abweichungen zwischen den von den Modellen und den von den Proben gemessenen relativen Meeresspiegelpositionen aufzeigen. Die Studie wurde schließlich in zwei Analyseeinheiten aufgeteilt, die zum einen die Wahrscheinlichkeiten des gesamten Datensatzes im Vergleich zu den Modellen berechnet und die zusätzlich auch die Wahrscheinlichkeit jedes einzelnen Index-Punktes im Vergleich zu den Modellen aufzeigt. Daraus resultierend zeigt sich, dass in drei Fällen, die Ergebnisse beider Analyseeinheiten deutliche Unterschiede aufzeigen, wobei in weiteren fünf Regionen nur niedrige Wahrscheinlichkeiten für die Position der Abweichungen berechnet wurden. Letzteres impliziert das hier die glazialisostatische Bodenbewegung nicht der einzige Grund für die von den Proben abgeleitete relative Meeresspiegelposition ist. Im Gegensatz dazu, zeigen acht Regionen sehr hohe Wahrscheinlichkeiten für die Abweichungen, was darauf hinweist, dass die glazialisostatische Bodenbewegung in diesen Regionen der hauptsächliche Grund für die relativen Meeresspiegelpositionen ist.

In dem folgenden Kapitel 1, erkläre ich allgemein die Bedeutung von historischen Meeresspiegeluntersuchungen, welchen Beitrag sie bei der Bestimmung der zukünftigen Meeresspiegelvariabilität leisten und was die hauptsächlichen Antriebsprozesse der glazialisostatischen Anpassungen sind, die den relativen Meeresspiegel beeinflussen. Im 2. Kapitel zeige ich die Methoden, die für das Zusammenstellen der Datenbank, die Probennahme und für die Altersbestimmung während und nach der Feldarbeit angewendet wurden. Desweiteren wird erklärt wieso GIA Modelle immer mit in Meeresspiegelstudien einbezogen werden müssen. Die Kapiteln 3 bis 7 präsentiere ich die Hauptresultate meiner Arbeit, worin die veröffentlichten und entworfenen Manuskripte beinhaltet sind. Schließlich, beweise ich in 8. Kapitel, dass eine Standardisierung von Meeresspiegeldaten unverzichtbar für das Vergleichen verschiedener Meeresspiegelstudien ist, um die relative Meeresspiegelgeschichte für eine größere Studienregion bestimmen zu können und um dabei außerdem Regionen zu identifizieren die ein erhöhtes Risiko haben überflutet zu werden. In diesem Kapitel zeige ich außerdem, dass eine statistische Wahrscheinlichkeitsberechnung dazu genutzt werden kann GIA Modelle besser auf Meeresspiegeldaten zu beschränken, sollten diese Anpassungen für die relativen Meeresspiegelanstiege im Holozän und in der Studienregion hauptverantwortlich sein. Zuletzt fasse ich in Kapitel 9 den Beitrag dieser Arbeit zur Wissenschaft zusammen und gebe einen Anstoß für die zukünftige, weiterführende Forschung.

III. Acknowledgement

In the last 3 years of my PhD, I learnt a lot. I learned a lot about science, about sea-level research, about field work and about people. I experienced good times and interestingly crazy times. Many people made the last three years special to me and many of them I really like and would like to keep in touch with.

First of all, there is Alessio Rovere. My Supervisor. I thank you for your guidance and help in so many aspects and at so many points during my PhD. It was a trip. A good one. It was challenging, interesting, motivating exhausting in some parts adventures, short: awesome. I will remember so many funny moments and situations with you and I am grateful for this. I thank very much also for your support and your good-will.

Thomas Mann, I would like to thank for your support in Indonesia and your help and thoughtful comments during the whole time of my PhD and Tilo Schöne, for your help in all my mean sea-level problems.

I thank the University of Bremen, MARUM and ZMT for the cooperation and the chance for this PhD. Further, I would like to thank the Special Priority Program (SPP)-1889 "Regional Sea Level Change and Society" where my project was implemented in and the Deutsche Forschungsgemeinschaft for the funding of my project.

I would like to thank my Sea level and Coastal Changes working group colleagues, Elisa Casella, Thomas Lorscheid, Jan Drechsel, Deirdre Ryan and Patrick Boyden, I had a great time with you, inside and outside the office.

Samira, I would like to thank you for the time you spend with me in Makassar, on the Boat and on the Islands. I cannot imagine how field work would have been without you and you positive attitude.

A special thanks to Thomas L., Patrick and Julia who helped me a lot in the last days of finishing my thesis and in the years before, when we became good friends and spend many hours together, having fun, talking nonsense and being awesome. Thank you. Let´s keep going.

I thank my friends Vanessa, Lena, Lina, Henriette, Sarah, Sebastian and Julia for being my friends. I never want to miss one of you.

Thanks to my dear Husband who stayed awake with me during the night to finish this thesis, thank you for loving me even if I was awful while my writing problems and after short nights when my mood was bad. I love you and the last years with you were the best in my life, so far.

Ich möchte außerdem ganz besonders meiner Mutter Elke und meiner Oma Hilde und meinem Onkel Wolfgang danken. Ihr seid immer zur Stelle, wenn ich euch brauche. Ihr habt immer einen Rat, ihr seid immer eine Unterstützung, ihr seid liebevoll, herzlich und ihr seid einfach die wundervollsten Menschen in meinem Leben. Ich bin so dankbar euch zu haben. Ich liebe und danke euch.

Zuletzt möchte ich nun einem weiteren Teil meiner Familie ganz herzlich für alles Danken. Heike, Reini, Annika, Paul, Swantje, André, Lasse, Jannes und Klaas. Annika und Swantje, Danke dass ihr nicht aufgehört habt zu fragen, wann ich endlich abgebe, das hat mich stets motiviert. Danke für schöne die Zeit die wir bisher zusammen hatten und danke für eure Unterstützung. Ich habe euch lieb.

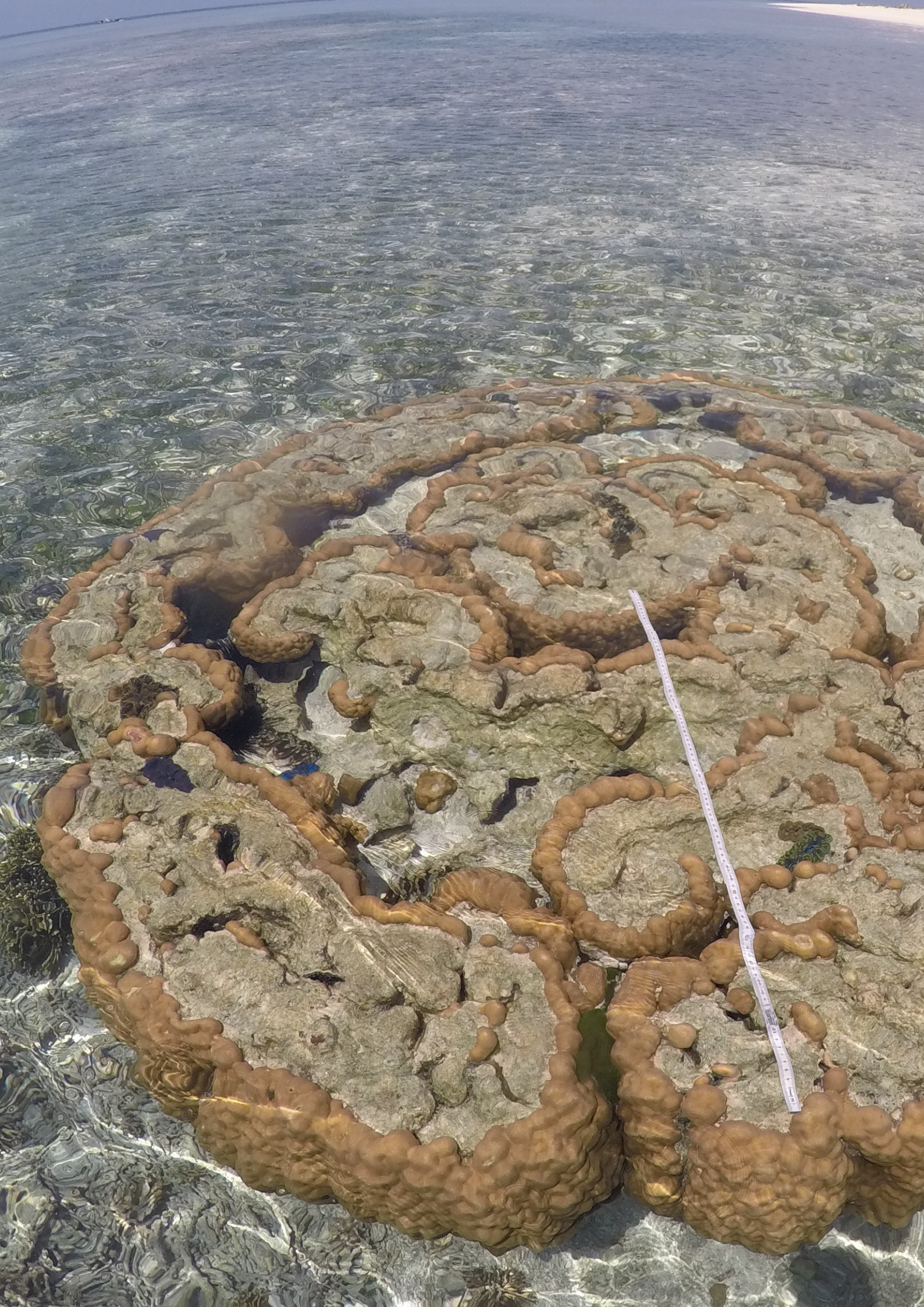

IV Table of Contents

IV. Table of contents

V. List of figures

VI. List of tables

VII. List of Abbreviations

^{14}C. *Radiocarbon dating method*

AD. *Anno Domini*

AMS. *Accelerated mass-spectrometry*

ANICE. *GIA model*

APC. *Average Probability Calculation*

BB. *Bone Batang*

BL. *Barrang Lompo*

BP. *Before Present, 1950*

Br. *Beachrock*

cal a. *calculated age*

Co. *Corals*

delta R. *Ocean Reservoire correction and error*

DPC. *Detailed Probability Calculation*

E. *Elevation of a microatoll*

Er. *Erosion error*

FMA. *Fossil Microatoll*

GIA. *Glacial Isostatic Adjustment*

GNSS. *Global Navigation Satellite System*

GPS. *Geographic Positioning System*

H. *sample elevation after Chappell and Polach, 1991*

HLC. *Height of living coral*

ICE5g. *GIA model*

ICE6g. *GIA model*

IGSN. *International Geo-Sample Number*

IM. *Indicative Meaning*

IR. *Indicative Range*

KK. *Kodingareng Keke*

LAT. *Lowest Astronomical Tide*

Lc. *Loamy clays*

LGM. *Last Glacial Maximum*, *Last Glacial Maximum*

LM. *Lower Mantle*

LMA. *Living Microatoll*

Ma. *Mangrove swamp*

MHHW. *Mean Higher High Water*

MLLW. *Mean Lower Low Water*

MLW. *Mean Low Water*

MLWN. *Mean Low Water Neaps*

MLWS. *Mean Low Water Springs*

Mo. *Mollusks*

MSL. *Mean Sea Level*

MTL. *Mean Tide Level*

n=. *number of sample points*

NetCDF. *Network Common Data Format*

Oy. *Oyters*

PDB. *PeeDee Belemnite*

pMC. *Percent Modern Carbon*

PPB. *Panambungan*

PS. *Pulau Suranti*

VII. List of Abbreviations

PT. *Pulau Tambakulu*

RSL. *Relative Sea Level*

RWL. *Reference Water Level*

S .*Sanane*".

SB. *Sanrobengi*, *Sanrobengi*

SEAMIS. *Southeast Asia, Maldives, India and Sri Lanka*

Sh. *Shell accumulations*

SM1. *Supplementary Material 1*

tc. *Radiocarbon age after Chappell and Polach 1991*

U. *Uplift / Subsidence rate*

U/Th. *Uranimum-Thorium age dating isotops*

UM. *Upper Mantle*

Visco. *Mantle Viscosity*

VLM. *Vertical Land Movements*

VM. *Mantle Viscosity*

XRD. *X-ray diffraction*

δ^13 C. *isotope fractionation correction factor*

σEr. *estimated erosion error*

σIR/2. *half of idicative range for error calculation*

σMAE. *Microatoll elevation error*

1 Introduction

1.1 Importance of paleo sea-level investigations

The study of global Holocene sea-level changes is important for both societal and scientific reasons (Church et al., 2001; IPCC, 2001; Nicholls, 2004), while there are several complex and intertwined processes affecting sea level that need to be unraveled. In fact, sea-level variability causes a mass imbalance affecting the Geoid and the Earth rotation (Box 1) (Milne et al., 2009; Toscano et al., 2011; Nakada and Lambeck, 1989). When ice sheets stopped melting in the Late Holocene, the variability in the height of the ocean surface is mostly due to re-distribution of water masses initiated by Glacial Isostatic Adjustment (GIA) (Box 2) (Clark and Farrell, 1976; Kopp et al., 2015a; Milne et al., 2002; Peltier, 1998; Peltier et al., 1978; Peltier and Fairbanks, 2006). In contrast, nowadays GIA is not the main contributing factor to ongoing sea-level changes. However, to predict future sea-level variability the processes triggered by GIA that affected the paleo sea-level and circumstances affecting the sea-level today need to be understood and disentangled (Overpeck et al., 2006; Gehrels et al., 2011).

The start of modern sea-level acceleration may be timed with the industrial revolution (ca. 1880 AD) and sea level currently rises by 3 to 4 mm/a globally (Watson et al., 2015; Yi et al., 2015). The increase in the global ocean and air temperature started when greenhouse gas emissions increased, contributing to initiating climate change and sea-level rise. The latter is initiated by changes in global surface temperature that induces thermal expansion, which changes global mean sea level by increasing the ocean volume (Church et al., 2001; Milne et al., 2009; Peltier, 1998). Thermal expansion differs geographically depending on the ocean stratification and on water temperature, while due to the large heat capacity of the ocean, resulting sea-level change can continue for centuries (Church et al., 2001). Besides thermal expansion, the main driver of sea-level rise (Church et al., 2001), land-ice melting also contributes to ongoing sea-level rise. Major ice-sheets from Greenland and Antarctica increased in mass loss since the 1990s (Rignot et al., 2011; Allison et al., 2009) while Rignot et al. (2011) reports a combined ice-mass loss of 475±158 Gt/a from both ice-sheets in 2006, which is equivalent to a sea-level rise of 1.3±0.4 mm/a. Furthermore, Church et al. (2001) summarizes, that the contribution to global sea-level rise of the Greenland ice-sheet is ranging from 0.01 m and 0.03 m between 1990 and 2090 and the contribution from Antarctica varies from -0.07 m to -0.01 m. However, these calculations exclusively result from ice-sheet reactions to recent and future climate change predictions, and do not include ongoing ice-sheet adjustments lasting from past climate changes (Church et al., 2001). Further resulting global changes, include changes in weather patterns, melting of sea ice, and increased fresh-water load on global oceans from ice-melting of smaller ice-caps and glaciers (Church and White, 2011; Church et al., 2006).

Results from Warrick et al. (1996), summarized in Nicholls and Mimura (1998), show that sea-levels rose 0.1 m to 0.25 m within the 19th century and predict a general rise of additional ~0.5 m until year 2100, likely initiating an immense land inundation or loss. As summarized by Vitousek et al. (2017), sea-level variability also causes:

- passive inundation of low-lying areas by high-tides
- increases and intensifications of the flood rate at coastal areas
- intensification of beach erosion
- inundation of groundwater
- variations in wave dynamics
- and the displacement of coastal communities.

Box 1: Short explanation of the Geoid and water masses re-distributions due to changing surface mass or internal deformations of the mantle.

The Geoid and the gravitational potential

The geoid is an equipotential surface of gravity that corresponds to the mean sea surface at rest over the oceans. Therefore, changes in the gravitational potential due to surface loads displacements and solid Earth deformations force meltwater re-adjustments to compensate for the gravitational difference under the requirement of mass conservation (Milne et al., 2009; Toscano et al., 2011). A clear example of this process is the so-called "equatorial ocean siphoning", where water migrates from the equatorial regions towards the subsiding peripheral forebulges of the polar regions (Mitrovica and Peltier, 1991).

This is particularly relevant for regions that are more vulnerable to flooding or drowning because of very low coastlines above mean sea level (MSL) as it is in e.g. South and Southeast Asia (Cazenave and Cozannet, 2013; Nicholls et al., 1999; Nicholls and Cazenave, 2010). At the close of the 20th century, already more than 50 % of the global population were living along low-lying coastlines, (Houghton, 1996). Now, in the 21st century, the growth of coastal populations, expansion of mega cities (i.e. cities exceeding 8 million inhabitants), and extensive groundwater extraction have destabilized the basement geology and causing localized and regional subsidence. This accelerates local sea-level rise and increases the risk of flooding (Nicholls, 1995; Horton et al., 2005; Geyh et al., 1979). Eleven of fourteen coastal mega-cities are located in Asia (Tibbetts, 2002; Geyh et al., 1979), where the number of people at risk to flooding is the highest, as the coastlines of India, Indonesia and Vietnam belong to the most populated regions in the world (Neumann et al., 2015). For Indonesia, an increase of 0.60 m in RSL can already cause land inundation of 34.000 km² (1.9% of the entire land mass) and for Vietnam, an increase in RSL of 1 m, is supposed to cause land loss of 40.000 km² (12.1% of the entire land mass) (Warrick et al., 1996). As Indonesia is composed of many thousand low-lying islands (~17.500 Islands cover a coastline length of 88.000 km) (Marfai and King, 2007; Kench and Mann, 2017), the land loss will affect the inhabitants dramatically. Some other regions in SE Asia that are also vulnerable to sea-level rise and the consequences of climate change are Bangladesh, parts of China, the Mekong River Delta in Vietnam, or the Bangkok region of Thailand (Yusuf and Francisco, 2009; Neumann et al., 2015). However, as explained by Nicholls and Mimura (1998), predicting the effect of how future sea-level scenarios might affect the society and environment is difficult due to the incomplete knowledge of all processes affected by sea-level rise or the lack of analytical methodologies convenient for several impacts. Thus to prevent catastrophic events in regions that are at elevated risk from sea-level rise and to predict its future rates and distribution, an understanding of the driving mechanisms of sea-level variability and their interactions, is essential (Overpeck et al., 2006).

Modern sea-level fluctuations and paleo RSL changes can be tracked with different methods. While for today's mean sea-level variability tide gauges (RSL changes) and satellite altimetry (sea surface changes) are the common methods to record sea-level changes, paleo RSL positions are assessed using paleo sea-level indicators (i.e. index points; Shennan, 1982; Van de Plassche, 1986) or indirect sea-level proxies e.g. stable oxygen isotopes of foraminifera (Rohling et al., 2008). Holocene RSL studies are based on the estimation of paleo RSL variability using a combination of geophysical observations and geological proxy reconstructions (Cazenave et al., 2009; Church et al., 2006; Kopp et al., 2015a; Toscano et al., 2011; Mann et al., 2019b). While geophysical GIA models encompass calculations of ice melting, mantle properties, and convection processes, geological indicators are studied in the field to derive former local sea-level positions. In general, there are two types of sea-level samples: limiting indicators and index points. While marine or terrestrial limiting points form, respectively, below or above the tidal range, (Shennan and Horton, 2002) index points give a direct indication of paleo sea level, that is called the indicative meaning (Van de Plassche, 1986; Shennan, 1986; Woodroffe et al., 1990). The indicative meaning includes the indicative range (elevation range in which the indicator

forms within a tidal datum) and the reference water level (midpoint of indicative range). The calculation of both is required to define an index point (Shennan, 1986; Shennan and Horton, 2002).

In addition to studies detailing the Holocene sea-level history, sea-level positions from the Common Era (last 2 ka BP) (Kopp et al., 2016) are also a vitally important in focus of RSL studies. They fill the chronology gap between modern tide gauge recordings and the pre-industrial era (Church et al., 2006; Kopp et al., 2015a; Kopp et al., 2016). However, samples from that period are rare in South and Southeast Asia. Both types of indicators (limiting and index points) provide valuable insights in the continental response to changing water masses (Engelhart et al., 2011; Lambeck et al., 2001; Melis et al., 2018). Thus, they contribute to the improvement and adjustment of GIA and Earth rheology models (Engelhart et al., 2011; Lambeck, 1998; Melis et al., 2018; Milne and Peros, 2013). The studies of paleo patterns and ongoing sea-level changes help to predict future sea-level prognoses. The individual local RSL history from Holocene disentangles how water masses were distributed due to GIA and show the paleo sea-level fluctuation for each location that was carefully studied, while ongoing sea-level variability records the rates of changes, which help to combine paleo results with ongoing rates, to match the sea-level curve and refine the future predictions.

Box 2: Short explanation of hydro- and isostatic processes and changes during the transition from glacial to interglacial. Both adjustments interact with each other and affect the Geoid (references in the text).

From glacial to interglacial & Holocene highstand

In glacial periods: mass accumulates especially at the poles where local ice load causes continental subsidence of the underlying crust. This subsidence induces convection processes forcing mantle material to migrate away from the loaded region to unloaded areas, causing an uplift of the crust. Mantle material accumulates directly below the regions adjacent to the ice, deforming the crust and forming a forebulge that surrounds the ice covered region (Peltier, 1998). The gravitational equipotential drives a poleward migration of water as land based ice sheets increase the pole mass (Milne et al., 2002; Mitrovica and Peltier, 1991; Toscano et al., 2011). This causes a disequilibrium of the Geoid in ice-free regions (far field areas), as the RSL is higher in the near field than in the far field during this time (Milne et al., 2009; Peltier, 1998).

The transfer from glacial to interglacial: is marked by a redistribution of mass. As temperatures increase after the Last Glacial Maximum (~26 ka BP), land ice starts melting, releasing fresh water into the oceans. As the gravitational ice-ocean water attraction diminishes, ocean water starts to migrate away from the polar regions and the ice retreat allows continental uplift. This causes the near field RSL to begin to fall (Hay et al., 2014). With the onset of Holocene (~11.5 ka BP) equatorial regions experienced a rapid sea-level rise in a rate of ~15 m/ka (Lambeck et al., 2014). Ongoing water load at the equator causes a downward flexure of continental shelfs and the ocean floor inducing continental levering (Clark et al., 1978; Nakada and Lambeck, 1989).

During Mid to late Holocene highstand: south and southeast Asia experienced a highstand in RSL between ~3 ka BP in the Maldives (Kench et al., 2009) and ~5 ka BP in e.g. Indonesia (Mann et al., 2016; Bender et al., 2020, *proof stage*.). In this period, RSL positions varied (dependent on the location) from 0.5 to ~4.5 m above modern sea-level (e.g. Bird et al., 2010; Geyh et al., 1979; Horton et al., 2005; Kench et al., 2009; Mann et al., 2016; Woodroffe et al., 1990; Mann et al., 2019b).

These processes make the understanding of sea-level variability more complex and intricate, underlying the importance of such studies, especially in the period of modern global warming and eustatic sea-level rise.

Therefore, the results of this thesis contribute to:

- expanding the knowledge of Holocene RSL variability in SE Asia,
- offer new paleo constrains to assess future impacts
- provide improved GIA models for Southeast Asia.

State of the Art (previous work)

Pirazzoli and Pluet (1991), date the beginning of sea-level observation at the time when Celsius, in 1733, noticed a sea-level fall in the Baltic Sea, which he explained with an increase in ocean evaporation. While in contrast, first tide measurements are traced back to the 17th century when the Dutch, in 1682, built a provisional tide gauge in Amsterdam. They needed to survey daily tides as, for the subsiding Netherlands, a rising sea-level was (and still is) an important threat (Van Veen, 1954). Few hundred (200 to 300) years later, in the late 19th and in the early 20th century, Suess (1885), Thomson (1888), Daly (1920b, 1920a) and Daly (1934) concluded a relation between changes in lithosphere, sea levels and climatic conditions with water mass migration due to mass compensation, mass attraction and other Glacial-isostatic effects affecting sea-level and continents (Pirazzoli and Pluet, 1991). Finally, in the late 1970s, Clark and Farrell (1976) developed a sea-level equation, which is used to calculate the RSL changes based on the mass flux from ice and ocean and continental response. It was later improved by including all GIA feedbacks (Mitrovica and Peltier, 1991).

Research focusing especially on Holocene sea-level reconstructions has been conducted since the 1930s (Baden-Powell, 1937; Pirazzoli and Pluet, 1991), whereas the indicative meaning provided by index points was only introduced 50 years later in the 1980s (Van de Plassche, 1986; Shennan, 1982). The use of limiting indicators was developed in the early 21st century (Shennan and Horton, 2002). To document the history of Holocene sea-level studies, Pirazzoli and Pluet (1991) published "The World Atlas of Holocene Sea Level Changes", which is a compilation of all Holocene sea-level datasets published before 1991. It includes 750 sea-level studies and provides 800 sea-level curves (Pirazzoli and Pluet, 1991). In the 21st century, RSL studies are an integrated part of marine sciences with established measurement methods and procedures as well as standardized protocols. Thus, Shennan et al. (2015) published the "Handbook of Sea-Level Research" were they summarize all important field and laboratory techniques and provide explanations of methodologies related to sea-level sciences accepted by the sea-level community and commonly published in literature.

Nowadays, there is a high amount of literature documenting global RSL history. Nevertheless, there are still many regions lacking published sea-level information. Due to climate change and the on-going land ice melt, scientists need to unravel the RSL history from Holocene to improve the future predictions of sea-level rise. Especially areas far from polar regions (i.e. far-field, Khan et al., 2015) are of high interest for RSL studies as these regions mainly experience a sea-level highstand in Holocene that documents the paleo sea-level paleo position after the last ice melt stopped. Two of these less studied far-field regions are South and Southeast Asia. These areas are composed of many low-lying, inhabited and locally subsiding coastlines (Nicholls et al., 1999; Nicholls and Cazenave, 2003; Chaussard et al., 2013). Future sea-level variability predictions are important for determining which areas in South and Southeast Asia are at risk to flooding or drowning. However, only one semi-recent and one recent Holocene sea-level database (Horton et al., 2005; Mann et al., 2019b, the latter included in this thesis) compiled all relevant publications since 1972 from these two areas. In Chapter 4, 31 studies are discussed and compared to GIA, as published in Mann et al. (2019b). While, so far, the Malay-Thai Peninsula in the central Sunda Shelf is one of the most studied regions in Southeast Asia (Chapter 5), there are many regions represented by a small number of data points. Only one example of these regions is the Spermonde Archipelago. It is represented by 21 data points (Mann et al., 2019a; Mann et al., 2019b) compiled in three Holocene sea-level studies available from literature (Mann et al., 2016; Tjia et al., 1972; De Klerk, 1982) and further 24 newly investigated index points (Bender et al., *proof stage*).

1.2 Motivation

Understanding and unraveling the RSL history in South and Southeast Asia is essential to indicate areas that are at risk to flooding or drowning due to modern and future sea-level rise. Besides the lack of paleo sea-level data in the literature for these regions, there are also inconsistencies within datasets in the same study areas. This complicates the identification of critical regions. The reasons for these inconsistencies need to be understood to better frame the paleo RSL histories within the broader regions. Furthermore, field data and GIA predictions for the area of interest are important to constrain the glacial-isostatic adjustments for the area of interest. However, many study locations present field data disagreeing with GIA model predictions while others match the models perfectly. The mismatch of field data and GIA models need to be analyzed statistically, to evaluate if RSL observations from field data and predicted by GIA models show comparable RSL histories mismatching only in small ranges, or if reasons for significantly deviating results are based either on complications in the data analysis or discrepancies in RSL predictions by the GIA models. The result will expand the knowledge of local RSL history and improve data analysis.

To investigate the above-described concerns, this thesis addresses the following questions:

1. Why is a standardized analysis of sea-level data indispensable for the compilation of a database and how does this improve data handling?
2. Can the database and new data collected in this thesis help to highlight critical areas in South and Southeast Asia for which concern flooding risk?
3. Does a statistical probability calculation help to constrain GIA model predictions for all tectonically stable study sites in South and Southeast Asia and can the models be applied for locations without field data?

Question 1 will be addressed in chapter 4 and 5, where I will present a new standardized Holocene sea-level database and 23 sample sets that show analyzing sea-level data by using standardized methods and errors improves the quality of paleo relative sea-level predictions.

Afterward, question 2 will be investigated in chapter 4, 5, and 6, where inconsistencies within datasets or a lack of data imped to predict the local RSL history. Chapter 6 presents the study of a new dataset for the rarely studied area of the Spermonde Archipelago and shows that sampling following standardized methods is essential for the RSL predictions derived from fossil and living microatolls.

Finally, question 3 will be analyzed in chapter 7, where a statistical probability calculation is provided that is based on 54 GIA models and 246 sea-level data points from 22 studies located in tectonically stable areas of South and Southeast Asia.

2 Methods

The following paragraphs summarize all methods I used during the work on the Holocene sea-level database, my fieldwork in Indonesia, and for the related data analysis. The detailed method explanations are provided in the related chapters.

Radiocarbon dating

Chapter: 4.4.4, 6.4.4

All samples collected in the field were cut at least into two slices using a carbonate saw in the geology laboratory of the Centre for Tropical Marine Research (ZMT). One piece of each sample is archived at MARUM and the second piece of each sample was pulverized by mortar and pestle to analyze the carbon percentage and possible diagenetic alterations of the aragonite in the coral skeleton or to detect other contaminating minerals. The pulverized samples were analyzed via X-ray (powder) diffraction (XRD) scan at the Central Laboratory for Crystallography and Applied Material Sciences (ZEKAM), University of Bremen, Germany. For the final accelerated mass-spectrometry (AMS) radiocarbon dating and calibration into calendar years, a small solid piece of each sample was sent to Beta Analytic Laboratory, Miami, USA. As no delta R value for reservoir corrections of the sample are available on literature the value of 0±0 was used (Southon et al., 2002). An IGSN number (International Geo-Sample Number) was assigned to each fossil microatoll sample.

Re-analysis of sea-level indicators for the compilation of a database

Chapter: 4.4.2

For the compilation of the database, all data points were split into two groups, where the second group is subdivided into two types. The first group includes RSL index points and the second group compiles limiting indicators subdivided into marine and terrestrial limiting points. Terrestrial or marine limiting indicators provide relevant information depending upon whether they formed above the highest astronomical tide (HAT) (terrestrial) or below the lowest astronomical tide (LAT) (marine) (Shennan and Horton, 2002). To be considered as an index point, four essential criteria are required:

- Sample elevations are benchmarked to a tidal datum and were surveyed with high-precision techniques
- Index points are providing an individual indicative meaning (IM) (Shennan, 1982; Van de Plassche, 1986) calculated from the indicative range (IR) and the reference water level (RWL).
- The indicator age was dated with ^{14}C, and corrected for radiocarbon activity in the ocean termed reservoir correction (δR±uncertainty), or it was dated with U/Th.
- The location of the sample shows coordinates and is retrievable

Expressed in a formula the IR is the upper tidal limit minus the lower tidal limit:

$$HAT - LAT$$

while the RWL is expressed as

$$\frac{(HAT+LAT)}{2}$$

In general, the meaning for marine and terrestrial limiting indicators can be expressed as

- below mean tide level (marine samples)

and

- above mean tide level (terrestrial samples).

Sample age re-calculation

Chapter: 4.4.4

In the Holocene sea-level database, some data point ages derived from studies older than ~1980s provided incomplete information about radiocarbon isotope fractionation (Törnqvist et al., 2015) or the explanation of the radiocarbon age analysis. For these studies, a $\delta^{13}C$ isotope fractionation correction was applied and age re-analysis with the MARINE 13 or IntCal 13 curve, both provided by the Calib 7.1 Radiocarbon Calibration website Calib.org or usable as the download version 7.0.0. (Stuiver et al., 2017).

Glacial-Isostatic Adjustment (GIA) models

Chapter: 4.4.7, 5.2, 6.4.5, 7.4

GIA models include all geophysical processes ongoing on Earth induced by changes from ice and ocean volume due to mass re-distributions. These processes initiate related convectional processes deforming the Earth's interior and affect the planetary gravitation. For the analysis of relative sea-level variability in the Holocene after the last glacial period, GIA models are important instruments as they take into account sea-level variation and crustal deformations and calculate the relative sea-level position based on mantle convection, flow velocities, ice mass loss, freshwater intrusion into the ocean, sea-level fall due to continental uplift and further related processes. This study comprises of results from the ice sheet models ICE-5G, ICE-6G and ANICE coupled to SELEN (Peltier, 2004; De Boer et al., 2015; Peltier et al., 2015; De Boer et al., 2017). Both models vary, among others, in the flow velocities of the upper and lower mantle or the transition zone and the lithosphere thickness.

Seametrics PT2X sensors

Chapter: 6.4.2

Seametrics PT2X pressure and temperature sensors were used to record local tide levels at all field sites. They were attached to jetties or corals below sea level for the longest possible period. The sensor adjustments, data extraction and processing were performed with the Aqua4Plus software.

Leveling and sampling

Chapter: 6.4.2, 6.4.4

All microatoll elevations were measured with an automatic level and meter stick. The benchmark was a Seametrics PT2X sensor, installed on each study site. For sampling, a hammer and chisel were the best instruments to cut out small pieces from most fossil microatolls as they were covered by water. Those elevated above sea level, were sampled with a hand drill to extract material for ^{14}C dating. For the propagation of measurement errors, we used the root mean square of the sum of squares of :

- automatic level survey error = 0.02 m (Mann et al., 2016). Added twice if the level had to be moved
- referencing error from one island logger to Panambungan MSL (ranging from 0.01 to 0.07 m)
- referencing error Panambungan to Makassar MSL = 0.04 m
- Makassar MSL calculation error from 8.9 years = 0.05 m.

Relative sea-level calculation

Chapter: 6.4.3

For the microatolls surveyed in this thesis, RSL calculations are based on the concept of the indicative meaning (Shennan, 1986), the height of living corals (HLC) as the living analog to the fossil microatolls, and of the following formula:

$$RSL = E - HLC + Er$$

This formula includes the surveyed elevation of the fossil microatoll (E), the average height of living coral (HLC) and if given, the missing cm of eroded fossil microatoll surface material (Er).

The related RSL error calculation of all uncertainty term is expressed as follows:

$$\sigma RSL = \sqrt{(\sigma MAE^2 + \sigma(\frac{IR}{2})^2 + \sigma Er^2)}$$

And it includes the individual fossil and living microatoll elevation error (σMAE), the half of the related indicative range represented by the standard deviation of the HLC divided by 2(σIR/2) and the uncertainty of the estimated coral erosion (= 0.19 m), in case a microatoll was eroded (σEr).

Processing and refining software

Chapter: 4, 5, 6, 7

All maps included in this thesis were produced with ESRI ArcGIS™, while graphs were plotted with the Golden Software, Inc. Graphing System Grapher – version 10.5. or the MathWorks Matlab ®. Resulting plots and figures were finally embellished or created in CorelDRAW® 2017 version 19.1.

3 Outline of manuscripts

The thesis is compiled of three papers and one "data in brief" article. These publications cover the main chapters, and are summarized in a few points and the main research highlights as well as all author contributions are listed below. My own work on each manuscript is also detailed.

Manuscript 1 – Holocene sea levels in Southeast Asia, Maldives, India and Sri Lanka: The SEAMIS database

&

Manuscript 2 – Data article; Relative sea-level data from the SEAMIS database compared to ICE-5G model predictions of glacial isostatic adjustment

Thomas Mann, **Maren Bender,** Thomas Lorscheid, Paolo Stocchi, Matteo Vacchi, Adam D. Switzer, Alessio Rovere

Published in Quaternary Science Reviews (2019)

Research highlights:

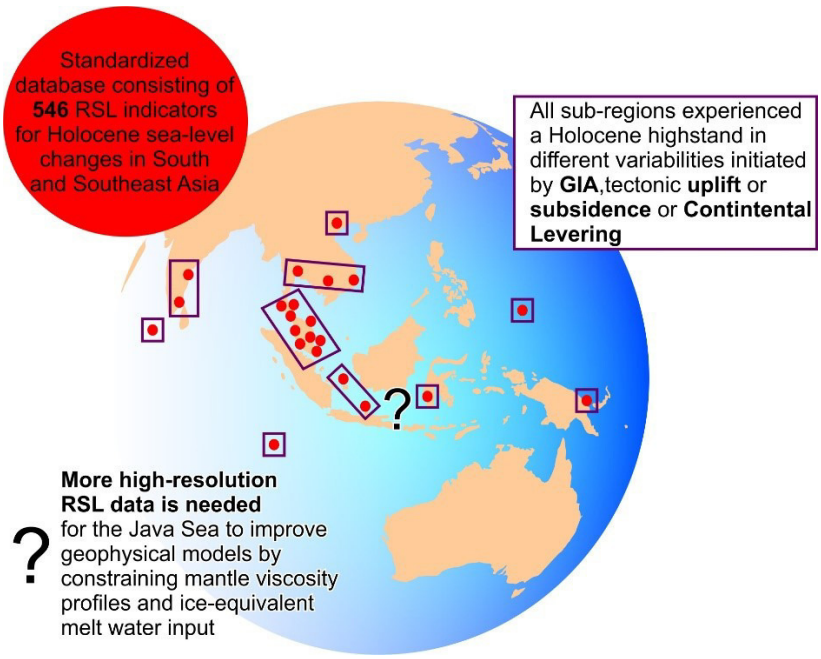

Author contributions: AR, TM, MV, PS and AS conceived the project; **MB determined the indicative meaning for each indicator type present in the relevant literature, reviewed and standardized the published RSL data** with support from AR, TM and MV; **MB prepared figures** with support from TM and AR; TL determined tidal datums for each geographic sub-region; PS performed GIA modeling for each geographic sub-region; TM wrote the initial manuscript that has been revised and approved by all authors.

Detailed own contribution: For manuscript 1 and 2, I reviewed the entire existing literature on Holocene sea-level indicating data in Southeast Asia, the Maldives, the eastern and southeastern parts of India, and Papua New Guinea in the western, central pacific. I reviewed all papers, and I inserted the data in

the database template. As this was done early in my thesis, TM, MV and AR helped me to, interpret and analyze all the information included in the papers I reviewed. For each paper, I reviewed information about the sampling and measurement methods, and the original interpretation of each sample. In case any of the basic information about a sample, e.g. elevations, methods, ^{14}C, calendar ages or its origin (if it was sampled in situ) was missing, these points were rejected and an explanation for this was added to the database. I carefully transmitted all information into the excel file and recalibrated radiocarbon ages without isotope fractionation information or if an old calibration software was used for the calculation of ^{14}C ages into calendar years. In case information was missing or uncertain, I also tried to contact the original authors or the laboratories where the analysis was done. Further, I was responsible for all figures (except Figure 4) and I provided the first author with information about all reviewed papers while the paper was being written.

Manuscript 3 – Late Holocene (0-6 ka) sea-level changes in the Makassar Strait, Indonesia

Maren Bender, Thomas Mann, Paolo Stocchi, Dominik Kneer, Tilo Schöne, Julia Illigner, Jamaluddin Jompa, Alessio Rovere

Accepted – In publication (proofs stage) – Climate of the Past

Research highlights:

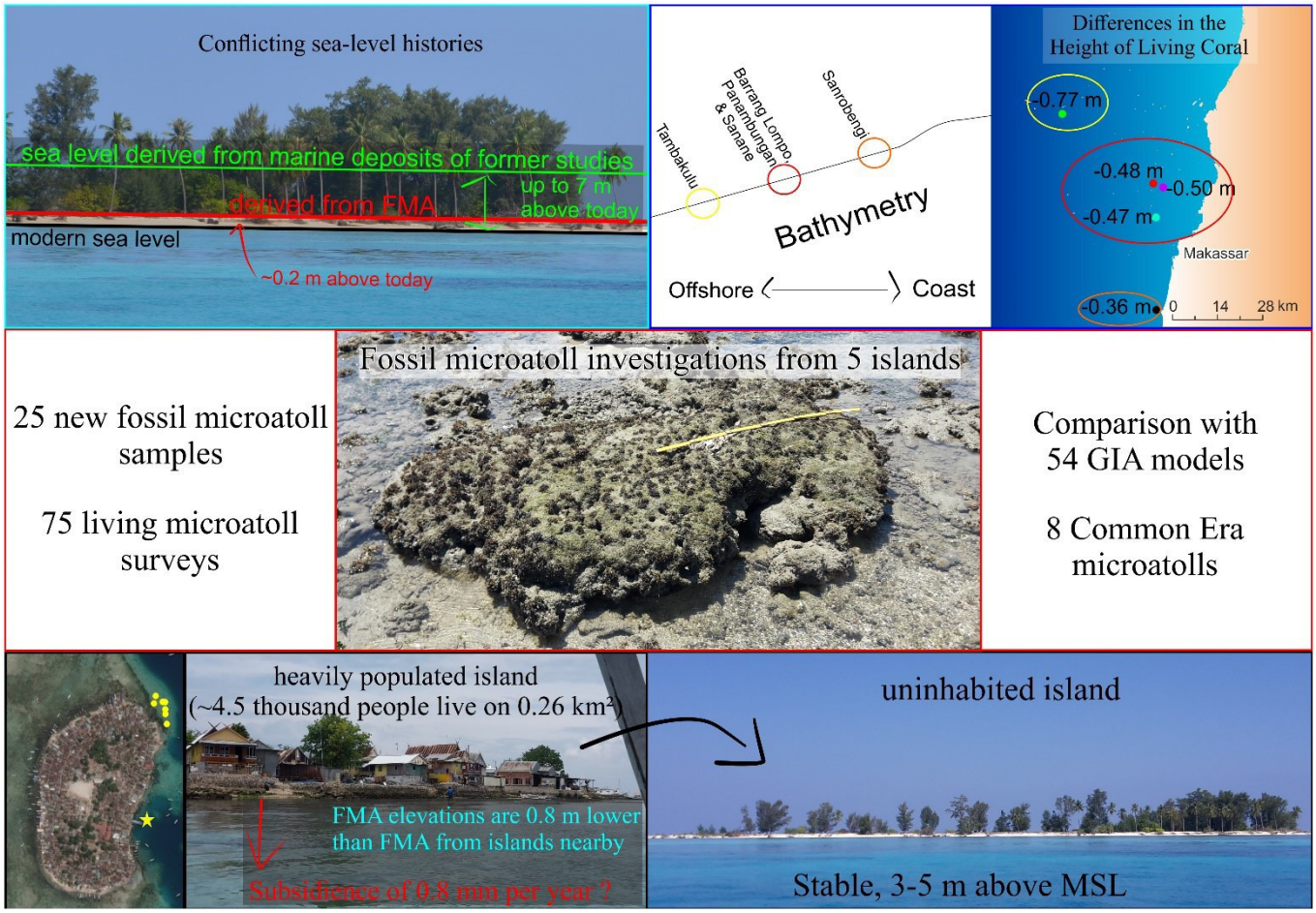

Author contributions: **MB organized fieldwork and sampling**, which were conducted in collaboration with TM and DK. JJ gave on-site support in Makassar and provided essential support with sampling and research permits in Indonesia. **MB organized the data analysis**, with supervision and inputs by TM and AR. AR wrote the python codes provided in the Supplementary material. TS and JI analyzed the tidal datum and calculated MSL, providing expertise on modern sea-level processes. PS offered expertise, performed model runs and provided discussion inputs on Glacial-Isostatic Adjustment. **MB drafted the first version of the manuscript. MB and AR wrote the final version of the manuscript jointly**. All authors revised and approved the content of the manuscript.

Detailed own contribution: For manuscript 3, I planned and conducted fieldwork in the Spermonde Archipelago in Indonesia (including research and export permits). Together with TM and DK, we sampled 25 fossil microatolls and surveyed 81 living microatolls to indicate local paleo sea-level positions on 5 small and low-lying islands. I prepared and ran the pressure sensors to record the tides on 7 islands and I further downloaded and prepared the data for the analysis. I also prepared the samples for the XRD scan at the Central Laboratory for Crystallography and Applied Material Sciences (ZEKAM), University of Bremen and the Beta Analytics Laboratory for the AMS analysis. With the support of TM and TS, I analyzed the results of the pressure sensors and the fossil and living microatoll surveys to reference them to relative mean sea level. I led the writing of the paper, including handling revisions.

Manuscript 4 – Probability difference analysis between geological sea-level indicators and GIA model predictions

Maren Bender, André Düsterhus, Alessio Rovere

In preparation

Research highlights:

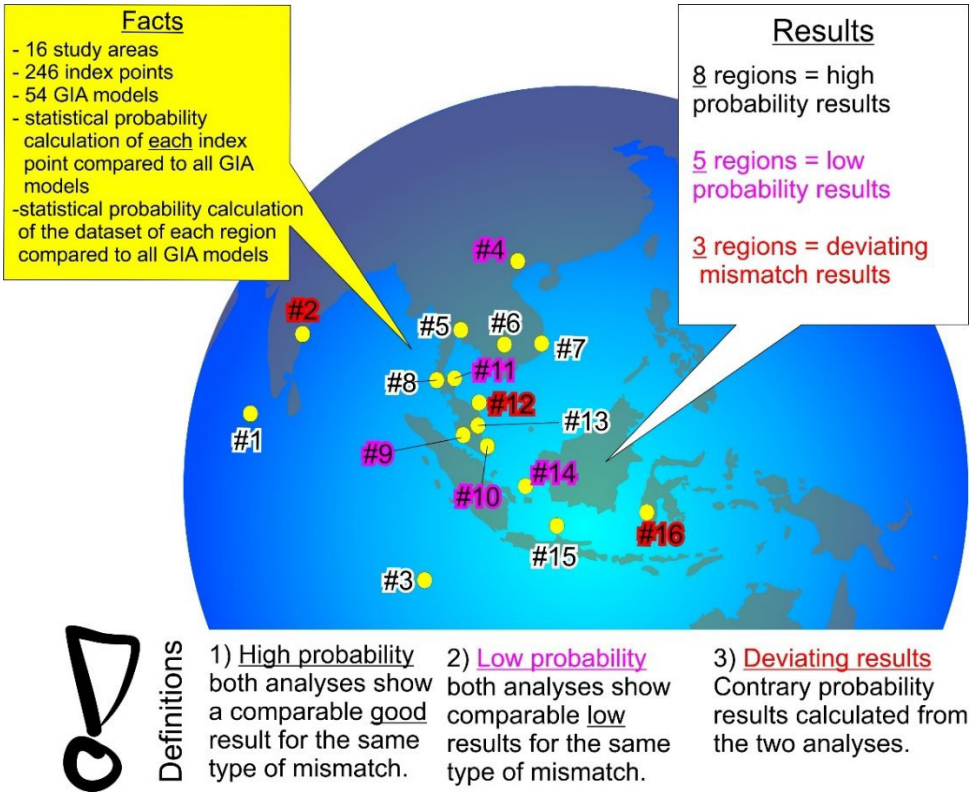

Author contributions: **MB provided the improved and expanded database** that was compiled by her for the first manuscript 0 and 0. AD tested, wrote and modified the used GIA scripts. **MB compared the results and wrote the MS**. AR supported the writing, the analysis, and the modification of the figures.

Detailed own contribution: Due to my experiences from the previous papers (chapters 4, 5 and 6) I was able to use the database and field data from the Spermonde Archipelago accordingly for this analysis. Thus, I used and combined all data points from stable regions provided in MS 1, 2 and 3 (chapter 4, 5 and 6) and an additional reference that was not presented in the SEAMIS database for this analysis. I interpreted and produced additional figures and wrote the MS.

4 Holocene sea levels in Southeast Asia, Maldives, India and Sri Lanka: The SEAMIS database

4.1 Abstract

We assembled a database of Holocene relative sea-level indicators (n=213), marine (n=213) and terrestrial (n=122) limiting points for the broader South and Southeast Asian region including the Maldives, India and Sri Lanka. The standardized review of published age-elevation information from corals, deltaic, estuarine and mangrove deposits, beachrocks and tidal notches, yielded a new suite of relative sea-level index and limiting points produced according to a standardized protocol. Expected spatial variability in Holocene relative sea-level due to glacial isostatic adjustment was accounted for, by first subdividing the study area into ten geographic sub-regions from the Central Indian Ocean to the Western Tropical Pacific, and second by comparison of the sub-regional relative sea-level data to model predictions of glacial isostatic adjustment. Results show that some of the regionally constrained relative sea-level data are characterized by significant inconsistencies that cannot be explained by glacial isostatic adjustment. Such inconsistencies of standardized relative sea-level data becomes particularly obvious in areas around the Red River Delta in Vietnam, the Gulf of Thailand, the northwest coast of Malaysia and the Spermonde Archipelago in Indonesia. Based on a critical evaluation of the reviewed relative sea-level indicators, we discuss possible sources of local divergence and identify regions where data are currently insufficient to constrain glacial isostatic adjustment predictions. The remaining quality-controlled and consistent relative sea-level data show that glacial isostatic adjustment and syn-/post-formational influences such as tectonic uplift, subsidence and compaction were the dominant local drivers of Holocene relative sea-level change. Collectively, the results of this review suggest that Holocene sea levels in South and Southeast Asia and surrounding regions have been controlled by a variety of global and local drivers and imply that additional index points from the Java Sea in Indonesia would be valuable to better assess the spatial variability, and to calibrate geophysical models of glacial isostatic adjustment.

4.2 Introduction

Coastal areas in South and Southeast (SE) Asia are among the world´s most vulnerable in terms of flooding due to climate induced sea-level rise and the associated land and economic loss (Nicholls and Cazenave, 2010; Cazenave and Cozannet, 2013). Throughout much of Asia, socio-economic risks primarily emerge from high rates of relative sea-level (RSL) rise in coastal megacities that are largely a product of subsidence resulting from groundwater extraction (Chaussard et al., 2013). Subsidence-driven RSL rise exacerbates the climatic signal and is most problematic in rapidly developing coastal megacities where population growth and urbanization will further increase the exposure to climate-related weather extremes and sea-level rise in the future (Hanson et al., 2011).

Located far field of ice-sheets that covered vast regions in higher and middle latitudes during the Last Glacial Maximum (LGM, ~21 ka before present, BP), deglacial RSL changes within the equatorial ocean basins of SE Asia resulted from a combination of eustatic, isostatic and local factors (Sieh et al., 2008; Mann et al., 2016; Meltzner et al., 2017). In contrast to near- and intermediate-field regions such as Greenland, Northern Europe and North America (Long et al., 2006; Hijma and Cohen, 2010; Engelhart and Horton, 2012; Horton et al., 2013; Engelhart et al., 2015), the Holocene RSL record in the far field is minimally influenced by isostatic deformation of the mantle resulting from weight relief after the melting of thick LGM ice sheets (Shennan and Horton, 2002; Gehrels and Long, 2008). Rather, the melting of ice sheets in high-latitudinal regions induced a collapse of the peripheral forebulge, which had been surrounding the former ice margins, and thereby caused a redistribution of water masses away from the tropics and towards higher latitudes (i.e. ocean siphoning; Mitrovica and Peltier, 1991; Peltier, 1999).

As a result, a Holocene RSL highstand in equatorial ocean basins in SE Asia is predicted by geophysical models, unless the eustatic contribution and subsequent redistribution of water following the subsidence of the peripheral forebulge has been compensated by contemporaneous hydro-isostatic subsidence of the oceanic crust (i.e. continental levering; Lambeck et al., 2002; Mitrovica and Milne, 2002; Lambeck et al., 2010; Woodroffe et al., 2012). Noteworthy, however, hydro-isostasy and continental levering also contribute to the presence of a Holocene RSL highstand far field from ice-sheets. The interplay between these processes (i.e. ocean siphoning and hydro-isostasy/continental levering) predominantly determines glacial isostatic adjustment (GIA) patterns in equatorial ocean basins and influences Holocene RSL change in the far field accordingly. Furthermore, in regions such as South and SE Asia, the possibility of tectonically-induced, post-formational changes in the elevation of RSL indicators is often relevant, potentially adding additional uncertainty to reconstructions.

Regional sea-level databases summarizing RSL index and limiting points since the LGM provide meaningful insights to disentangle the primary driving mechanisms of RSL change and its potential environmental and societal impacts (e.g. Love et al., 2016; Yousefi et al., 2018). Accurate and precise RSL reconstructions are essential to understand variability in Earth´s rheology (Engelhart et al., 2011; Roy and Peltier, 2015), identify ice-volume equivalent melt-water contributions (Lambeck et al., 2014; Bradley et al., 2016) and to reconstruct shoreline responses to RSL changes as a valuable benchmark against which to assess modern and ancient hominin dispersals (Lambeck and Chappell, 2001; Carto et al., 2009; Armitage et al., 2011; Fontana et al., 2017; Melis et al., 2018).

In SE Asia, RSL studies summarizing some of the hitherto existing deglacial RSL data from within this region, as well as from the broader Indo-Pacific region are provided by Horton et al. (2005) for the Malay-Thai Peninsula and Woodroffe and Horton (2005). For example, Horton et al. (2005) analyzed the facies of ancient mangrove and freshwater swamps in the Great Songkhla Lakes at the southwest coast of Thailand, and compared their results to earlier RSL reconstructions from the Malay-Thai Peninsula. In this region, they identified strong spatial variability of RSL signals across the study sites culminating in a maximum mid-Holocene highstand of ~5 m above present-day mean sea level (msl) by ~ 4.9 – 4.5 ka BP. The spatial spread of Holocene RSL variability is explained by regional differences in the hydro-isostatic response of the ocean floor affecting the sea-level signal in that area. Such datasets therefore provide valuable contributions to the growing awareness of Holocene sea-level variability, and, at the same time, call for an updated, quality-controlled and standardized framework summarizing the spatial and temporal variability of Holocene RSL change for the broader SE Asian region.

In this paper, we have standardized data from terrestrial, intertidal and marine deposits into 548 RSL index and limiting points for ten regions within South and SE Asia, including the Indo – West Pacific. To produce the RSL data points along with their associated uncertainty, we followed the protocols described by International Geoscience Correlation Programme (IGCP) projects 61, 200, 495, 588, and 639 (e.g. Preuss, 1979; Van de Plassche, 1986; Gehrels and Long, 2008; Horton et al., 2009; Shennan et al., 2015). Our results represent the first standardized Holocene RSL database for broader SE Asia, Maldives, India and Sri Lanka (hereafter abbreviated to SEAMIS). The new SEAMIS dataset allows for an examination of driving mechanisms of RSL change within individual sub-regions as well as the identification of those areas where focussed efforts to produce high-quality RSL data are required.

4.3 Regional Setting

4.3.1 Geography

SE Asia is a vast geographic zone comprising countries located on the southeastern extension of continental Asia (Myanmar, Thailand, Laos, Cambodia, Vietnam, Malaysia, Singapore), the island of Borneo (comprising Brunei and parts of Indonesia and Malaysia) and the archipelagos of Indonesia and the Philippines. In the SEAMIS dataset, we have furthermore included RSL studies from the Maldives (Kench et al., 2009) and Cocos (Keeling) Islands (Woodroffe et al., 1990) in the central and eastern

Indian Ocean, southeastern India (Vaz and Banerjee, 1997; Banerjee, 2000), the Palau Islands in the western tropical Pacific (Kayanne et al., 2002) and the Huon Peninsula, Papua New Guinea (Chappell and Polach, 1991). This results in a geographical extension of the study area ranging between 20°N – 20°S latitudes and 70°E – 150°E longitudes (Figure 1).

4.3.2 Tectonics

The geographic region of this study is in many parts characterized by active tectonics, which have shaped the regional geomorphology through earth history and continue to influence the behavior of the lithosphere today (Hall and Blundell, 1996; McCaffrey, 1996; Simons et al., 2007; Hall and Spakman, 2015) and inherently affect records of Holocene RSL change. The study area comprises approximately 20 different tectonic plates and micro-plates and an accordingly high number of plate boundaries (Bird, 2003; Figure 1). If considered in terms of absolute length within the study area, the dominant structural units delineating the different plates from each other are subduction zones, followed by divergent plate boundaries and transform faults. For example, along the Sunda Megathrust, the Australian Plate is subducted beneath the Sunda and Timor plates and have thereby created a volcanic arc comprising the Indonesian islands of Sumatra, Java and Nusa Tenggara (Darman and Sidi, 2000). In the SEAMIS database, we attempt to exclude areas where tectonics are poorly constrained or represent a first-order control on RSL variability (e.g., south coast of Sumatra and Java and much of the Philippines).

4.3.3 Climate

Located between 20°N – 20°S latitudes (Figure 1), virtually all countries in the study area experience tropical to sub-tropical climates with predictable reversals in monsoon wind directions and associated changes between wet and dry seasons. As reefs and mangrove environments cover large parts of the coastal landscape of the region, RSL indicators that have been included in this database are dominated by corals (many of which surveyed as coral microatolls) and sediment from mangrove swamp deposits.

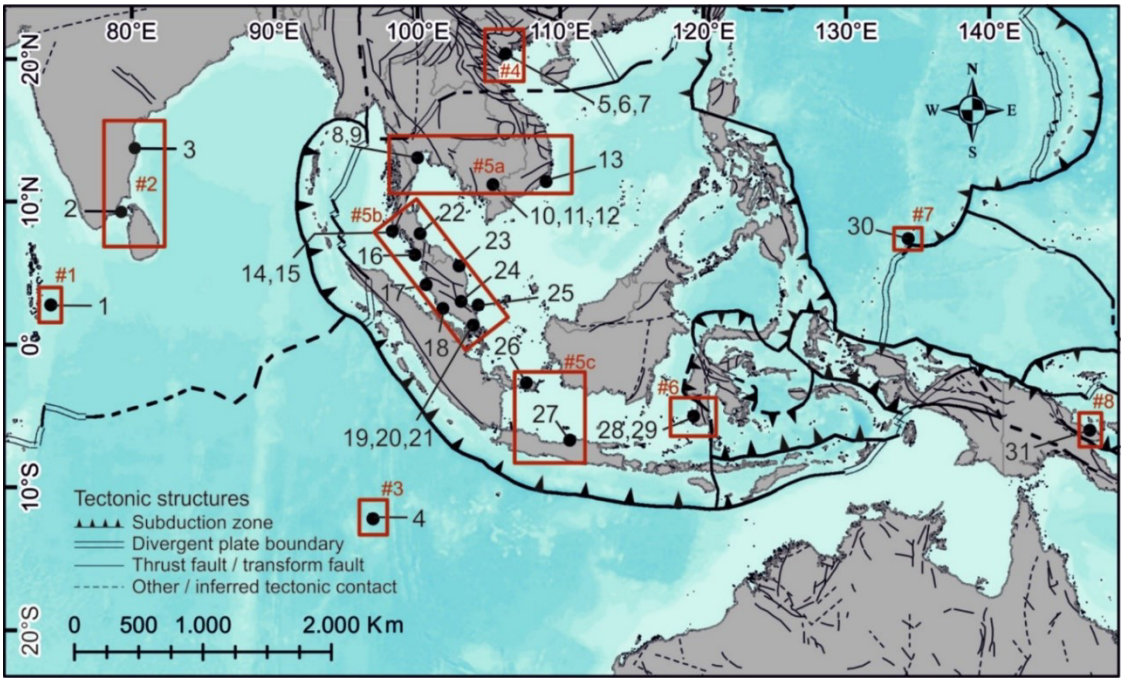

Figure 1: Overview map of the broader SE Asian region showing the study sites of published RSL reconstructions implemented in this paper. Black numbers refer to studies listed in Table 1. Red rectangles and numbered hashtags indicate the positions of geographical sub-regions. (For interpretation of the references to color in this figure legend, the reader is referred to the Web version of this article.)

4.4 Material and Methods

4.4.1 Studies reviewed and types of sea-level indicators

Sea-level changes in SE Asia have been studied since the 1970s (e.g. Tjia et al., 1972). Most RSL indicators that have been analyzed are of biological origin such as coral reefs and microatolls (e.g. Chappell and Polach, 1991; Hesp et al., 1998; Kayanne et al., 2002; Mann et al., 2016; Meltzner et al., 2017), or result from the partial decay of plant material and leaf litter that accumulate in peatlands and mangrove swamps (Geyh et al., 1979; Horton et al., 2005). Other RSL indicators are preserved within beach deposits (Stattegger et al., 2013) and deltas (Hori et al., 2004; Tamura et al., 2009), or reconstructed from geomorphic characteristics such as tidal notches (Scheffers et al., 2012). Table 1 summarizes all studies from which data have been incorporated to the SEAMIS database and gives the locations of the respective study sites.

4.4.2 Compilation of the dataset

The criteria to compile a standardized dataset of sea-level index and limiting points has been primarily described and formalized during the International Geological Correlation Program (IGCP) Project 61 (Bloom, 1977; van de Plassche, 1982) and was subsequently refined in the follow-up IGCP projects 200, 274, 367, 437, 495 and 588 (Van de Plassche, 1986; Pirazzoli and Pluet, 1991; Shennan, 1992; Murray-Wallace and Scott, 1999; Hopley and Gehrels, 2007; Gehrels and Long, 2008; Switzer et al., 2012). Most of these earlier works have been recently summarized by Shennan et al. (2015), stating that four fundamental criteria need to be reported for any index point:

(1) elevation measurements need to be undertaken using high-precision topographic survey techniques where the obtained results can be benchmarked to a tidal datum;

(2) for every sea-level index point, the Indicative Meaning (IM), comprising the Indicative Range (IR) and the Reference Water Level (RWL), need to be calculated. IR represents the elevation range occupied by a sea-level index point relative to contemporary tidal datums. The RWL is the midpoint of the IR. Accordingly, the smaller the IR of a certain sea-level index point, the lower its vertical uncertainty in the final RSL reconstruction;

(3) the age of a sea-level index point must be obtained using radiometric dating techniques and eventually (in the case of ^{14}C) calibrated to take into account the variation of radiocarbon activity in the ocean and atmosphere over time;

(4) the location of a sea-level index point must be determined relative to national or international conventions.

These data must also be reported in a standardized way (Hijma et al., 2015).

4.4.3 Reconstructions of sea-level positions

In order to standardize the RSL positions obtained from literature and apply the aforementioned criteria, we have critically reviewed published RSL evidence and allocated each RSL indicator with an IR and a RWL (Table 2).

Table 1: Summary of reviewed RSL studies and respective locations within SE Asia.

Map reference	Literature reference	Geographic subregion (map reference #)	Latitude[a]	Longitude[a]
1	Kench et al. 2009	Central Indian Ocean (#1)	5.19	73.00
2	Banerjee 2000	Southeastern India (#2)	9.29	79.22
3	Vaz and Banerjee 1997	Southeastern India (#2)	13.75	80.21
4	Woodroffe et al.1990	Eastern Indian Ocean (#3)	-11.83	96.82
5	Hori et al. 2004	Red River Delta (#4)	20.68	105.90
6	Tanabe et al. 2003a	Red River Delta (#4)	20.37	106.15
7	Tanabe et al. 2003b	Red River Delta (#4)	20.63	105.99
8	Somboon and Thiramongkol 1992	Gulf of Thailand (#5a)	14.34	100.96
9	Somboon 1988	Gulf of Thailand (#5a)	13.50	100.50
10	Tamura et al. 2007	South China Sea (#5a)	11.48	105.12
11	Tamura et al. 2009	South China Sea (#5a)	11.19	105.28
12	Hanebuth et al. 2012	South China Sea (#5a)	10.75	105.71
13	Stattegger et al. 2013	South China Sea (#5a)	11.40	109.00
14	Scheffers et al. 2012	Malay-Thai-Peninsula (#5b)	7.92	98.24
15	Scoffin and Le Tissier 1998	Malay-Thai-Peninsula (#5b)	7.75	98.42
16	Tjia et al. 1972	Malay-Thai-Peninsula (#5b)	6.28	99.82
17	Tjia and Fuji 1992	Malay-Thai-Peninsula (#5b)	4.18	100.60
18	Geyh et al. 1979	Malay-Thai-Peninsula (#5b)	2.52	101.77
19	Hesp et al. 1998	Malay-Thai-Peninsula (#5b)	1.33	103.75
20	Bird et al. 2007	Malay-Thai-Peninsula (#5b)	1.34	103.89
21	Bird et al. 2010	Malay-Thai-Peninsula (#5b)	1.31	103.89
22	Horton et al. 2005	Malay-Thai-Peninsula (#5b)	7.75	100.17
23	Parham et al. 2014	Malay-Thai-Peninsula (#5b)	5.49	102.89
24	Kamaludin 2001	Malay-Thai-Peninsula (#5b)	3.00	103.25
25	Tjia et al. 1983	Malay-Thai-Peninsula (#5b)	2.75	104.25
26	Meltzner et al. 2017	Java Sea (#5c)	-3.23	108.08
27	Azmy et al. 2010	Java Sea (#5c)	-7.61	110.71
28	Mann et al. 2016	Strait of Makassar (#6)	-5.04	119.33
29	De Klerk 1982	Strait of Makassar (#6)	-5.59	119.49
30	Kayanne et al. 2002	Western Tropical Pacific (#7)	7.37	134.38
31	Chappell and Polach 1991	Huon Peninsula (#8)	-6.00	147.05

[a] Decimal degrees

Table 2: Derivation of the indicative meanings for different indicator types implemented in this paper to calculate RSL positions for the SEAMIS database. Highest astronomical tide (HAT), mean tide level (MTL), mean higher high water (MHHW), mean lower low water (MLLW) and lowest astronomical tide (LAT).

Sample type	Evidence	Reference Water Level	Indicative Range
Index points			
Mangrove swamp	Sedimentological information and plant macrofossils referring to a general marsh environment (Hesp et al., 1998; Bird et al., 2007). Foraminiferal, diatom and pollen assemblages dominated by swamp taxa (Kamaludin, 2001; Engelhart et al., 2007; Horton et al., 2007; Tam et al., 2018).	(HAT to MTL)/2	HAT to MTL
Mangrove upper swamp	Sedimentological information and plant macrofossils referring to a high swamp environment (Horton et al., 2005; Tam et al., 2018).	(HAT to MHHW)/2	HAT to MHHW
Tidal beach	Clayey fine sand with silt beds, fining or coarsening upward, few organic spots, few foraminifers and shell fragments (Hanebuth et al., 2012).	(HAT to MHHW)/2	HAT to MHHW
Intertidal beachrock	Inter-granular aragonitic or high-magnesium calcite cements and sedimentary architecture characterized by seaward-dipping parallel lamination (Michelli, 2008; Stattegger et al., 2013; Mauz et al., 2015).	(HAT to MLLW)/2	HAT to MLLW
Intertidal mudflat	Sedimentary facies consisting of laminated sand with mud drapes and low-angle bi-directional cross-lamination (Tamura et al., 2009).	(HAT to LAT)/2	HAT to LAT
Microatoll (Individual, not ponded)	Discoid-shaped reef-flat corals with flat 'dead' upper surface and 'living' polyps around the perimeter (Scoffin and Stoddart, 1978; Smithers and Woodroffe, 2000).	(MLW to LAT)/2	MLW to LAT
Microatoll (Individual, ponded)	Microatolls for which ponding cannot be excluded (Scoffin and Stoddart, 1978).	(MHWN to LAT)/2	MHWN to LAT
Microatoll (Highest level of survival)	Diedowns identified from slabbed and x-rayed specimens (Meltzner and Woodroffe, 2015; Meltzner et al., 2017).	(MLLW to LAT)/2	MLLW to LAT
Oyster belts	In situ belts of the oyster Saccostrea cucullata (Scheffers et al., 2012; Rovere et al., 2015).	(HAT to LAT)/2	HAT to LAT
Marine limiting	Subtidal beachrock. Inter-granular, aragonitic or high-magnesium calcite cements and trough-cross stratification (Stattegger et al., 2013; Mauz et al., 2015). In situ corals. Reef and fore-reef corals identified up to genus level in cores or in outcrops (Yokoyama and Esat, 2015). Marine shells without species description and microfossil assemblages. Found in sandy and silty sediments typical of mudflat, lagoonal, upper shoreface, prodelta or marine environments, or attached to hard substrates (Tamura et al., 2009). In situ corals. Considered marine limiting if no microatoll structure is clearly described.	LAT	Below LAT
Terrestrial limiting	Backshore deposits. Landward-dipping parallel sediment lamination and beach ridges (Michelli, 2008; Stattegger et al., 2013). Limnological sediments. Plant macrofossils and microfossil assemblages typical for freshwater environments (Hesp et al., 1998; Hori et al., 2004; Tamura et al., 2009).	HAT	Above HAT

If the IR for a given RSL indicator falls within the tidal range, then it is considered a RSL index point. RSL index points constrain the elevation of RSL positions at a given time most precisely as these provide upper and lower limits (Van de Plassche, 1986; Shennan and Horton, 2002; Engelhart et al., 2015; Shennan et al., 2015). For example, mangrove swamp deposits interpreted from sedimentological information, micro- and macrofossils and pollen assemblages (e.g. Horton et al., 2005; Bird et al., 2007; Engelhart, 2007) have been given an IR between Highest Astronomical Tide (HAT) and Mean Tide Level (MTL). Furthermore, if the information provided in the literature (i.e., text, figures and profiles) was sufficient to allocate the dated facies to an upper mangrove swamp environment, the IR is therefore better constrained to HAT to Mean Higher High Water (MHHW).

On the other hand, RSL positions that could not be allocated to a tidal datum but rather have formed with certainty below Lowest Astronomical Tide (LAT) or above HAT, have been considered as marine and terrestrial limiting points (Shennan and Horton, 2002). Such data indicate that at the time of formation, RSL has been respectively above or below the elevation of the respective indicators. This category includes, for example, deposits that have formed as part of the supratidal beach or in a freshwater environment (terrestrial limiting), or are derived from in situ corals and marine shells (marine limiting).

In the database, we treated microatolls in different ways. Microatolls comprise a relatively flat annular morphology, usually with living coral polyps around their rims and dead upper surfaces (Scoffin and Stoddart, 1978; Smithers and Woodroffe, 2000; Meltzner and Woodroffe, 2015; Meltzner et al., 2017). These type of intertidal reef-flat corals have often been used to reconstruct RSL histories in tropical areas (e.g. Kench et al., 2009; Woodroffe et al., 2012; Mann et al., 2016) as the elevation of their dead top surface approximates a tidal datum that falls between Mean Low Water Springs (MLWS) and Mean Low Water Neaps (MLWN) in semidiurnal tidal systems. In order to determine the RWLs for microatolls that have been growing in an open reef-flat environment (i.e. that were not ponded during their lives) with the OSU Tidal Prediction Software (see 4.4.2 (2)), we used the range between LAT and Mean Low Water (MLW) as nearly equivalent substitutes for MLWS and MLWN (Table 2). If instead fossil microatolls have been subject to ponding during their lifetime, their indicative range is larger and RWL would fall between LAT and Mean High Water Neaps (MHWN) (Scoffin and Stoddart, 1978). In the SEAMIS database, all microatolls were interpreted as non-ponded due to the descriptions in the reviewed works.

Recent studies demonstrated that an improved resolution in the final RSL reconstructions can be achieved if die-downs within individual microatolls are used as RSL index points (Meltzner and Woodroffe, 2015; Meltzner et al., 2017). This requires the analyzed fossil microatolls to be surveyed, slabbed and x-rayed. In order to account for both, the newer (slabbing) and rather classic (surface surveying) interpretation of microatolls as RSL indicators, we have defined microatoll data as RSL index points with lower precision (RWL between LAT and MLW) if the surface of individual fossil colonies have been used to determine time-averaged RSL data. These data will provide a broader timeframe of RSL change where potential small-scale fluctuations due to dynamic oceanographic and steric factors might not be resolved. If however Holocene microatolls have been slabbed and die-downs have been identified, these have been considered as RSL index points with higher precision (RWL between LAT and MLLW) (e.g. Meltzner et al., 2017).

Due to lack of sufficient information within the original sources, some RSL data were also rejected. This was the case when (i) there was no sample location mentioned, (ii) no sample elevation given, (iii) it was not possible determine a relation between the sample elevation and msl, (iv) there was no information about which specific horizon of the respective indicator has been surveyed (eventually, in that case, RSL positions have not necessarily been rejected but were commonly “downgraded” from index to limiting points), (v) no age was given, (vi) the upper bound calibrated age was older than 12 ka BP, (vii) the radiocarbon age was too young to be calibrated, or, (viii) if the original reference was not available (see Supplementary Table 1 (4.9) for details on rejected data).

4.4.4 Age of RSL indicators

All radiocarbon age calibrations were done with the latest version of the software CALIB using the Marine13 curve for marine samples and the Intcal13 curve for terrestrial samples (Reimer et al., 2013). Marine reservoir corrections have been applied according to the closest available data in the Indian Ocean and Southeast Asia (Southon et al., 2002). If a study site was located evenly distant from two or more localities from which Delta-R values are known, the average value with average uncertainty has been used for calibration. A notable concern is the lack of a correction for isotopic fractionation for old radiocarbon dates (Törnqvist et al., 2015). This became a standard procedure in most radiocarbon laboratories by the late 1970s, but some have only applied fractionation corrections (e.g., normalized to -25% PDB) since the mid 1980s (Stuiver and Polach, 1977; Hijma et al., 2015). We performed a correction for $\delta^{13}C$ fractionation, and for these calculations a special radiocarbon table with further information about the sample age details (e.g. the lab code or whether a bulk error was added) is available in Supplementary Table 1 (4.9).

U-series ages and uncertainties (+/-) were taken from the original sources. Reviewed ages and uncertainties are placed in a related U-series table with further information about the measured thorium isotopes or the U/Th isotope combination that was used (Supplementary Table 1; 4.9).

4.4.5 Elevation of RSL indicators

RSL positions have been calculated as the height difference between the indicator elevation and RWL (Shennan and Horton, 2002) relative to local msl obtained from the OSU Tidal Prediction Software (Egbert and Erofeeva, 2002) for each geographic sub-region (see 4.4.6). The total vertical uncertainty associated with every RSL indicator includes any possible error related to the production of index and limiting points (Shennan and Horton, 2002; Vacchi et al., 2016). It comprises the IR and the error associated with calculating the sample altitude (Shennan and Horton, 2002), a sampling error (Hijma et al., 2015), a survey and benchmark uncertainty error (Törnqvist et al., 2004; Engelhart et al., 2011) and an error associated with the modeled tidal information (Vacchi et al., 2016). We also accounted for possible post-formational changes in the position of an index point by sediment compaction from coring (which would result in lower RSL positions), depending on the original position of a sample within the surrounding substrate (i.e. basal vs intercalated; Engelhart et al., 2015).

Such uncertainties, related to the depth of a dated sample in a core that has shortened due to different coring techniques, have been treated following the suggestions from Hijma et al. (2015) in cases where exact errors have not been reported in the respective papers. Additionally, if no precise sample elevation was provided, the sample thickness uncertainty has been defined as half of the sample thickness. Details on the individual vertical errors for each RSL indicator defined as index point are reported in Supplementary Table 1 (4.9). The resulting total vertical upper and lower 2-sigma uncertainty is calculated as the root sum square of each individual source of uncertainty (Shennan and Horton, 2002).

4.4.6 Subdivision into geographical sub-regions

Deglacial RSL histories are characterized by notable spatial and temporal variability, particularly with regards to the magnitudes of Holocene highstands after meltwater input decreased (e.g. Lambeck et al., 2002; Mitrovica and Milne, 2002; Lambeck et al., 2010; Woodroffe et al., 2012. For the Malay-Thai Peninsula, for example, this was demonstrated by Horton et al. (2005). In order to account for the spatial Holocene RSL variability, we have subdivided our dataset into ten regions, based on a number of criteria such as data availability, inferred tectonic activity and homogenous GIA patterns. The SEAMIS database comprises four and five individual studies respectively west and east of the Sunda Shelf, all of which have been allocated an individual sub-region in order to minimize the risk of potentially erroneous

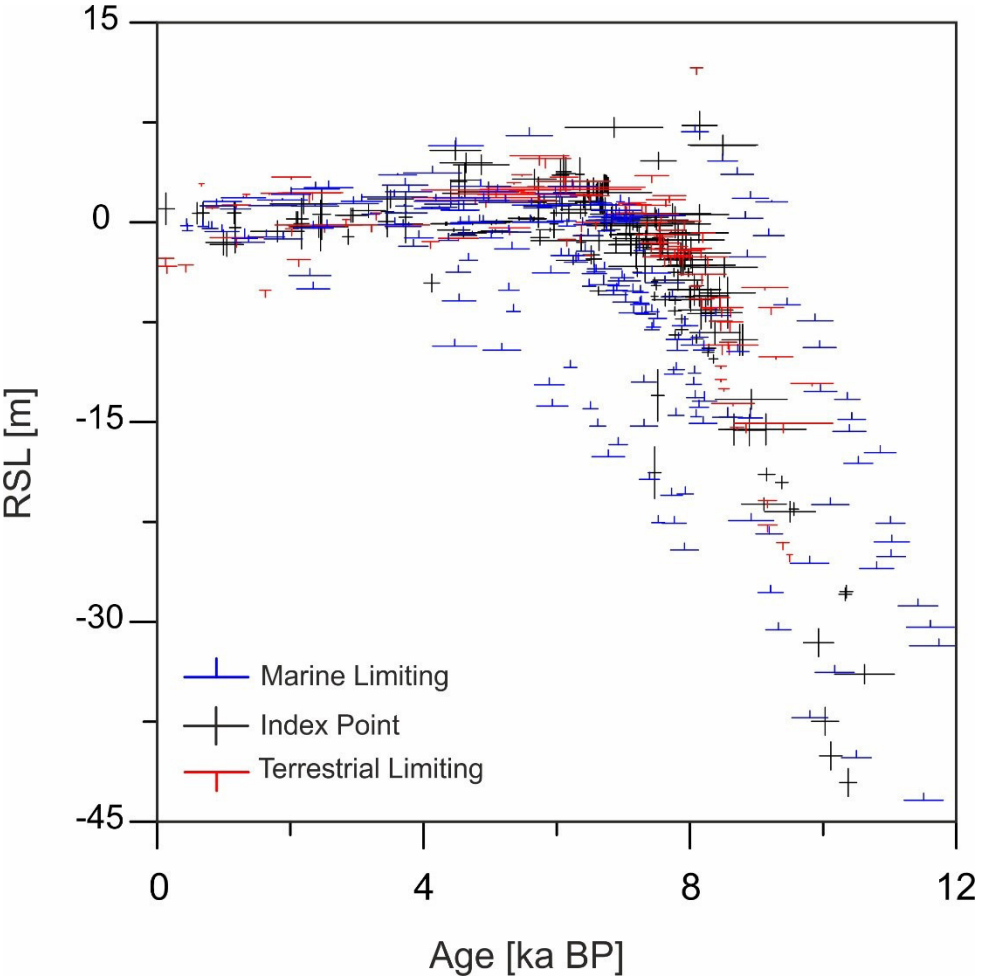

Figure 2: Age-elevation plot of standardized Holocene RSL indicators compiled in the SEAMIS database.

compilations resulting from naturally variably RSL signals due to GIA, and also to capture longitudinal variability in Holocene RSL signals, if they clearly exist.

The Sunda Shelf itself, which marks the central portion of the study area, contains the majority of RSL studies included in the present dataset. This relatively shallow platform connects the South China Sea, the Gulf of Thailand and the intervening seas between Sumatra, Java and Borneo. It is the largest shelf area within the tropics and covers an area of approximately 1.8×10^6 km^2 (Hanebuth et al., 2000). During the LGM, when the global eustatic sea-level lowstand reached a maximum value of -130 m msl (Yokoyama et al., 2018), large parts of the shelf were subaerially exposed, with late-glacial flooding initiated around 14.5 ka BP (Hanebuth et al., 2000; Hanebuth et al., 2011).

The Sunda block in the central part of the Sunda Shelf has relative tectonic stability in recent decades, with vertical crustal plate motions < 0.1 mm/yr (Tjia, 1996) and horizontal deformation rates < 0.4 mm/yr (Simons et al., 2007). It is widely assumed that the Sunda block is tectonically stable at least since the Pliocene/Pleistocene boundary (Simandjuntak and Barber, 1996; Tjia and Liew, 1996). Accordingly, RSL studies from the Sunda Shelf provide a good opportunity to constrain GIA models.

4.4.7 Glacial Isostatic Adjustment models

The primary aim of this study is to review and standardize RSL indicators in SE Asia, Maldives, India and Sri Lanka, and to assess the quality and rigor of the published datasets. For those sub-regions where

the individual study sites are distributed over a large area, we use a set of GIA model predictions to identify potentially significant differences in RSL at a given time due to GIA between the study sites within one sub-region (see section 4.6.1). Furthermore, because RSL also records tectonic uplift/subsidence, we use robust results from those localities, where RSL is reliably constrained by index and limiting points and where the presumed tectonic overprint can be approximately corrected for, to compare these against the output of GIA models (Mann et al., 2019a). This allows us to (i) discuss the relationship of robust and corrected RSL data with the predictions, (ii) evaluate potential post-formational changes in the elevations of RSL data where tectonic influences and sediment compaction rates are unknown, and (iii) validate the GIA model parameters considered here (see 4.6.2). Details on how the model runs were performed can be found in Table 1 of Mann et al. (2019a).

4.5 Results

We present our results subdivided into eight geographical regions (#1 – #8), including three sub-regions (#5a - #5c), as shown in Figure 1. Overall, we standardized 548 RSL indicators divided into 213 index points, 122 terrestrial and 213 marine limiting points. Our data spans the past 12 ka and cover RSL signals from -45 m msl to +12 m msl (Figure 2). Detailed information on the age-elevation information of each RSL indicator as well as additional evidence such as species information or other supporting evidence for the extraction of a RSL signal from each data point can be found in Supplementary Table 1.

4.5.1 Central Indian Ocean (#1)

Holocene RSL data for the central Indian Ocean originates from a study that was conducted in Hulhudhoo and Funadhoo islands, South Maalhosmadulu Atoll, Maldives by Kench et al. (2009). The dataset consists of 23 marine limiting points, obtained from three reef cores extracted from the southern Hulhudhoo reef platform, and three index points formed by in situ fossil microatolls surveyed on the reef flats of Hulhudhoo and Funadhoo (Figure 3a). Early Holocene reefs in the central Indian Ocean initiated upward growth at ~8 ka BP when RSL was above -14 m below msl. Marine limiting points indicate a continuous rise in RSL until it reached msl for the first time at around 4.5 ka BP. The three reviewed index points from the Maldives date between 3.5 – 2.0 ka BP and place RSL a few decimeters above msl, thus providing evidence for a mid- to late-Holocene RSL Highstand in the central Indian Ocean.

4.5.2 Southeastern India (#2)

RSL data for the eastern and southern part of the sub-continent India are provided by Vaz and Banerjee (1997) and Banerjee (2000) and consist of one index point obtained through a peat layer and 13 marine limiting points comprising corals and marine molluscs (Figure 3b). One RSL index point with an age of 8 ka BP lies ~ 4.5 m above present-day msl and it is followed by a series of marine limiting points that indicate RSL was above 1 m msl between 8 ka BP and 6 ka BP, and likely higher than 2 - 3 m msl between 6 ka BP and 4 ka BP. From 4 ka BP to present, RSL is constrained to above -4 m msl at 2 ka BP, and above -1.5 m msl since 2 ka BP.

4.5.3 Eastern Indian Ocean (#3)

The Holocene RSL history of the eastern Indian Ocean is currently limited to three index points from in situ Holocene *Porites* microatolls on the Cocos (Keeling) Islands (Woodroffe et al., 1990). The microatoll record, from which the index points have been deduced place RSL between ~0.5 – 1 m above msl at approximately 3 ka BP (Figure 3c), therefore providing evidence for a RSL highstand of similar magnitude and timing as in the Central Indian Ocean (#1).

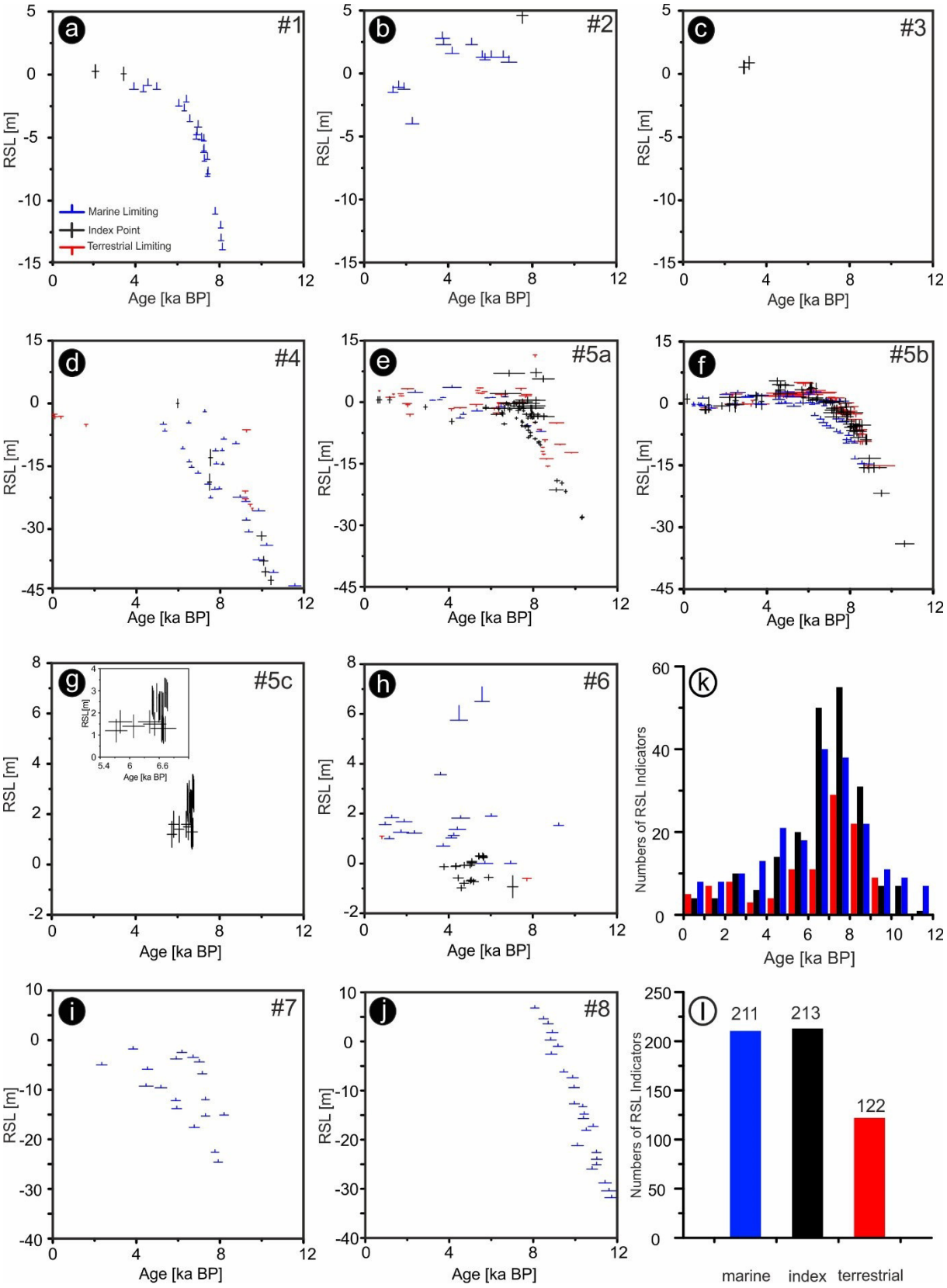

Figure 3: Holocene RSL data for all sub-regions. a) Central Indian Ocean. b) Southeastern India. c) Eastern Indian Ocean. d) Red River Delta. e) South China Sea. f) Malay-Thai-Peninsula. g) Java Sea. h) Strait of Makassar. i) Western Tropical Pacific. j) Huon Peninsula. k) Frequency distribution of index and limiting points in the SEAMIS database. L) Histogram showing the absolute numbers of different RSL indicators implemented in the SEAMIS database.

4.5.4 Red River Delta (#4)

Early Holocene RSL data from the southeastern coast of Vietnam comes from rotary drilling in the Red River Delta region and has been provided by Tanabe et al. (2003a), Tanabe et al. (2003b) and Hori et al. (2004). The entire dataset consists of 27 marine limiting points, mainly marine molluscs and shell fragments from prodelta deposits, ten terrestrial limiting points containing laminated sediment samples enriched with organic material and characterized by freshwater macro- and microfossil assemblages, and seven index points interpreted as mangrove saltmarsh deposits or intertidal mudflat accumulations (Figure 3d). There is considerable internal data inconsistency between index and limiting points. Index points, for example, put RSL at ~-40 m at around 10 ka BP reaching its modern position at approximately 6 ka BP. In contrast, marine limiting points places RSL at above ~-20 m msl at 10 ka BP rising to present-day msl by about 7 ka BP.

4.5.5 The Sunda Shelf (#5)

4.5.5.1 Gulf of Thailand/South China Sea (#5a)

The Gulf of Thailand/South China Sea region is characterized by a temporally well-distributed dataset of 15 marine and 40 terrestrial limiting points, and 67 index points throughout the Holocene (Somboon, 1988; Somboon and Thiramongkol, 1992; Tamura et al., 2007; Tamura et al., 2009; Hanebuth et al., 2012; Stattegger et al., 2013). Nevertheless, the resulting age-elevation plot of reviewed RSL data for this area appear ambiguous (Figure 3e). For example, Tamura et al. (2009) present a series of terrestrial limiting points based on massive clayey to silty deposits containing freshwater diatom assemblages and interpreted as having been deposited on a flood plain or as levee. These deposits are increasing in elevation from -15 m msl to -10 m msl between 9 – 8 ka BP (thus indicating that RSL was lower at that time). In contrast, index and marine limiting points from Somboon (1988), Somboon and Thiramongkol (1992) and Tamura et al. (2009) indicate a RSL that was substantially higher (on average -6 m msl) at that time. Allowing for some internal variability, another dataset consisting of marine limiting and index points place RSL at or slightly below modern msl between 8 – 2 ka BP Hanebuth et al. (2012). Constraining the late Holocene history from 1 ka BP, only three RSL index points from Stattegger et al. (2013) based on intertidal beachrock samples were found. They indicate a slightly higher-than-present RSL during the Late Holocene in the region.

4.5.5.2 Malay-Thai-Peninsula (#5b)

The most extensive RSL data subset comes from the central part of the Sunda Shelf, the Malay-Thai Peninsula (Figure 3f). It comprises 79 index points, 68 terrestrial limiting and 68 marine limiting points, representing the results from 12 individual studies conducted between 1972 and 2014 (Tjia et al., 1972; Geyh et al., 1979; Tjia et al., 1983; Tjia and Fujii, 1992; Hesp et al., 1998; Scoffin and Le Tissier, 1998; Kamaludin, 2001; Horton et al., 2005; Bird et al., 2007; Bird et al., 2010; Scheffers et al., 2012; Parham et al., 2014). An almost continuous series of RSL index points (flanked by limiting points) depicts a rise of RSL from -33 m msl at 10.5 ka BP (peat from mangrove swamp; Geyh et al., 1979) to approximately present-day msl at 7 ka BP (wood from mangrove saltmarsh; Bird et al., 2007). A higher-than-present RSL is recorded by the index point data between 6 ka BP and 4 ka BP, with amplitudes between 2 m msl and 5 m msl. After 4 ka BP, RSL has been falling and likely reached msl probably during the past two millennia.

4.5.5.3 Java Sea (#5c)

The Java Sea RSL record is limited to two studies, both of which used fossil microatolls as RSL indicators (Azmy et al., 2010; Meltzner et al., 2017), resulting in a total of 31 index points and 22 marine limiting points. Marine limiting points from Azmy et al. (2010) date between 7.2 ka BP and 6.9 ka BP and indicate that RSL was above ~1.5 m msl at that time, followed by a period (until 5.5 ka BP) where

RSL was at about 1.5 m msl. During a similar time period, from 6.8 ka BP to 6.4 ka BP, Meltzner et al. (2017) provide index points obtained from slabbed and x-rayed fossil microatolls, showing that RSL within that timeframe fluctuated on decimeter-scales between 1.8 m and 1.2 m above msl (Figure 3g).

4.5.6 Strait of Makassar (#6)

The Holocene RSL history of the Spermonde Archipelago, southwest Sulawesi, is limited to two studies (Kench and Mann, 2017) and contains 21 index points, 20 of which from fossil microatolls (Mann et al., 2016), 18 marine limiting points e.g. from bivalves such as *Anadara* sp., and unspecified oysters, and two terrestrial limiting points (De Klerk, 1982). A number of marine limiting points indicate that RSL was above present-day msl during the past 8 ka with a peak elevation at least 6.5 m above msl between approximately 6 – 4 ka BP (Figure 3h). Notably, these marine limiting points contrast with the mid-Holocene microatoll record from the region that reaches a maximum elevation of ~0.2 m msl between 6 – 5 ka BP (Mann et al., 2016).

4.5.7 Western Tropical Pacific (#7)

Kayanne et al. (2002) provide 18 marine limiting points from massive (*Porites* sp. and *Montipora* sp.) and branching (*Acropora* sp.) corals as well as algal crusts that give minimum elevations to the RSL history of the western tropical Pacific between 8 ka BP and 2 ka BP (Figure 3i). From this dataset, it can be deduced that RSL was above -15 m msl at 8 ka BP, reaching an elevation above -2 m msl at 6 ka BP.

4.5.8 Huon Peninsula (#8)

Chappell and Polach (1991) reconstructed one of the earliest RSL records from a coral drill core on uplifted reef terraces at the east coast of Huon Peninsula, Papua New Guinea. The reviewed dataset consists of 29 marine limiting points (Figure 3j), resulting in a continuous early Holocene RSL record between 12 ka BP and 8 ka BP. During the early phase of the record, core data indicate a RSL position above -30 m msl. Core material dated to 8 ka BP indicate a continuous rise of RSL up to a position somewhere above 8 m relative to msl.

4.6 Discussion

The SEAMIS database shows that the broader SE Asian region experienced variable RSL histories during the Holocene. Our synthesis of RSL index points reviewed and standardized for the SEAMIS database provide records that constrain the first indicators of early Holocene sea-level rise from 12 ka BP to 8 ka BP (Figure 2, Figure 3a-j). After 8 ka BP, the rate of eustatic sea-level rise slowed down from approximately 9 mm/year to about 1 mm/ year (Lambeck et al., 2014), with a further and possibly stepwise decrease until the onset of recent global sea-level rise some 150 years ago. It is likely that many of the index and limiting points that are younger than 8 ka record the effects of GIA, the predominant control on RSL change in the far-field after 9 - 8 ka BP (Milne et al., 2005; Lambeck et al., 2010; Lambeck et al., 2014). Taking into account that the effects of GIA on RSL are spatially and temporally variable (Lambeck et al., 2002; Mitrovica and Milne, 2002), it is reasonable to expect considerable variability in the RSL records from different regions within South and SE Asia.

It is particularly apparent that the timing and magnitude of RSL highstands that occurred after 9 ka BP in the far-field are affected by GIA. When the number of RSL index and limiting points is plotted against time, ~ 61% occur between 9 ka BP and 6 ka BP (Figure 3k). By looking solely at the number of index points within this time window (143 points), the percentage is even higher (67%; cf. Figure 3l). This may imply that in most of the investigated regions, within this time window RSL was higher than present, thus leaving behind RSL samples that are more easily accessible than, for example, submerged indicators. Yet RSL data from several sub-regions of the SEAMIS database clearly show the occurrence

of RSL highstands later than 6 ka BP (e.g. Woodroffe et al., 1990; Kench et al., 2009. Therefore, the prevalence of RSL data between 9 ka BP and 6 ka BP in the SEAMIS database might be a geographical artifact as the majority of RSL studies in the present database have been carried out in the Gulf of Thailand, the South China Sea and the Malay-Thai Peninsula, all regions where RSL data indicate a highstand that occurred earlier and more pronounced than on the atolls of the Indian Ocean.

There are also many instances of inconsistency between sub-regional RSL records (e.g., terrestrial limiting points lying below index or marine limiting points) in the SEAMIS database. Intrinsically contradicting results are mostly evident from the Red River Delta (#4, Figure 3d), the Gulf of Thailand/South China Sea (#5a, Figure 3e), the Malay-Thai-Peninsula (#5b, Figure 3f) and the Strait of Makassar (#6, Figure 3h). In these areas, further field studies would be required to confirm whether the reported in situ indicators are instead affected by reworking or other post-formational influences on the original elevation. In the SEAMIS database, we have attempted to exclude areas with noted tectonics of variable vertical nature. However, the study area undoubtedly comprises unmapped active fault zones and the site-specific inconsistencies between RSL data within the individual sub-regions indicate that in some locations there might be a tectonic overprint. Similarly, the results of many of the studies compiled in the SEAMIS database are based on evidence from mangrove and delta deposits, both of which are environments prone to subsidence, bioturbation and compaction during sediment sampling (Brain et al., 2012; Brain et al., 2015). Ultimately, in the sub-regions #5a and #5b, the study sites are spread over a large area and therefore, RSL data inconsistencies in single age-elevation plots for those sub-regions might also result from the spatial variability in RSL due to GIA. In the following section, we aim to resolve possible sources of discrepancies between site-specific RSL data and identify the most robust data.

4.6.1 Data inconsistency assessment

4.6.1.1 Red River Delta (#4)

RSL data from the Red River Delta derive from three studies that describe facies variations within a number of sedimentary drill cores (Tanabe et al., 2003a; Tanabe et al., 2003b; Hori et al., 2004). In some instances, interpretations of the depositional environment are based on the presence and absence of brackish-water molluscs. For example, Unit 2 (consisting of Facies 2.1 – 2.3) in core ND1 of Tanabe et al. (2003a) is interpreted as having completely been deposited in a brackish-marine environment based on the occurrence of *P. amurensis* (Shrenck) and *Corbicula* sp. For the SEAMIS database, we have carefully re-interpreted sub-sections of the individual facies as marine or terrestrial limiting. Furthermore, reworking of the dated material (shells, roots and plant fragments) cannot be excluded, and delta sediments are also prone to natural subsidence over time. These processes that cause post-depositional distortions of the sedimentary sequences have not likely been adequately taken into account in the studies from the Red River Delta. Even though we put additional uncertainty of ±0.15 m onto those samples as suggested by Hijma et al. (2015), the degree of compaction is likely different across different coring techniques and through different sediment facies. This complicates the determination of the original sample position and elevation during deposition.

4.6.1.2 Gulf of Thailand/South China Sea (#5a) and Malay-Thai-Peninsula (#5b)

In order to determine whether or not significant variations in RSL due to GIA can be expected in the sub-regions #5a and #5b, we use the output of GIA models for the past 10 ka at 2-ka increments (Figure 4). At each analyzed time step between 10 – 2 ka BP, all combinations of different model parameters considered here (see Mann et al., 2019a for details) predict a significantly lower RSL in the area around the Mekong Delta in South Vietnam (Tamura et al., 2007; Tamura et al., 2009; Hanebuth et al., 2012) than at the east coast of Vietnam (Stattegger et al., 2013) or the west coast of Thailand (Somboon, 1988; Somboon and Thiramongkol, 1992). Likewise, GIA models predict a higher RSL along the west coast of the Malay-Thai-Peninsula (Tjia et al., 1972; Geyh et al., 1979; Tjia and Fujii, 1992; Hesp et al., 1998;

Scoffin and Le Tissier, 1998; Bird et al., 2007; Bird et al., 2010; Scheffers et al., 2012) than on the east coast (Tjia et al., 1983; Kamaludin, 2001; Horton et al., 2005; Parham et al., 2014)(Parham et al. 2014). However, when the study sites are considered individually (Figure 4; Mann et al., 2019a), it becomes clear that the age-elevation information for sub-region #5a is mostly inconsistent between approximately 8 – 6 ka BP, where numerous index points plot above terrestrial limiting points. The majority of these inconsistent RSL data stem from two studies that have been conducted around the Chao Phraya Delta in Thailand (Somboon, 1988; Somboon and Thiramongkol, 1992). The interpretation of the depositional environment in these studies is based on faunal and floral assemblages without considering the opportunity of reworking based, for example, on the recognition of shell disarticulation or a comparison with the modern pollen distribution. An additional shortcoming in these studies is that no ^{14}C laboratory code is provided, which prevents us from obtaining information on how the samples have been treated before radiocarbon dating (Millard, 2014). Such imprecise descriptions result in additional uncertainties regarding both age and elevation of RSL data that cannot be quantified.

The remaining studies from the Gulf of Thailand part of sub-region #5a (Tamura et al., 2007; Tamura et al., 2009; Hanebuth et al., 2012) and those studies from sites susceptible to compaction within sub-region #5b (Geyh et al., 1979; Hesp et al., 1998; Kamaludin, 2001; Horton et al., 2005; Bird et al., 2007; Bird et al., 2010) all consider and discuss the possibilities of reworked dated material and sediment compaction. We were largely able to follow the original interpretations of intertidal index or limiting points contained in these studies. Therefore, the individual datasets themselves should be considered robust.

4.6.1.3 Strait of Makassar (#6)

In sub-region #6, the Strait of Makassar, marine limiting points from De Klerk (1982) plot considerably higher than the index points presented by Mann et al. (2016). In a discussion on the potential reasons for the inconsistent pattern, Mann et al. (2016) argue that the previous dataset might be less robust due to uncertainties in the IM of the implemented indicators and the lack of detail in the description of the survey methods. With regards to the offset between microatoll records from two islands in the Spermonde Archipelago, Mann et al. (2016) discuss the possibility of a localized subsidence. This assessment is based on the analysis of microatoll morphologies on the different study sites.

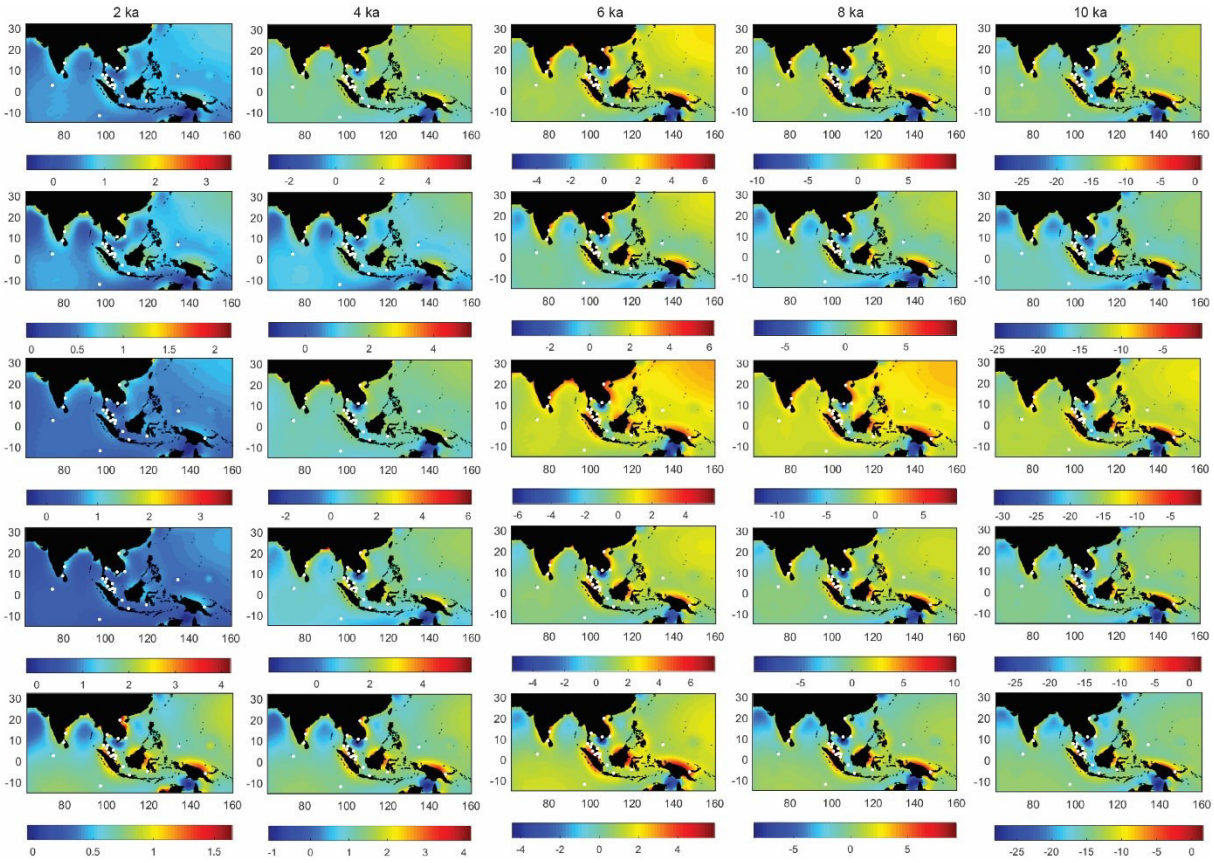

Figure 4: RSL predictions for the broader SE Asian region between 10 ka BP and 2 ka BP based on different iterations of ice and earth models. Numbers along the left and bottom map edges indicate latitudes and longitudes. Color scales below maps indicate RSL in m relative to present-day msl. Note differences for RSL in the color values for each map. Top row: ICE5g-VM2-90km. 2nd row: ICE5g-VM2-120km; 3rd row: ICE5g-VM2b-90km; 4th row: ICE5g-VM3-90km; Bottom row: ICE5g-VM4-90 km. See Mann et al. (2019a) for details of simulations. (For interpretation of the references to color in this figure legend, the reader is referred to the Web version of this article.)

4.6.2 Driving processes of RSL change in SE Asia, Maldives, India and Sri Lanka

Following the discussion about possible sources for RSL data inconsistencies in the SEAMIS database, site-specific discrepancies between Tanabe et al. (2003a), Tanabe et al. (2003b) and Hori et al. (2004) (sub-region #4), Somboon (1988) and Somboon and Thiramongkol (1992) (sub-region #5a), Tjia et al. (1972) (sub-region #5b) and De Klerk (1982) and Mann et al. (2016) (sub-region #6) must be resolved with additional high-accuracy RSL data before the existing datasets can be used to decipher regional driving processes of Holocene RSL change within SE Asia. The remaining data indicate reliable RSL curves that allow assessment of driving processes of Holocene RSL change for the different sub-regions in the SEAMIS database. Moreover, the comparison between quality-controlled and tectonically corrected RSL data can potentially be used to validate model output for the suite of parameters considered here (Mann et al., 2019a).

In the Central Indian Ocean, the Western Tropical Pacific, and the Huon Peninsula, the elevation of the Pleistocene unconformity underlying the Holocene reefs (Kench et al., 2009; Kayanne et al., 2002) or the last interglacial barrier reef (Chappell and Polach, 1991) is commonly known. These elevations are -14.12 m msl (Central Indian Ocean; Kench et al., 2009), -15.70 m msl (Western Tropical Pacific; Kayanne et al., 2002) and +226 m msl (Huon Peninsula; Chappell and Polach, 1991). Taking into account the timing (116 – 129 ka BP) and most recent constraints on the position of global mean sea level (6 – 9 m msl) during the Last Interglacial (Dutton and Lambeck, 2012; Dutton et al., 2015), it is

possible approximate subsidence and uplift rates, and replot these three RSL records corrected accordingly (Mann et al., 2019a). We remark that this is a simplified assessment, not taking into account possible perturbations to the elevation of the Last Interglacial sea level caused by GIA or mantle dynamic topography (Austermann et al., 2017)

After tectonic correction, it is instructive to see that Holocene reefs in all three study sites plot considerably lower than the GIA predictions used here. In the Central Indian Ocean, Holocene reef growth initiated some 8 ka BP when RSL (from GIA modeling) was as much as 10 m above the Pleistocene unconformity. Corals continued to grow upwards with a reconstructed mean rate of reef growth of 4.7 m/ka until sea-level rise slowed and the reef reached an intertidal environment at around 6 ka BP. The reef crest core from the Western Tropical Pacific (PL-I; Kayanne et al., 2002) similarly indicates that the Pleistocene unconformity was flooded at approximately 8 ka BP, which is comparable to the Central Indian Ocean record. Furthermore, the initiation of Holocene reef growth in the Western Tropical Pacific took place when the model-derived relative water depth accounted for 10 – 12 m and the mean reconstructed growth rate of corals between 8 – 6 ka BP was 6.1 m/ka. On Huon Peninsula, the corrected reef record spans from 12 – 8 ka BP and is characterized by an increasing rate of growth of 7.8 m/ka until 10 ka BP, and 15.6 m/ka from 10 – 8 ka BP and a decreasing vertical lag to modeled RSL from 20 m at 11 ka BP and 11 m at 8 ka BP.

Based on the estimated paleo-bathymetry of particular coralgal species assemblages associated with algal crust thickness, vermetid gastropods and benthic foraminifera, paleo-water depth ranges of distinct coral reef core sections can be reconstructed (Yokoyama and Esat, 2015). The reviewed coral descriptions from within the cores are limited to genus level, which prohibits us to constrain the paleo-water depth range of the dated facies to less than 10 – 15 meters (Hibbert et al., 2016). This uncertainty precludes a coherent estimate of whether the corrected coral reef records reveal a uniform catch-up reef response during the early and middle Holocene RSL rise (Davies and Montaggioni, 1985; Neumann and Macintyre, 1985).

A number of observations regarding the driving processes of RSL change can be made from the comparison of quality-controlled RSL indicators with the modeled RSL. First, in all study sites within the SEAMIS database, the primary driving process of RSL change is GIA. This becomes especially obvious in the results from the Central Indian Ocean (Kench et al., 2009), Southeastern India (Vaz and Banerjee, 1997), the Eastern Indian Ocean (Woodroffe et al., 1990), the Malay-Thai Peninsula Geyh et al., 1979; Hesp et al., 1998; Kamaludin, 2001) and the Java Sea (Azmy et al., 2010; Meltzner et al., 2017), where quality-controlled, tectonically corrected and intrinsically consistent Holocene RSL index points plot significantly above the eustatic sea-level curve (Mann et al., 2019a).

Second, RSL data from several studies considered in the SEAMIS database appear to be affected by syn- and post-formational sediment compaction and subsidence when compared to the modeled RSL predictions. This accounts for sites in the South China Sea (Tamura et al., 2007; Tamura et al., 2009; Hanebuth et al., 2012) and the Malay-Thai-Peninsula (Bird et al., 2007; Bird et al., 2010; see Mann et al., 2019a).

Lastly, for a few study sites, it appears that the mismatch between model output and RSL data cannot be explained by local tectonics, compaction or subsidence. For example, the Geyh et al. (1979) study indicates a RSL rise from – 22m at 9.5 ka BP to – 2m at 8 ka BP, followed by a RSL highstand at ~5 ka BP. Here, the model likely overestimates the early Holocene RSL rise and underestimates the magnitude of the highstand (see Mann et al., 2019a). The inconsistent deviations between RSL based on field evidence and modeled RSL during the early and middle Holocene suggests that for this part of the Malay-Thai Peninsula, the model output is invalid. Similarly, RSL data from microatolls in the Java Sea (Meltzner et al., 2017) show that RSL was 1.2 – 1.8 m above present between 6.8 and 6.4 ka BP. The models used here however do not predict a highstand at this time or of this magnitude (see Mann et al., 2019a). Accordingly, additional data from these sites could be helpful to better constrain mantle

viscosities for modeling sea-level change since the Last Interglacial and to better understand the Earth-Ocean-Ice system in general.

4.7 Conclusion

A solid understanding of the primary driving mechanisms of future RSL rise is one of the fundamental requirements for effective and sustainable coastal management on regional scales in South and SE Asia. In order to identify the processes that were responsible for Holocene RSL changes in that region, we have standardized 568 published data points in the SEAMIS database. The geographical range of the SEAMIS database stretches from the Maldives in the west to Papua New Guinea in the east, and from Vietnam in the north to Cocos (Keeling) Islands in the south. Our results show that the individual sub-regions experienced RSL histories of considerable variance. In particular a clear signal in RSL highstand variability has been detected between the Central Indian Ocean, Southeastern India, the Eastern Indian Ocean, the Malay-Thai-Peninsula, the Java Sea and the Strait of Makassar. However, neither latitudinal nor longitudinal patterns can be well constrained in the reviewed RSL data and therefore we assume that continental levering, which causes strong gradients of RSL perpendicular to the coast, is one dominant driver of the spatial variability in the magnitudes of the observed highstands.

We have furthermore identified several instances of inconsistency between grouped RSL records that do not arise from spatial variability of GIA. Following a detailed assessment of robustness we considered each data point based on the quality and RSL-related detail provided within the original sources. We then identify a number of datasets (i.e. some specific studies) that are likely responsible for the discrepancies observed. It should be noted however that the datasets are not invalid. These data meet, in the first place, the criteria for RSL index and limiting points and have accordingly been included in the SEAMIS database. It is conceivable that with more data this initial assessment on data inconsistency may change. However for the moment, we recommend end-users of the database put more weight on the consistent and quality-controlled data sets.

The SEAMIS RSL data reveal that besides GIA, Holocene RSL in the region has also been affected by syn- and post-formational tectonics, compaction and subsidence. This becomes particularly evident in some sites of the central and eastern Indian Ocean, the South China Sea, the Malay-Thai-Peninsula, the Western Tropical Pacific and Huon Peninsula. However, study sites in the Strait of Malacca and the Java Sea appear to be relatively unaffected by post-formational influences. Accordingly, additional high-quality RSL data, especially from the Java Sea where little data is available so far, could be useful to calibrate competing GIA models with different eustatic history, in order to better constrain earth rheology and ice-equivalent melt-water input after 9 ka BP.

4.8 Acknowledgments

This work was supported through grant SEASCHANGE (RO-5245/1-1) from the Deutsche Forschungsgemeinschaft (DFG) as part of the Special Priority Program (SPP)-1889 "Regional Sea Level Change and Society". TM, MB TL and AR are supported by the Leibniz-Centre for Tropical Marine Research (ZMT). TL, MB and AR's research was further supported by the Institutional Strategy of the University of Bremen, funded by the German Excellence Initiative [ABPZuK-03/2014]. The authors acknowledge the working groups HOLSEA - Modelling Paleo Processes (INQUA CMP project 1601P) and PALSEA (PAGES/INQUA) for useful discussions during the 2016 workshop in Mt. Hood, Oregon. This paper also contributes to IGCP639 "Sea level change: from Minutes to Millennia". We thank two anonymous reviewers and Glenn A. Milne for their thoughtful comments that helped to substantially improve a first draft of this paper. Thanks also to our Co-PIs and collaborators Hildegard Westphal, Benjamin P. Horton, Jamaluddin Jompa, Robert E. Kopp, Muhammad Lukman and Tilo Schöne.

4.9 Supplementary Material

The supplementary material can be found on the DVD attached to this Thesis or online at https://doi.org/10.1016/j.quascirev.2019.07.007.

4.10 Data availability

The SEAMIS database is available in a Mendeley data repository (https://doi.org/10.17632/wp4ctb4667.1). Updates to the database, netCDF files of ICE-5G model output and a MATLAB script to plot the data is accessible at https://github.com/Alerovere/SEAMIS.

5 Data article; Relative sea-level data from the SEAMIS database compared to ICE-5G model predictions of glacial isostatic adjustment

5.1 Abstract

The SEAMIS database (Mendeley data repository; doi:10.17632/wp4ctb4667.1) contains 548 relative sea-level indicators from 31 different study sites within the broader Southeast Asian region including the Maldives, India and Sri Lanka. Here we compare quality-controlled and site-specific relative sea-level data from the SEAMIS database to a suite of ICE-5G glacial isostatic adjustment models. The relation between robust and, if applicable, tectonically corrected relative sea-level data with the broad predictions of glacial isostatic adjustment models is interpreted and discussed in the article "Holocene sea levels in Southeast Asia, Maldives, India and Sri Lanka: The SEAMIS database" (Mann et al., 2019b) in Quaternary Science Reviews.

Specifications Table

Subject area	*Earth Sciences*
More specific subject area	*Coastal geomorphology*
Type of data	*Tables, graphs, figures, netCDF files*
How data was acquired	*Standardization of published data; modeling*
Data format	*Published RSL data: standardized and quality-controlled; netCDF files of modeled RSL: raw*
Experimental factors	*Data considered originate from previous studies carried out in Southeast Asia, Maldives, India and Sri Lanka and contain Holocene RSL information*
Experimental features	*Data were collected from literature review*
Data source location	*Southeast Asia, Maldives, India and Sri Lanka*
Data accessibility	*SEAMIS database and updates, netCDF files of ICE-5G model output and MATLAB script to plot data at https://github.com/Alerovere/SEAMIS; SEAMIS database containing RSL indicators also at https://doi. org/10.17632/wp4ctb4667.1*

Value of the data

- Data are useful to calibrate earth- and ice-models in glacial isostatic adjustment simulations
- Data is beneficial for modelers of glacial isostatic adjustment processes and field geologists in Southeast Asia
- Data can be easily updated by other researchers and compared to other models of glacial isostatic adjustment
- Data allow an evaluation of potential post-formational changes in the elevations of relative sea-level markers
- Data allow a validation of model parameters

5.2 Data

The SEAMIS database currently (as of May) comprises 548 Holocene relative sea-level indicators for Southeast Asia and surrounding regions (Mann et al., 2019b). Age-elevation information of published relative sea-level data have been transformed into comparable relative sea-level indicators using a standardized protocol (Shennan et al., 2015). Site-specific relative sea-level indicators are here

compared to modeled relative sea-level change at each site generated with the ICE-5G geophysical model (Peltier, 2004).

Table 3: Details on the Earth model parameters and different mantle viscosity profiles employed to simulate glacial isostatic adjustment in combination with the Ice model ICE-5G in the areas of interest. Model short names refer to the different model curves on Figure 5–Figure 26.

Model short name	Ice model	Earth model parameters
ice5g-vm2-90km.nc	ICE-5G	Upper Mantle = 0.25×10^{21} Pa•s Transition Zone = 0.5×10^{21} Pa•s Lower Mantle = 5×10^{21} Pa•s Lithosphere Thickness = 90 km
ice5g-vm2b-90km.nc	ICE-5G	Upper Mantle = 0.25×10^{21} Pa•s Transition Zone = 0.25×10^{21} Pa•s Lower Mantle = 5×10^{21} Pa•s Lithosphere Thickness = 90 km
ice5g-vm2-120km.nc	ICE-5G	Upper Mantle = 0.25×10^{21} Pa•s Transition Zone = 0.5×10^{21} Pa•s Lower Mantle = 5×10^{21} Pa•s Lithosphere Thickness = 120 km
ice5g-vm3-90km.nc	ICE-5G	Upper Mantle = 0.25×10^{21} Pa•s Transition Zone = 0.5×10^{21} Pa•s Lower Mantle = 10×10^{21} Pa•s Lithosphere Thickness = 90 km
ice5g-vm4-90km.nc	ICE-5G	Upper Mantle = 0.25×10^{21} Pa•s Transition Zone = 0.5×10^{21} Pa•s Lower Mantle = 100×10^{21} Pa•s Lithosphere Thickness = 90 km

The present dataset comprises a collection of RSL data from 23 studies that have been conducted in 22 locations. Figure 5–Figure 26 present site-specific, standardized, quality-controlled and, if possible (see Ref. Mann et al., 2019b), tectonically corrected age-elevation information of relative sea-level indicators together with the modeled relative sea level.

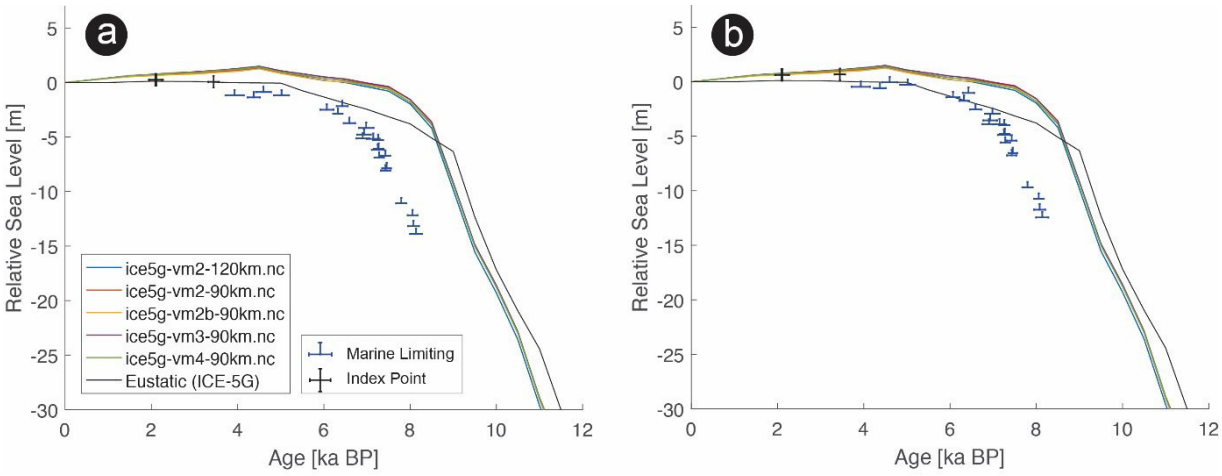

Figure 5: Standardized Holocene relative sea-level data obtained from Kench et al. (2009) in comparison to glacial isostatic adjustment geophysical model predictions for South Maalhosmadulu Atoll, Maldives. a) Original sample elevations are shown. b) Data corrected for subsidence based on a number of constraints regarding the timing and elevation of Last interglacial sea level and the magnitude of karstification resulting from subaerial exposure of the Last interglacial reef carbonate during the glacial (see Mann et al., 2019b and above).

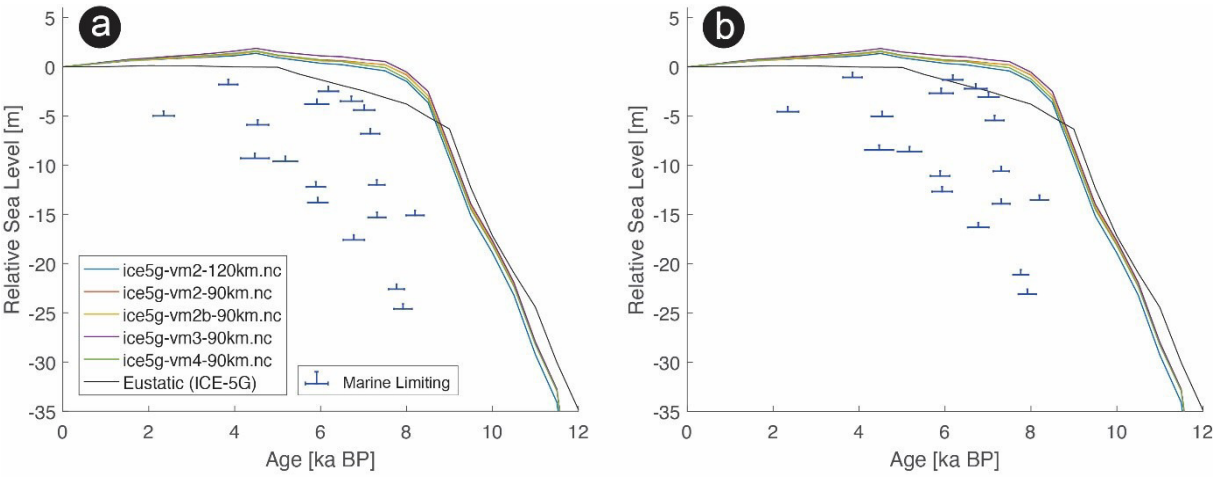

Figure 6: Standardized Holocene relative sea-level data obtained from Kayanne et al. (2002) in comparison to glacial isostatic adjustment geophysical model predictions for Palau Islands in the western Pacific. a) Original sample elevations are shown. b) Data corrected for subsidence based on a number of constraints regarding the timing and elevation of Last interglacial sea level and the magnitude of karstification resulting from subaerial exposure of the Last interglacial reef carbonate during the glacial (see Mann et al., 2019b and above).

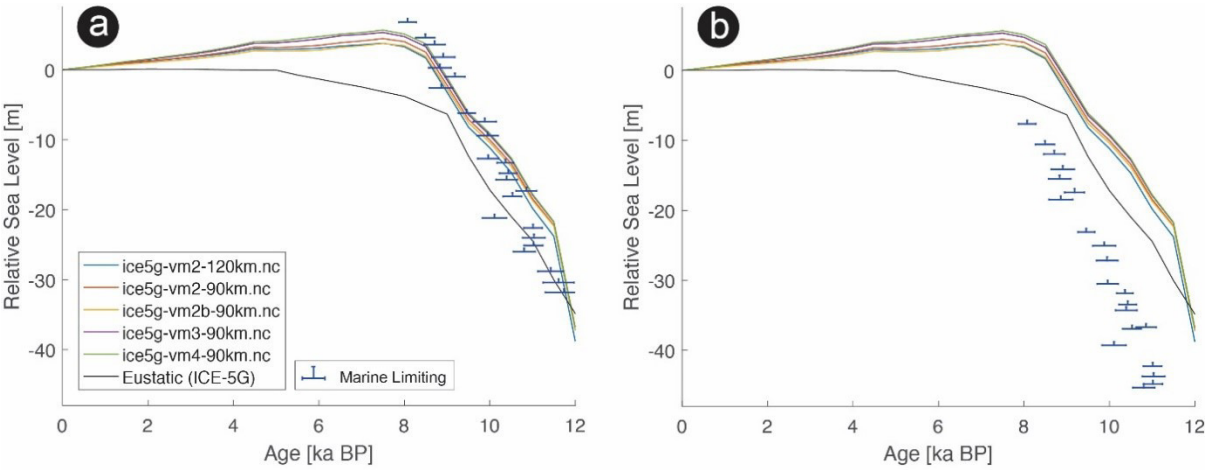

Figure 7: Standardized Holocene relative sea-level data obtained from Chappell and Polach (1991) in comparison to glacial isostatic adjustment geophysical model predictions for Huon Peninsula, Papua New Guinea. a) Original sample elevations are shown. b) Data corrected for tectonic uplift based on a number of constraints regarding the timing and elevation of Last interglacial sea level and the magnitude of karstification resulting from subaerial exposure of the Last interglacial reef carbonate during the glacial (see Mann et al., 2019b and above).

5.3 Experimental design, materials and methods

5.3.1 Relative sea-level data

The methods that have been applied to compile a standardized dataset of sea-level index and limiting points meet the criteria recently summarized by Shennan et al. (2015). In those sites where the elevation of the Pleistocene unconformity relative to the analyzed sequence of Holocene relative sea-level data is known (i.e., Kench et al., 2009; Kayanne et al., 2002; Chappell and Polach, 1991), the tectonic overprint resulting from active uplift or long-term subsidence has been calculated. First, the average uplift/subsidence rate U has been calculated at each site. In doing so, minimum and maximum rates have

been determined by dividing the minimum/maximum vertical displacements (based on the actual position of the Pleistocene Reef and a Last Interglacial sea level between 6 and 9 m above present) by the minimum/maximum time elapsed (based on a Last Interglacial between 116 ka BP and 129 ka BP). The average rate U is the sum of the minimum and maximum rates divided by 2 (negative rate for uplift, positive rate for subsidence). Calculated rates U are 0.18 m/ka for South Maalhosmadulu Atoll, Maldives (Kench et al., 2009), 0.19 m/ka for Palau Islands in the western Pacific (Kayanne et al., 2002) and -1.79 m/ka for Huon Peninsula, Papua New Guinea (Chappell and Polach, 1991). The corrected relative sea-level position at each site is then calculated as H + U × tc (following Chappell and Polach, 1991) where H is the actual sample elevation and tc the radiocarbon age of the sample. Details on the reconstructions of site-specific relative sea-level positions can be found in Mann et al. (2019b).

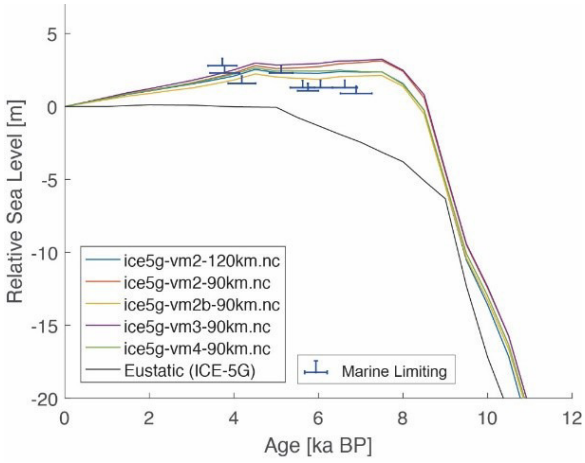

Figure 8: Standardized Holocene relative sea-level data obtained from Banerjee (2000) in comparison to glacial isostatic adjustment geophysical model predictions for the section between Cape Comorin and Rameswaram in Southeastern India.

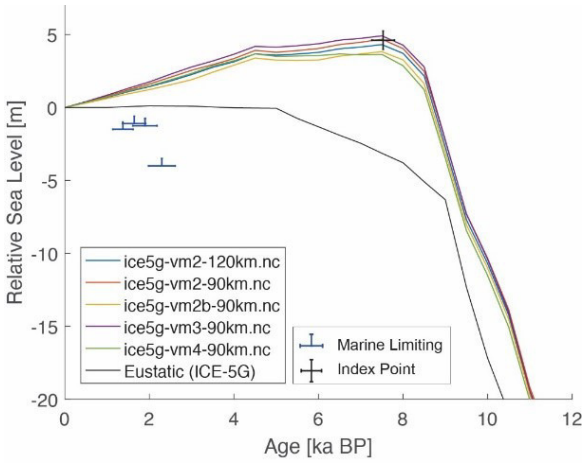

Figure 9: Standardized Holocene relative sea-level data obtained from Vaz and Banerjee (1997) in comparison to glacial isostatic adjustment geophysical model predictions for the Pulicat Lagoon in Southeastern India.

5. Data article; Relative sea-level data from the SEAMIS database compared to ICE-5G model predictions of glacial isostatic adjustment

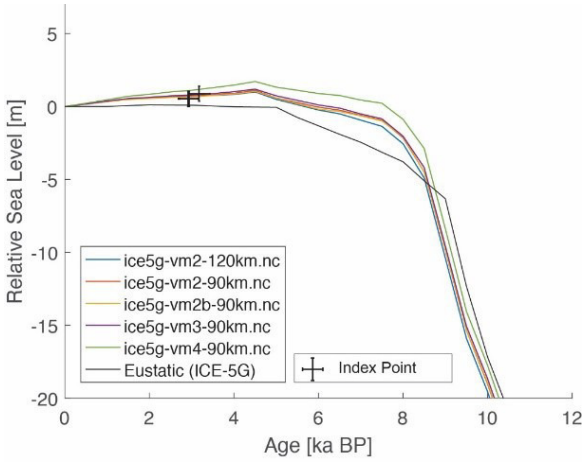

Figure 10: Standardized Holocene relative sea-level data obtained from Woodroffe et al. (1990) in comparison to glacial isostatic adjustment geophysical model predictions for the Cocos (Keeling) Islands in the eastern Indian Ocean.

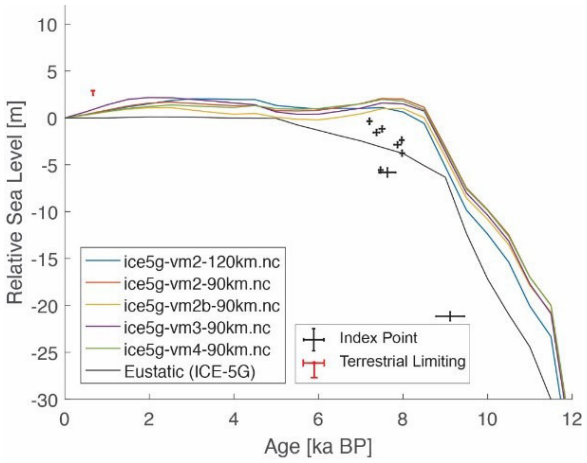

Figure 11: Standardized Holocene relative sea-level data obtained from Tamura et al. (2007) in comparison to glacial isostatic adjustment geophysical model predictions for the Mekong River lowland near Phnom Penh, Cambodia.

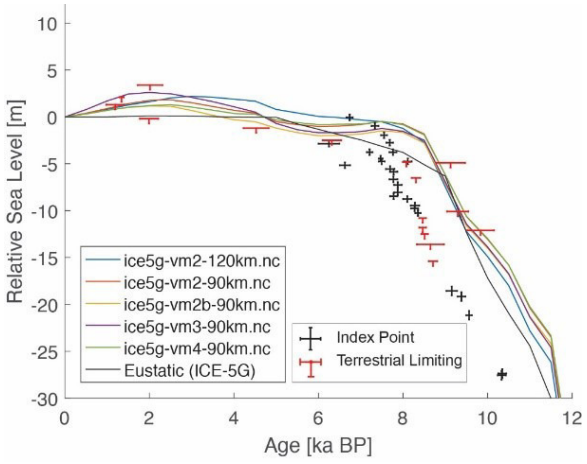

Figure 12: Standardized Holocene relative sea-level data obtained from Tamura et al. (2009) in comparison to glacial isostatic adjustment geophysical model predictions for the Mekong River lowland near Phnom Penh, Cambodia.

5. Data article; Relative sea-level data from the SEAMIS database compared to ICE-5G model predictions of glacial isostatic adjustment

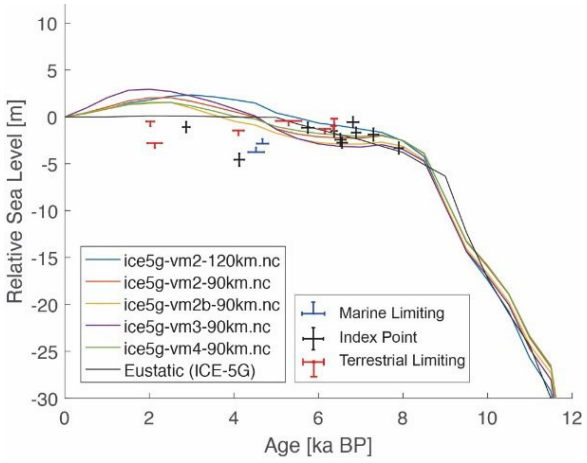

Figure 13: Standardized Holocene relative sea-level data obtained from Hanebuth et al. (2012) in comparison to glacial isostatic adjustment geophysical model predictions for the northeastern Mekong River Delta, Vietnam.

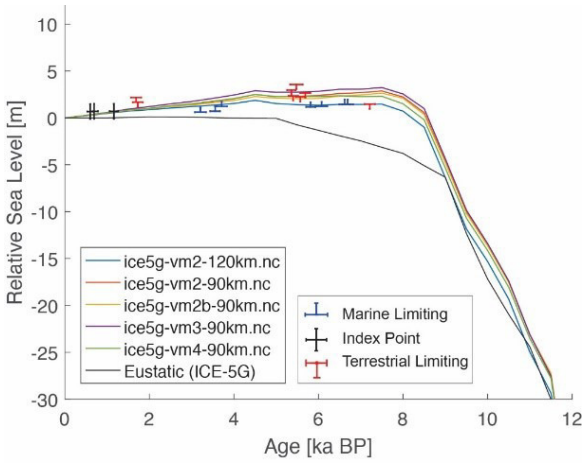

Figure 14: Standardized Holocene relative sea-level data obtained from Stattegger et al. (2013) in comparison to glacial isostatic adjustment geophysical model predictions for the section between Cà Ná and Son Hài in southeast Vietnam.

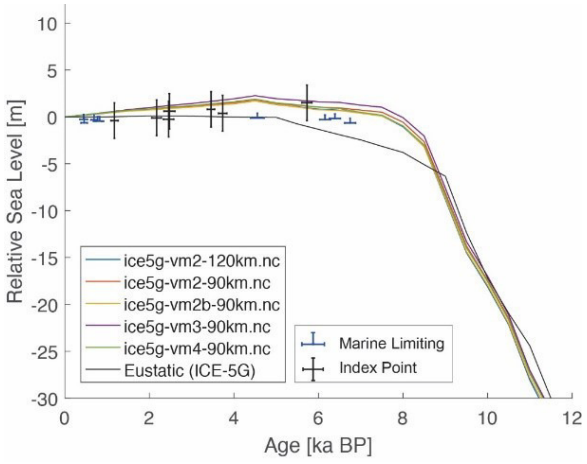

Figure 15: Standardized Holocene relative sea-level data obtained from Scheffers et al. (2012) in comparison to glacial isostatic adjustment geophysical model predictions for the Phang-nga Province, Thailand.

5. Data article; Relative sea-level data from the SEAMIS database compared to ICE-5G model predictions of glacial isostatic adjustment

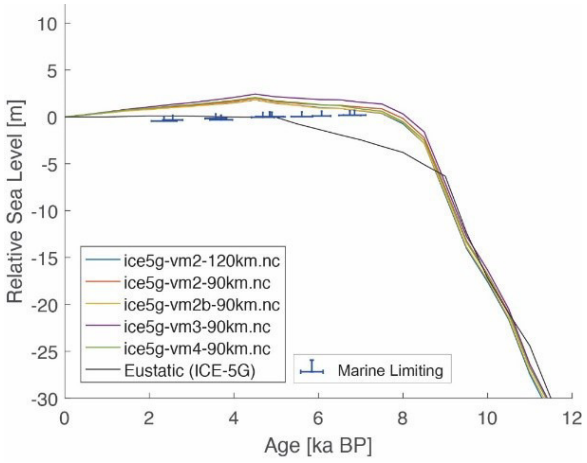

Figure 16: Standardized Holocene relative sea-level data obtained from Scoffin and Le Tissier (1998) in comparison to glacial isostatic adjustment geophysical model predictions for Phuket, South Thailand.

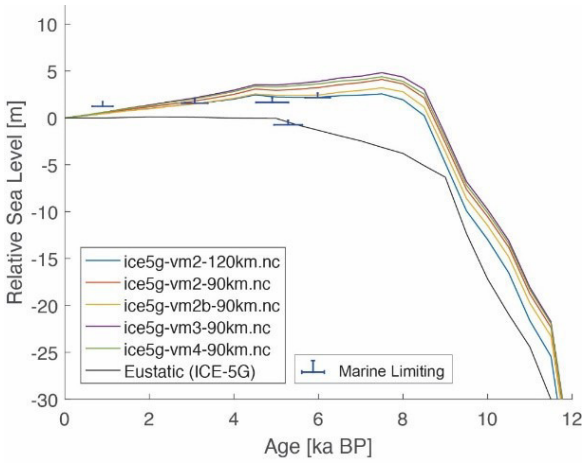

Figure 17: Standardized Holocene relative sea-level data obtained from Tjia and Fujii (1992) in comparison to glacial isostatic adjustment geophysical model predictions for the section between Langkawi and Terengganu-Pahang at the west coast of Peninsular Malaysia.

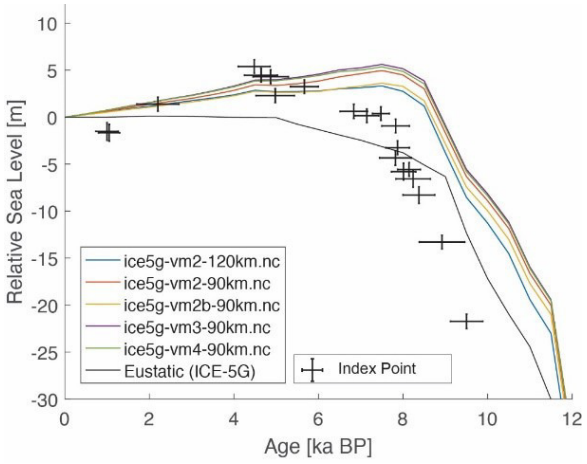

Figure 18: Standardized Holocene relative sea-level data obtained from Geyh et al. (1979) in comparison to glacial isostatic adjustment geophysical model predictions for the section between Port Dickinson, Malaysia and Singapore.

5. Data article; Relative sea-level data from the SEAMIS database compared to ICE-5G model predictions of glacial isostatic adjustment

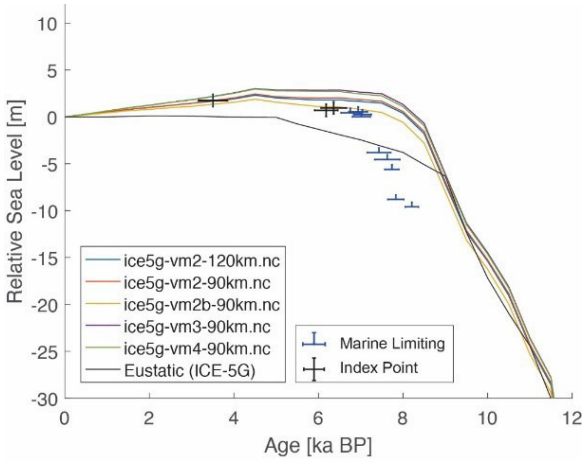

Figure 19: Standardized Holocene relative sea-level data obtained from Hesp et al. (1998) in comparison to glacial isostatic adjustment geophysical model predictions for the Sungei Nipah catchment, Singapore.

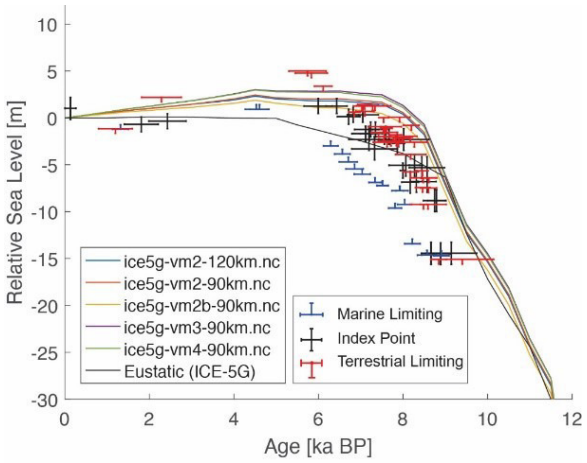

Figure 20: Standardized Holocene relative sea-level data obtained from Bird et al. (2007) and Bird et al. (2010) in comparison to glacial isostatic adjustment geophysical model predictions for the Geylang district, Singapore.

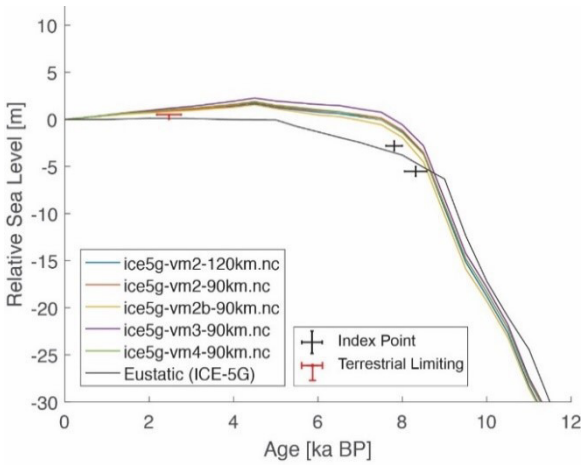

Figure 21: Standardized Holocene relative sea-level data obtained from Horton et al. (2005) in comparison to glacial isostatic adjustment geophysical model predictions for the Great Songkhla Lakes, Malay-Thai Peninsula.

5. Data article; Relative sea-level data from the SEAMIS database compared to ICE-5G model predictions of glacial isostatic adjustment

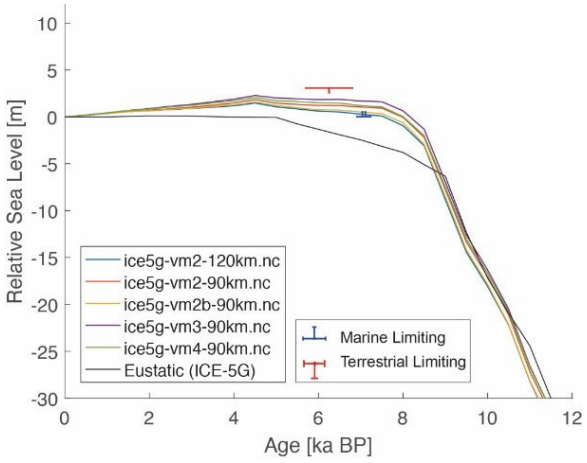

Figure 22: Standardized Holocene relative sea-level data obtained from Parham et al. (2014) in comparison to glacial isostatic adjustment geophysical model predictions for the area near Merang, Malaysia.

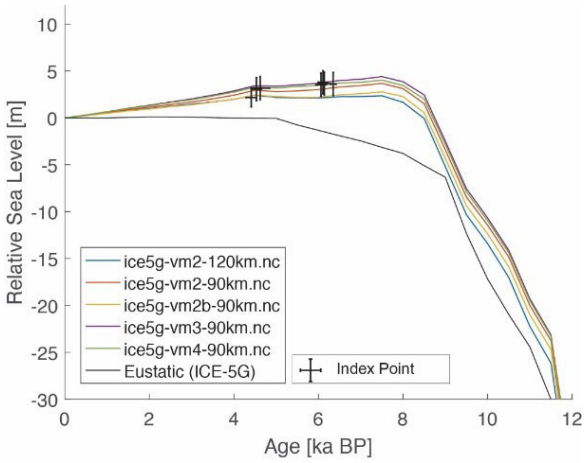

Figure 23: Standardized Holocene relative sea-level data obtained from Kamaludin (2001) in comparison to glacial isostatic adjustment geophysical model predictions for Kelang and Kuantan, Peninsular Malaysia.

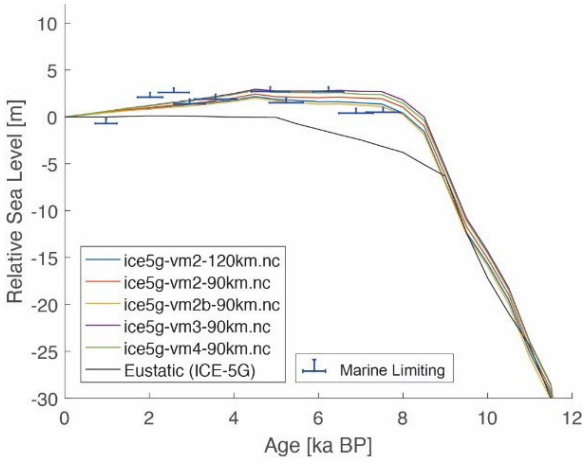

Figure 24: Standardized Holocene relative sea-level data obtained from Tjia et al. (1983) in comparison to glacial isostatic adjustment geophysical model predictions for Tioman Island, Malaysia.

5. Data article; Relative sea-level data from the SEAMIS database compared to ICE-5G model predictions of glacial isostatic adjustment

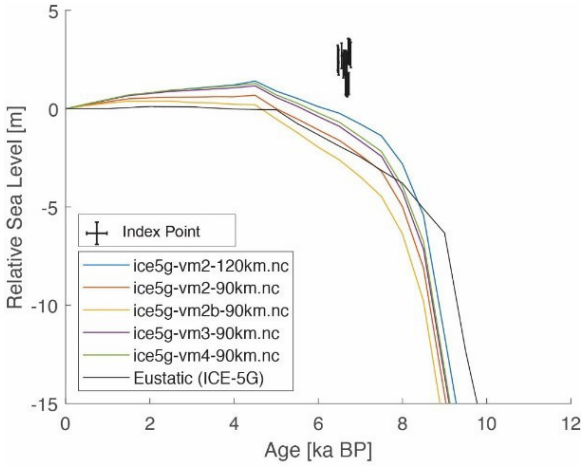

Figure 25: Standardized Holocene relative sea-level data obtained from Meltzner et al. (2017) in comparison to glacial isostatic adjustment geophysical model predictions for the Belitung area, Indonesia.

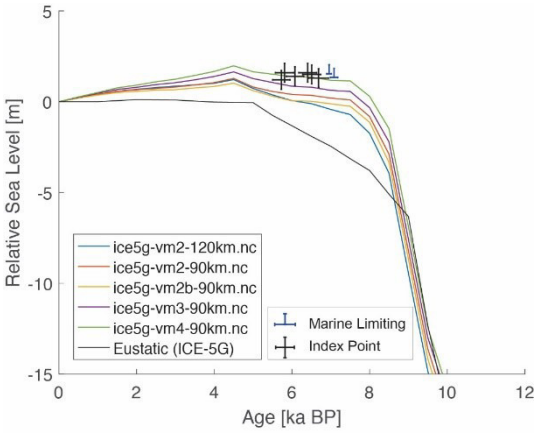

Figure 26: Standardized Holocene relative sea-level data obtained from Azmy et al. (2010) in comparison to glacial isostatic adjustment geophysical model predictions for Teluk Awur, Indonesia.

5.4 Glacial isostatic adjustment models

To compute the contribution of glacial isostatic adjustment to relative sea-level changes, we have solved the Sea Level Equation (Clark and Farrell, 1976; Mitrovica and Peltier, 1991) by means of the SELEN program (Spada and Stocchi, 2007). We employed a 1-D, radially stratified, self-gravitating, rotating, Maxwell viscoelastic and incompressible Earth model and the ice-sheet model ICE-5G (Peltier, 2004). To explore the sensitivity of the predictions to various aspects of the model, we employed different mantle viscosity profiles and lithosphere thicknesses (Table 3). All model runs include time varying coastline positions (Peltier, 2004, 1994).

5.5 Acknowledgements

This work was supported through grant SEASCHANGE (RO-5245/1-1) from the Deutsche Forschungsgemeinschaft (DFG) as part of the Special Priority Program (SPP)-1889 "Regional Sea Level Change and Society". TM, TL and AR are supported by the Leibniz-Centre for Tropical Marine Research (ZMT). TL and AR's research is further supported by the Institutional Strategy of the University of Bremen, funded by the German Excellence Initiative [ABPZuK-03/2014]. The authors acknowledge the working groups HOLSEA - Modelling Paleo Processes (INQUA CMP project 1601P)

5. Data article; Relative sea-level data from the SEAMIS database compared to ICE-5G model predictions of glacial isostatic adjustment

and PALSEA (PAGES/INQUA) for useful discussions during the Oregon workshop (2016). We thank our Co-Pi´s and collaborators Hildegard Westphal, Benjamin P. Horton, Jamaluddin Jompa, Robert E. Kopp, Muhammad Lukman and Tilo Schöne.

6 Late Holocene (0-6 ka) sea-level changes in the Makassar Strait, Indonesia

6.1 Abstract

The Spermonde Archipelago, off the coast of Southwest Sulawesi, consists of more than 100 small islands, and hundreds of shallow-water reef areas. Most of the islands are bordered by coral reefs that grew in the past in response to paleo relative sea-level changes. Remnants of these reefs are preserved today in the form of fossil microatolls. In this study, we report the elevation, age and paleo relative sea-level estimates derived from fossil microatolls surveyed in five islands of the Spermonde Archipelago. We describe 24 new sea-level index points, and we compare our dataset with both previously published proxies and with relative sea-level predictions from a set of 54 Glacial Isostatic Adjustment (GIA) models, using different assumptions on both ice melting histories and mantle structure and viscosity. We use our new data and models to discuss Late Holocene (0-6 ka) relative sea-level changes in our study area and their implications in terms of modern relative sea-level estimates in the broader South and Southeast Asia region.

6.2 Introduction

After the Last Glacial Maximum, sea level rose as a result of increasing temperatures and ice loss in Polar regions. Rates of sea-level rise due to ice melting and thermal expansion (i.e., eustatic) progressively decreased between 8 to 2.5 ka BP (Lambeck et al., 2014), remaining constant thereafter (until the post-industrial sea-level rise). In areas far from Polar regions (i.e., far-field, Khan et al., 2015) the rapid eustatic sea-level rise after the Last Glacial Maximum was followed by a local (i.e., relative) sea-level highstand between ~6 and ~3 ka BP, and a subsequent sea-level fall towards present-day sea level. It has been long shown that the higher-than-present relative sea level (RSL) in the middle Holocene (e.g. Grossman et al., 1998; Mann et al., 2016) is not eustatic in origin, but was caused by the combined effects of glacial isostatic adjustment (GIA) (Milne and Mitrovica, 2008), that includes ocean siphoning (Milne and Mitrovica, 2008; Mitrovica and Milne, 2002; Mitrovica and Peltier, 1991) and redistribution of water masses due to changes in gravitational attraction and Earth rotation following ice mass loss (Kopp et al., 2015b).

Due to the spatio-temporal variability of the processes causing it, the Late Holocene highstand differs regionally in both time and elevation. The occurrence and elevation of RSL indicators deposited during the highstand are dependent not only on the processes mentioned above but also on the magnitude of Holocene land-level changes due to geological processes, such as subsidence resulting from sediment compaction or tectonics (e.g., Tjia et al., 1972; Zachariasen, 1998). Combining the use of precisely measured and dated RSL indicators with GIA models in areas where the highstand occurs, it is possible to improve our knowledge on long-term rates of land-level changes, which need to be considered in conjunction with local patterns and rates of current eustatic sea-level rise (e.g. Dangendorf et al., 2017) to gauge the sensitivity of different areas to future coastal inundation.

In this study, we present new Late Holocene sea-level data and GIA models from the Spermonde Archipelago (Central Indonesia, SW Sulawesi). In this region, a recent review (Mann et al., 2019b) indicated discrepancies between the RSL data reported by different studies. To reconstruct the local paleo RSL we surveyed microatolls, i.e. particular coral morphologies forming in close connection with sea-level datums (e.g., Scoffin and Stoddart, 1978; Woodroffe et al., 2012; Woodroffe et al., 2014). For reconstructing paleo RSL, we first studied living coral microatolls to calculate the range of depth where

corals are living at different islands. We then applied the results of the living microatolls (LMA) survey to fossil ones that we surveyed and dated using radiocarbon.

In total, we surveyed 24 fossil microatolls (FMA), with ages clustered around ~155 and ~5000 years Before Present (BP). We present this new dataset in conjunction with data provided by previous studies in the same region (Mann et al., 2016; Tjia et al., 1972; De Klerk, 1982) and new GIA models with varying ice histories and mantle properties. We use our data and models to discuss possible local subsidence mechanisms at the only heavily populated island (Barrang Lompo) among those we investigated, vertical land movements in the broader Spermonde Archipelago and implications of the different ice and earth models for modern sea-level estimates.

6.3 Regional Setting

The Spermonde Archipelago, located between 4°00’ S to 6°00’ S and 119°00’ E to 119°30’ E, hosts several low-lying islands, with average elevations of 2 to 3 m above mean sea level (Janßen et al., 2017; Kench and Mann, 2017). All these islands consist of table, platform, patch reefs crowned by coral cays (Sawall et al., 2011) and some are densely populated (Schwerdtner Máñez et al., 2012). Their low elevation above MSL and the fact that they are composed mostly of calcareous sediments makes them vulnerable to sea-level rise, inundation by waves and deficits in sediment supply (Kench and Mann, 2017). In the Spermonde Archipelago, the tidal cycle is mixed semi-diurnal with a maximum tidal range of 1.5 m (data from Badan Informasi Geospasial, Indonesia).

In this study, we focused on five islands in the Spermonde Archipelago. Here, we surveyed fossil microatolls that are complementary to those previously surveyed at two other islands in the same archipelago, reported in Mann et al. (2016) (Figure 27a, b). **Panambungan** (RSL data in Mann et al., 2016) (Figure 27g) is a small and uninhabited island, located 18 km northwest of Makassar City. **Barrang Lompo** (RSL data in Mann et al., 2016) (Figure 27i) is located 11.2 km northwest of Makassar and 11 km southwest of Panambungan, and is densely populated. **Bone Batang** (Figure 27h) is a narrow, uninhabited sandbank located south of the island of Panambungan and north of the island of Barrang Lompo. South of Barrang Lompo, and 13 km southwest from the city of Makassar, we surveyed **Kodingareng Keke** (Figure 27c), another uninhabited island. 25 km south of Kodingareng Keke lies the island of **Sanrobengi** (Figure 27d), a small, sparsely inhabited (less than 15 houses) reef island located close to the mainland of southern Sulawesi at the coast of Galesong, 21 km south of Makassar city. Sanrobengi is located south of the previous islands, which are close to each other off the coast of Makassar, towards the center of the Archipelago. The fourth and fifth study islands are located northwest of Makassar, bordering the edge of the Spermonde Archipelago. These two outer islands are **Suranti** (Figure 27f) and **Tambakulu** (Figure 27e) and both are uninhabited and located 58 km (Suranti) and 56 km (Tambakulu) from the City of Makassar. Another island already reported and studied by Mann et al. (2016) (**Sanane**) is included in this study only for the analysis of living microatolls, as fossil microatolls were not found on this island. Its location is 2.7 km northwest of Panambungan, and it is densely populated. The exact coordinates of the islands mentioned above are provided in SM1.

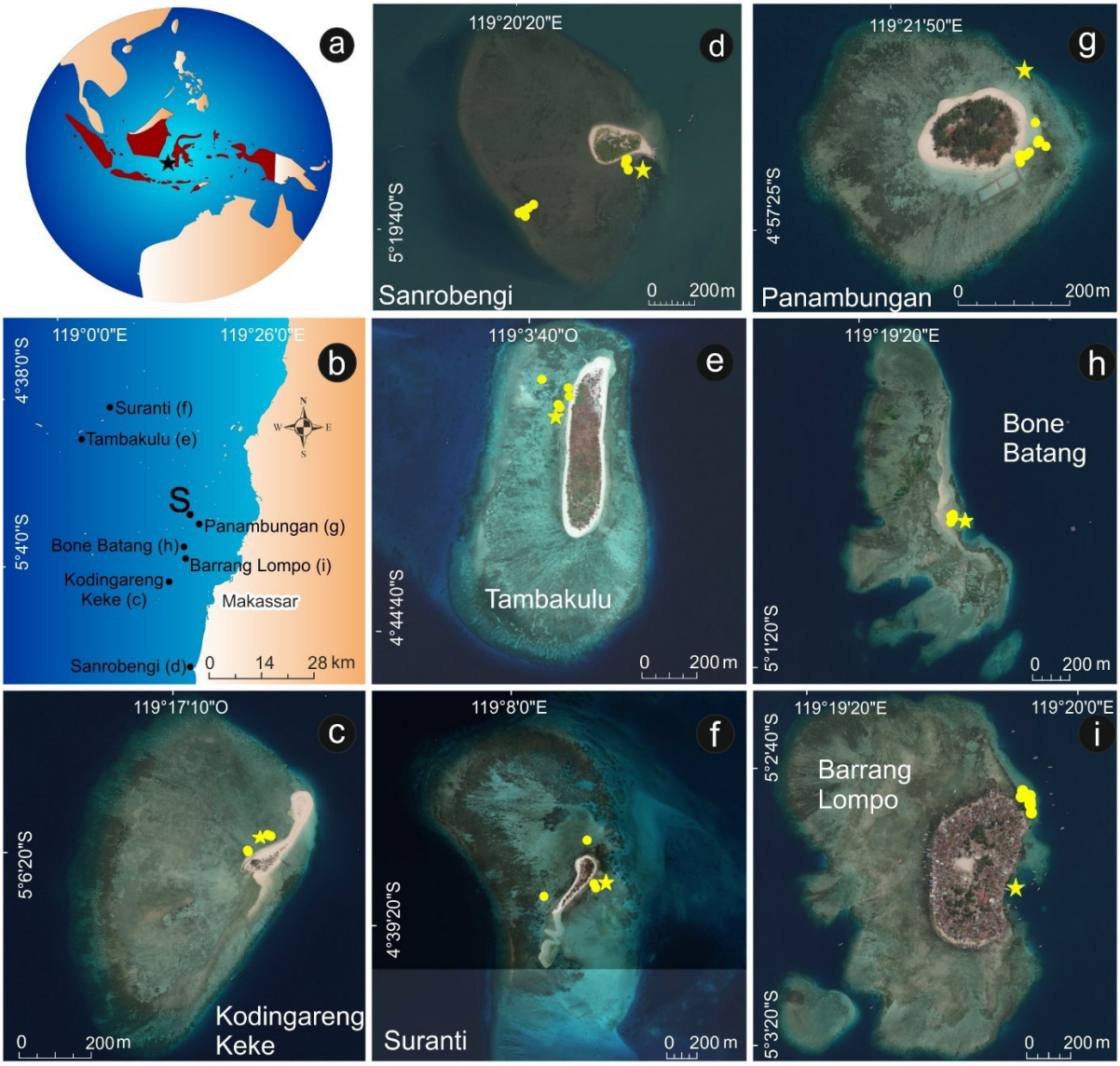

Figure 27: Overview map of the islands investigated in this study and the two islands studied by Mann et al. (2016) (Panambungan and Barrang Lompo). The star in a) indicates the location of the Spermonde Archipelago, off the coast of southwestern Sulawesi; b) indicates the position of each island, the dot labeled "S" indicates the position of Sanane, where only living microatolls were surveyed. Insets c) to i) show each island. The yellow dots in these panels indicate the location of sampled fossil microatolls, while the yellow asterisks indicate the position of the tide pressure sensor. Imagery sources for panels a) and b): Global Self-consistent Hierarchical High-resolution Shorelines from Wessel and Smith (2004) and for c) to i): Esri, DigitalGlobe, GeoEye, Earthstar Geographics, CNES/Airbus DS, USDA, USGS, AeroGRID, IGN, and the GIS User Community. The background maps in Figure 27 were created using ArcGIS® software by Esri. ArcGIS® and ArcMap™ are the intellectual property of Esri and are used herein under license. Copyright© Esri. All rights reserved. For more information about Esri® software, please visit www.esri.com.

6.4 Methods

6.4.1 Coral microatolls

In most tropical areas, Holocene RSL changes can be reconstructed using several types of RSL indicators (Khan et al., 2015), among which are fossil coral microatolls (e.g., Scoffin and Stoddart, 1978; Woodroffe et al., 2012; Woodroffe and Webster, 2014). Fossil microatolls are particular growth forms adopted by massive corals (e.g. *Porites*) when they reach the upper bounds of their living range, close to sea level. The coral colony generally grows upwards until they reach the lower part of the tidal range.

At this point, they keep growing horizontally at the same elevation forming "atoll-like" structures (Figure 1 in Scoffin and Stoddart, 1978 and Figure 8.1 in Meltzner and Woodroffe, 2015) that can widen up to several meters.

In the most standard definition, microatolls live at Mean Lower Low Water (MLLW), but their living range can span from Mean Low Water (MLW) down to the Lowest Astronomical Tide (LAT) (Mann et al., 2019b). If sea level falls below LAT, the coral polyps desiccate and die, retaining their carbonate calcium skeleton and their morphology (Meltzner and Woodroffe, 2015). Since they can survive within a narrow range related to tidal datums, fossil microatolls are often considered as an excellent RSL indicator (when found in good preservation state) as they constrain paleo RSL within a narrow range (Meltzner and Woodroffe, 2015).

While the relationship of coral microatolls with the tidal datums described above is often maintained, several authors (e.g. Mann et al., 2016; Smithers and Woodroffe, 2001; Woodroffe et al., 2012) pointed out that deviations from microatoll living range and tidal datums may occur due to site-dependent characteristics, such as wave intensity and broader reef morphology (Meltzner and Woodroffe, 2015). It is also worth highlighting that a tide gauge with long enough time series might not be available at remote locations where microatolls are often found. Therefore, it is both more practical and more accurate to reconstruct paleo RSL at the time of microatoll life starting from the height of living coral microatolls (Height of Living Coral microatolls, HLC). Under the assumption that tide, wave, and reef morphology did not change significantly in time, this allows determining the paleo RSL associated to fossil microatolls that were living in the same geographical setting as modern ones (i.e., the same island or group of islands). For this reason, in this study, we sampled both fossil and living microatolls elevations, and we determined the indicative meaning (i.e., the correlation with sea level) of the fossil microatolls from the HLC rather than to tidal datums.

As fossil microatolls are composed of calcium carbonate, they can be assigned an age, either with ^{14}C (Woodroffe et al., 2012) or U-series dating (e.g., Azmy et al., 2010). Recent studies showed that the accurate measurement, dating and standardized interpretation of coral microatolls have the further potential to detail patterns and cyclicities related to short-term (e.g. decadal to centennial) sea-level fluctuations (Meltzner et al., 2017; Smithers and Woodroffe, 2001; Kench et al., 2019).

6.4.2 Elevation measurements

Fossil and living microatoll (respectively, FMA and LMA) heights were surveyed on Sanrobengi, Kodingareng Keke, Bone Batang, Suranti and Tambakulu (Figure 27c–i) with an automatic level. FMA and LMA heights were always taken on the top microatoll surface. Elevations were initially referenced to locally deployed water level sensors (Seametrics PT2X) acting as temporary benchmarks. Locations of water level loggers are shown in Figure 27c–i (stars) and logged water levels are reported in SM1. The sensors were fixed to either jetties or living corals close to the survey sites and logged the tide levels at 30-second intervals. Tidal level differences between the sensors on the study islands were referenced to the tidal height of the water level sensor on Panambungan, for which we have the longest tide record of 8 days and 18 h. The Panambungan tidal readings were compared to readings at the national tide gauge at Makassar harbor (1.1.2011 – 19.12.2019, data courtesy of Badan Informasi Geospasial, Indonesia) to establish the reference of our sample sites to MSL. As a result of annual sea-level variability, the mean tidal level at Makassar during our surveys was slightly above (+0.014 m) the long-term MSL (1-Jan-2011 to 19-Dec-2019). Our elevation measurements were corrected accordingly.

FMA and LMA measurement error were propagated using the root mean square of the sum of squares of the following values (see SM1 for calculations and details):

- Automatic level survey error = 0.02 m, as in Mann et al. (2016). If the automatic level had to be moved due to excessive distance from the benchmark to the measured point, this error is added twice.
- Error referencing island logger to Panambungan MSL. This error has been calculated comparing water levels measured at each island against those measured at Panambungan, and varies from 0.01 to 0.07 m (see SM1 for details)
- Error referencing Panambungan to Makassar MSL = 0.04 m, as in Mann et al. (2016).
- Error in calculating Makassar MSL from a limited time (8.9 yrs, 1-Jan-2011 to 19-Dec-2019) and not for an entire tidal cycle (18.6 yrs). We estimated this error to be 0.05 m.

6.4.3 Paleo RSL calculation

After relating all microatoll elevations to MSL, we used FMA and LMA elevation measurements to calculate paleo RSL. We then applied the concept of indicative meaning (see Shennan, 1986 for definition and applications) to coral microatolls. The indicative meaning allows quantifying the relationship between the RSL indicator and the associated paleo sea level. To reconstruct paleo RSL from measured data we use the following formula:

$$RSL = E - HLC + Er$$

where **E** is the surveyed elevation of the fossil microatoll; **HLC** is the average height of living coral microatolls and **Er** is the estimated portion that was eroded from the upper fossil microatoll surface.

To calculate RSL, we measured HLC at each island individually or at the closest neighboring island where living microatolls could be found.

Concerning **HLC**, we surveyed living microatolls on Tambakulu (samples n=51) and Sanrobengi (n=24). On Suranti, Kodingareng Keke and Bone Batang, living microatolls were either restricted in number and with partly reworked appearance, or completely absent. Therefore, to calculate RSL at these islands, we used HLC elevations from Tambakulu (n=51) for Suranti, from Panambungan (from Mann et al., 2016; n = 20) for Bone Batang, and from Barrang Lompo (from Mann et al., 2016; n=23) for Kodingareng Keke.

The **Er** value was included in our calculation only in presence of visibly eroded microatolls (see Table 5 for details, comparison with non-eroded microatolls in Figure 28a, b) to account for the lowering of te top microatoll surface due to erosion. In Figure 29a and b, these microatolls are indicated with a light gray halo. Measurements on modern microatolls at Barrang Lompo, Panambungan and Sanane (Figure 30a) by Mann et al. (2016) showed that the average thickness of living microatolls in the Spermonde Archipelago is 0.48±0.19 m. Thus, to reconstruct the original fossil microatoll elevation for eroded FMAs, we added the missing centimeters to each eroded FMA thickness to reach 0.48 m. We remark that this approach does not take into account the fact that modern microatolls may be thicker than fossil ones because of the current rapidly rising sea level (that is forcing them to catch up, growing faster upwards). In contrast, under Late Holocene falling or stable sea-level changes, they were presumably getting wider, but not thicker. Hence, in our calculations, the added **Er** might be overestimated. In the absence of better constraints, we maintain this approach.

Final paleo RSL uncertainties were calculated using the root mean square of the sum of squares of the following values (see SM1 for calculations and details):

- Elevation errors of both FMA and LMA, calculated as described above
- Half of the indicative range, represented by the standard deviation of the measured heights of living corals
- Uncertainty in estimating erosion = 0.19 m, derived from (Mann et al., 2016) and discussed above.

Figure 28: Examples of a) non-eroded and b) eroded fossil microatoll at Sanrobengi.

6.4.4 Sampling and dating

The highest point of each FMA was sampled by hammer and chisel, or with a hand drill. Sub-samples from all samples taken in the field were analyzed via XRD at the Central Laboratory for Crystallography and Applied Material Sciences (ZEKAM), University of Bremen, Germany, to detect possible diagenetic alterations of the aragonite coral skeleton.

After the XRD screening, we performed one radiocarbon dating per sampled microatoll. AMS radiocarbon dating and age calibration to calendar years before present (a BP) was done at Beta Analytic Laboratory. We used the Marine 13 calibration curve (Reimer et al., 2013) and a delta R value (the reservoir age of the ocean) of 0±0 as recommended for Indonesia in Southon et al. (2002). To compare the new ages to the results from Mann et al. (2016), we recalculated their ages with the same delta R value.

The reason behind choosing a different delta R value than Mann et al. (2016) resides in the fact that the value they adopted (delta R = 89±70) was measured in southern Borneo (Southon et al., 2002) more than 900 km away from our study site. Their choice was based on the fact that there is no delta R value available between Sulawesi and southern Borneo that can be used for a radiocarbon age reservoir correction. Due to the long distance between Borneo and our study area and the presence of the Indonesian Throughflow between these two regions (Fieux et al., 1996), here we propose that there is no basis to assume a similar delta R value between southern Borneo and the Spermonde Archipelago. Therefore we follow the recommendation of Southon et al. (2002) to use a zero delta R, reported to be derived from unpublished data for the Makassar Strait.

All our samples were registered in the SESAR, the System for Earth Sample Registration, and assigned an International Geo-Sample Number (IGSN).

6.4.5 Glacial Isostatic Adjustment

To compare observations with RSL caused by isostatic adjustment since the Last Glacial Maximum, we calculated RSL as predicted by geophysical models of Glacial Isostatic Adjustment (GIA). These are based on the solution of the Sea-Level Equation (Clark and Farrell, 1976; Spada and Stocchi, 2007). We calculate GIA predictions using a suite of combinations of ice-sheets and solid Earth models. The latter are self-gravitating, rotating, radially stratified, deformable and characterized by a Maxwell viscoelastic rheology. We discretize the Earth's mantle in two layers: Upper and Lower Mantle (respectively, UM and LM). Each mantle viscosity profile is combined with a perfectly elastic lithosphere whose thickness is set to either 60, 90 or 120 km. We use 6 mantle viscosities for each lithospheric thickness, as shown in Table 4. We combine the Earth models with three different models: ICE5g, ICE6g (Peltier, 2009; Peltier et al., 2015) and ANICE (De Boer et al., 2015; De Boer et al., 2017). In total, we ran 54 different ice-earth model combinations (3 ice sheet models × 3 lithospheric thicknesses × 6 mantle viscosity profiles).

Table 4: Upper and lower mantle viscosities for the different Earth models.

Model name	**Upper Mantle [Pa s 10^{21}]**	**Lower Mantle [Pa s 10^{21}]**
VM1	0.25	2.5
VM2	0.25	5.0
VM3	0.25	10
VM4	0.5	2.5
VM5	0.5	5
VM6	0.5	10

6.5 Results

6.5.1 Living and fossil microatolls

Our dataset consists of a total of 25 fossil microatolls (FMA) surveyed in five islands of the Spermonde Archipelago (Table 5, see also SM1). Sixteen microatolls yield ages (calendar years) ranging from 5970 a BP to 3615 a BP (Figure 29a), while nine yield ages varying from 237 a BP to 37 a BP (Figure 29b). These are added to the 20 fossil microatolls and one modern microatoll from Barrang Lompo and Panambungan previously reported by Mann et al. (2016) (Figure 29a and Figure 29c, see also SM1) and the data from De Klerk (1982) and Tjia et al. (1972) (Figure 29c and Table 7, SM1). The microatoll PS_FMA 4 showed evidence of reworking, e.g., it was not fixed to the sea bottom, and thus it was subsequently rejected. Therefore, it is not shown in the results or discussed further. Among the 44 microatolls surveyed and dated in this study (n=24) and Mann et al., 2016 (n=20), 18 were eroded, and the erosion correction has been applied as reported in the methods section (gray bands in Figure 29a). The fact that these corrected data seem to plot consistently above the non-eroded microatolls might be indicative of the fact that our erosion correction may be overestimated. In absence of more precise data on the original thickness of fossil microatolls, we retain these indicators in our analyses.

Concerning living microatolls (LMA), our surveys included 51 individuals measured at the island of Tambakulu and 24 living microatolls measured at Sanrobengi (Figure 30b). The living microatolls in this survey complement those measured by Mann et al. (2016) at Panambungan (n=20), Barrang Lompo (n=23) and Sanane islands (n=17).

To reference the measured elevations of both LMA and FMA to MSL as described in the methods section, we measured water levels at Barrang Lompo, Panambungan, Suranti, Tambakulu, Kodingareng Keke, Bone Batang and Sanrobengi for a total of 688 hours, over the period 6-Oct-2017 to 15-Oct-2017 (see water levels in SM1). An example of measured water levels is shown in Figure 30b.

For which concerns XRD analyses (see SM1 for details), 17 over 24 samples show an average value of aragonite at 98.7±1.1%. Among the other samples, one (SB_FMA26) contains 7% of calcite, which might affect its age. Other potential sources of secondary carbon might be present in PT_FMA9 and BB_FMA13 where Kutnohorite was detected ($CaMn^{2+}(CO3)^2$, respectively 3 and 6%). All the remaining samples show relatively low aragonitic content, but the other minerals contained in them do not contain carbon that could potentially affect the ages reported in this study (see SM1 for details on XRD analyses).

The fossil microatolls of Suranti show age ranges from 237±97 a BP to 114±114 a BP. These samples indicate paleo RSL positions of -0.53±0.25 m and -0.11±0.25 m. On Tambakulu, ages range between 114±114 a BP and 37±12 a BP. In this time span, the elevations of the fossil microatolls at this island indicate RSL positions between -0.24±0.13 m and 0.11±0.23 m. The samples from Bone Batang cover ages from 5196±118 a BP to 3693±108 a BP and provide paleo RSL positions of 0.13±0.22 m to 0.20±0.22 m. Samples from fossil microatoll ages from Kodingareng Keke vary from 5869±99 a BP to 5343±88 a BP, indicating paleo RSL positions between -0.02±0.12 m and 0.10±0.12 m. Fossil microatoll samples from Sanrobengi range in age from 5970±89 a BP to 3615±99 a BP, with RSL from 0.14±0.12 m to 0.54±0.23 m.

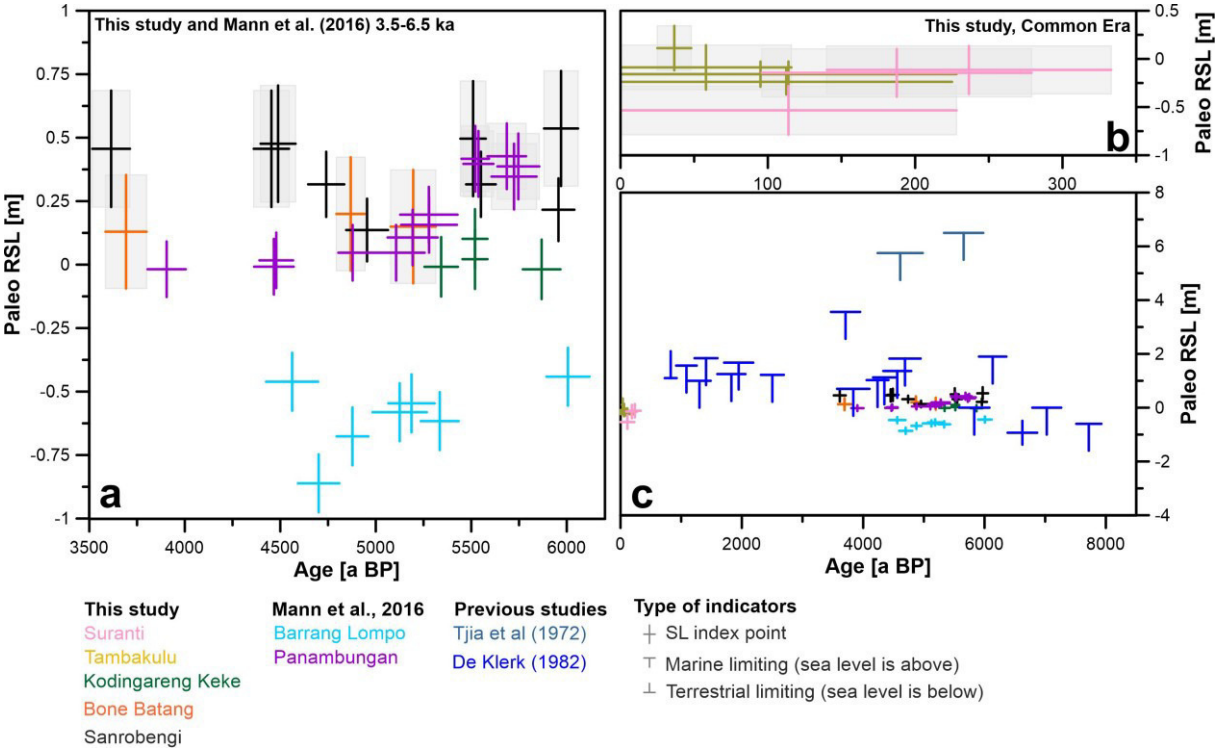

Figure 29: Representation of data reported in Table 5 and Table 6. a) RSL index points dating ~6.5 to ~3.5 ka and b) Common Era microatolls surveyed in this study. Gray bands in a) and b) represent the microatolls that were recognized as eroded in the field, and to which the erosion correction explained in the text has been applied. Panel c) shows the newly surveyed data in the context of previous studies.

Table 5: Fossil microatolls surveyed and dated at Suranti (PS_FMA 1 – 3), Tambakulu (PT_FMA 5 – 9), Bone Batang (BB_FMA 11 – 13), Kodingareng Keke (KK_FMA 14 – 17) and Sanrobengi (SB_FMA 18 – 26). All ages are recalculated with the delta R value of 0±0 (Southon et al., 2002). The elevation/age plot of these data is shown in Figure 29a, b.

IGSN	Lab Code	Sample Name	Island Name	14 C age	± 14 C error	Mean age [cal a BP]	± Error (yr)	Elevation [m] with respect to msl	HLC [m]	RSL [m]	± Vertical error [m]	+ Erosion error (σEr) [m]
IEMBMPSFMA1	Beta – 487554	PS_FMA1	Suranti	490	30	114	114	-1.48	-0.75	-0.53	0.25	0.2
IEMBMPSFMA2	Beta – 508373	PS_FMA2	Suranti	560	30	187.5	91.5	-1.22	-0.75	-0.14	0.25	0.33
IEMBMPSFMA3	Beta – 487555	PS_FMA3	Suranti	620	30	236.5	96.5	-1.19	-0.75	-0.11	0.25	0.33
IEMBMPTFMA5	Beta – 487558	PT_FMA5	Tambakulu	460	30	95	95	-0.91	-0.75	-0.16	0.13	0
IEMBMPTFMA6	Beta – 508375	PT_FMA6	Tambakulu	490	30	114	114	-0.91	-0.75	-0.16	0.13	0
IEMBMPTFMA7	Beta – 508376	PT_FMA7	Tambakulu	470	30	112.5	112.5	-0.99	-0.75	-0.24	0.13	0
IEMBMPTFMA8	Beta – 487559	PT_FMA8	Tambakulu	106.55	0.4 pMC	36.5	11.5	-0.84	-0.75	0.11	0.23	0.2
IEMBMPTFMA9	Beta – 508377	PT_FMA9	Tambakulu	420	30	58	58	-0.97	-0.75	-0.09	0.23	0.13
IEMBMBBFMA11	Beta – 487545	BB_FMA11	Bone Batang	4630	30	4869	75	-0.58	-0.50	0.20	0.22	0.28
IEMBMBBFMA12	Beta – 487546	BB_FMA12	Bone Batang	4910	30	5196	118	-0.65	-0.50	0.15	0.22	0.3
IEMBMBBFMA13	Beta – 508378	BB_FMA13	Bone Batang	3750	30	3692.5	107.5	-0.67	-0.50	0.13	0.22	0.3
IEMBMKKFMA14	Beta – 487556	KK_FMA14	Kodingareng Keke	4970	30	5342.5	87.5	-0.47	-0.47	-0.01	0.12	0
IEMBMKKFMA15	Beta – 508379	KK_FMA15	Kodingareng Keke	5500	30	5868.5	98.5	-0.48	-0.47	-0.02	0.12	0
IEMBMKKFMA16	Beta – 487557	KK_FMA16	Kodingareng Keke	5160	30	5519.5	65.5	-0.36	-0.47	0.10	0.12	0
IEMBMKKFMA17	Beta – 508380	KK_FMA17	Kodingareng Keke	5160	30	5519.5	65.5	-0.44	-0.47	0.02	0.12	0

IEMBMSBFMA18	Beta – 487547	SB_FMA18	Sanrobengi	4730	30	4954.5	109.5	-0.20	-0.34	0.14	0.12	0
IEMBMSBFMA19	Beta – 508371	SB_FMA19	Sanrobengi	5560	30	5956.5	83.5	-0.12	-0.34	0.22	0.12	0
IEMBMSBFMA20	Beta – 487548	SB_FMA20	Sanrobengi	5140	30	5509.5	66.5	-0.17	-0.34	0.50	0.23	0.33
IEMBMSBFMA21	Beta – 487549	SB_FMA21	Sanrobengi	5570	30	5970	89	-0.13	-0.34	0.54	0.23	0.33
IEMBMSBFMA22	Beta – 487550	SB_FMA22	Sanrobengi	5200	30	5550.5	77.5	-0.02	-0.34	0.32	0.13	0
IEMBMSBFMA23	Beta – 487551	SB_FMA23	Sanrobengi	4550	30	4740.5	94.5	-0.02	-0.34	0.32	0.13	0
IEMBMSBFMA24	Beta – 487552	SB_FMA24	Sanrobengi	4350	30	4488.5	91.5	-0.01	-0.34	0.48	0.23	0.15
IEMBMSBFMA25	Beta – 487553	SB_FMA25	Sanrobengi	4320	30	4453.5	92.5	-0.03	-0.34	0.46	0.23	0.15
IEMBMSBFMA26	Beta – 508372	SB_FMA26	Sanrobengi	3700	30	3614.5	98.5	-0.03	-0.34	0.46	0.23	0.15

Table 6: Fossil microatolls sampled by Mann et al. (2016) surveyed on Barrang Lompo (FMA 1 (BL) – FMA 7 (BL)) and Panambungan (FMA 8 (PPB) – FMA 21 (PPB). All ages are recalculated with a delta R value of 0 and an error of 0 (Southon et al., 2002). All erosion corrections are already included in the RSL as provided in Mann et al. (2016) but all details are provided in the supplementary SM1. The elevation/age plot of these data is shown in Figure 29a.

Lab Code	Sample Name	Island Name	14 C age	± 14 C error	Mean age [cal a BP]	± Error (yr)	Elevation [m] with respect to msl	HLC [m]	RSL [m]	± Vertical error [m]
Poz-63504	FMA1 (BL)	Barrang Lompo	4505	30	4701	108	-1.35	-0.47	-0.86	0.11
Poz-66838	FMA2 (BL)	Barrang Lompo	5600	40	6006.5	112.5	-0.93	-0.47	-0.44	0.11
Poz-63505	FMA3 (BL)	Barrang Lompo	4405	35	4562	136	-0.95	-0.47	-0.46	0.11
Poz-66839	FMA4 (BL)	Barrang Lompo	4900	35	5187	121	-1.03	-0.47	-0.55	0.11
Poz-63506	FMA5 (BL)	Barrang Lompo	4965	35	5335	99	-1.10	-0.47	-0.62	0.11
Poz-66840	FMA6 (BL)	Barrang Lompo	4640	35	4878	83	-1.16	-0.47	-0.68	0.11
Poz-66842	FMA7 (BL)	Barrang Lompo	4830	40	5125	142	-1.07	-0.47	-0.58	0.11
Poz-66843	FMA8 (PP)	Panambungan	5370	35	5746.5	109.5	-0.30	-0.50	0.39	0.13
Poz-66844	FMA9 (PP)	Panambungan	5185	35	5537.5	78.5	-0.29	-0.50	0.40	0.13
Poz-66845	FMA 10 (PP)	Panambungan	5165	35	5521	72	-0.27	-0.50	0.42	0.13
Poz-63507	FMA 11 (PP)	Panambungan	5325	35	5686	101	-0.26	-0.50	0.43	0.13
Poz-63511	FMA 12 (PP)	Panambungan	4915	35	5193	131	-0.38	-0.50	0.11	0.11
Poz-66846	FMA 13 (PP)	Panambungan	4940	40	5278	150	-0.29	-0.50	0.20	0.11
Poz-63512	FMA 14 (PP)	Panambungan	3920	30	3905	100	-0.50	-0.50	-0.02	0.11
Poz-63513	FMA 15 (PP)	Panambungan	4645	30	4879	75	-0.44	-0.50	0.05	0.11
Poz-66847	FMA 16 (PP)	Panambungan	4340	30	4479	88	-0.47	-0.50	0.02	0.11
Poz-66848	FMA 17 (PP)	Panambungan	4330	35	4466.5	103.5	-0.49	-0.50	-0.01	0.11
Poz-66849	FMA 18 (PP)	Panambungan	4810	40	5106.5	149.5	-0.44	-0.50	0.05	0.11
Poz-63515	FMA 19 (PP)	Panambungan	4940	35	5279	146	-0.33	-0.50	0.16	0.11
Poz-66850	FMA 20 (PP)	Panambungan	5350	40	5724	118	-0.34	-0.50	0.35	0.13
Poz-66852	FMA21 (PP)	Panambungan	106.08	0.33 pMC			-0.44	-0.50	0.04	0.11

*Table 7: Marine and terrestrial limiting indicators from De Klerk (1982) and Tjia et al. (1972) studied in different locations in SW Sulawesi and the Spermonde Archipelago. This table is an extract from the database of Mann et al. (2019b). * indicates samples from Tjia et al. (1972). The elevation/age plot of these data is shown in Figure 29c.*

Lab Code	Sample Name	Island Name	14 C age	± 14 C error	Mean age [cal a BP]	± Error (yr)	Elevation [m] with respect to msl	HLC [m]	RSL [m]	± Vertical error [m]
GrN-9883	-	Tanah Keke	4165	64	4237	180	1.025	n/a	n/a	n/a
GrN-9884	-	O. Pepe	4260	64	4349.5	186.5	1.125	n/a	n/a	n/a
GrN-9885	-	Talakaya	2755	126	2503	189	1.22	n/a	n/a	n/a
GrN-10559	-	Puntondo	1525	130	1086.5	169.5	1.565	n/a	n/a	n/a
GrN-10560	-	Puntondo	1840	136	1410	189	1.84	n/a	n/a	n/a
GrN-10561	-	Puntondo	6540	103	7026.5	238.5	0	n/a	n/a	n/a
GrN-10562	-	Puntondo	4380	128	4562	230	1.365	n/a	n/a	n/a
GrN-10563	-	Pamaroang	4520	141	4689.5	257.5	1.825	n/a	n/a	n/a
GrN-10564	-	Pangalasak	2230	136	1828	232	1.25	n/a	n/a	n/a
GrN-10565	-	Patene	2330	136	1948	240	1.675	n/a	n/a	n/a
GrN-10566	-	Samalona	5440	150	5831	251	0	n/a	n/a	n/a
GrN-10491	-	Tekolabua	905	50	827.5	98.5	1.1	n/a	n/a	n/a
GrN-10492	-	Tekolabua	6840	100	7719	207	-0.6	n/a	n/a	n/a
GrN-10493	-	Maros	6175	103	6624.5	243.5	-0.5	n/a	-0.93	0.44
GrN-10976	-	Bone Tambung	1735	83	1301.5	185.5	1	n/a	n/a	n/a
GrN-10978	-	Sarappo	3870	99	3837	267	0.7	n/a	n/a	n/a
GrN-10979	-	Pamaroang	3770	92	3709.5	240.5	3.56	n/a	n/a	n/a
GrN-10980	-	Tarallow	5740	106	6134.5	225.5	1.9	n/a	n/a	n/a
GrN-10981	-	Puntondo	8220	100	8738.5	261.5	1.53	n/a	n/a	n/a
GaK 3602*	-	Pamaroang	4460	139	4610	372	5.75	n/a	n/a	n/a
GaK 3603*	-	Pamaroang	5312	139	5656	323	6.5	n/a	n/a	n/a

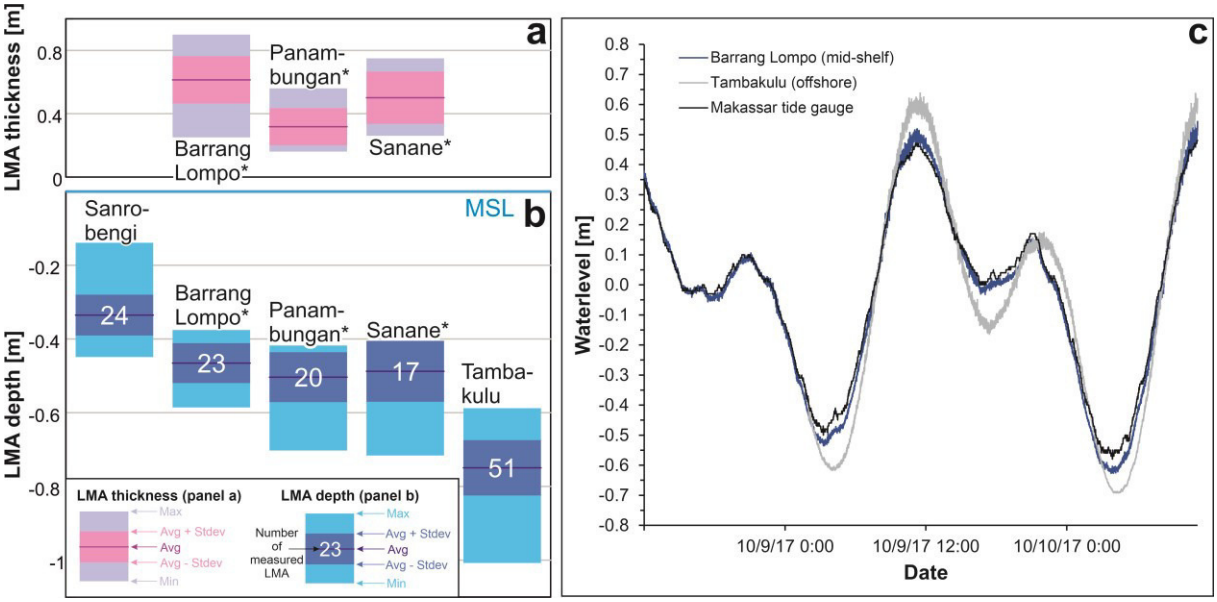

*Figure 30: a) Thickness of Living Microatolls (LMA) measured by Mann et al. (2016) in the Spermonde Archipelago. The average of the three islands reported is 0.48±0.19 m. b) Measured depth of LMA in this study (Sanrobengi and Tambakulu islands) and in Mann et al., 2016. * in a) and b) indicates the islands surveyed by Mann et al., 2016. In a) and b) the islands are ordered from the closest to the shore on the left side to the further away from the shore on the right side. c) Comparison between water levels measured at Barrang Lompo (located on the mid-shelf), Tambakulu (located offshore towards the edge of the shelf) and data recorded by the national tide gauge at Makassar harbor. Note that, in a and b), 'zero' refers to mean sea level, while in b) 'zero' refers to the average water level over the measurement period (here 10/8/2017 to 10/10/2017).*

6.5.2 GIA models

As described in the Methods section, we use different Earth and ice models to produce 54 different RSL predictions, from 16 ka BP to present (Figure 31b). The models are available in the form of NetCDF files including longitudes between 55.3° to 168.9° and latitudes between -28.6° and 38.6°. We provide the models in NetCDF format, with a Jupyter notebook to extract data at a single location and plot GIA maps (files can be retrieved from SM2).

An extract of the modeling results is shown in Figure 31 and Figure 32. While all models predict an RSL highstand in the Spermonde Archipelago (Figure 31a), the RSL histories predicted by each model show significant differences. ICE5g predicts the RSL highstand occurring ca. 2.5 ka later than ANICE and ICE6g. The maximum RSL predicted by ICE5g and ICE6g is higher than the one predicted by ANICE. ANICE is the only ice model for which at least one Earth model iteration (see the lowest line in Figure 5) does not predict an RSL highstand, but a quasi-monotonous sea level rise from 8 ka BP to present.

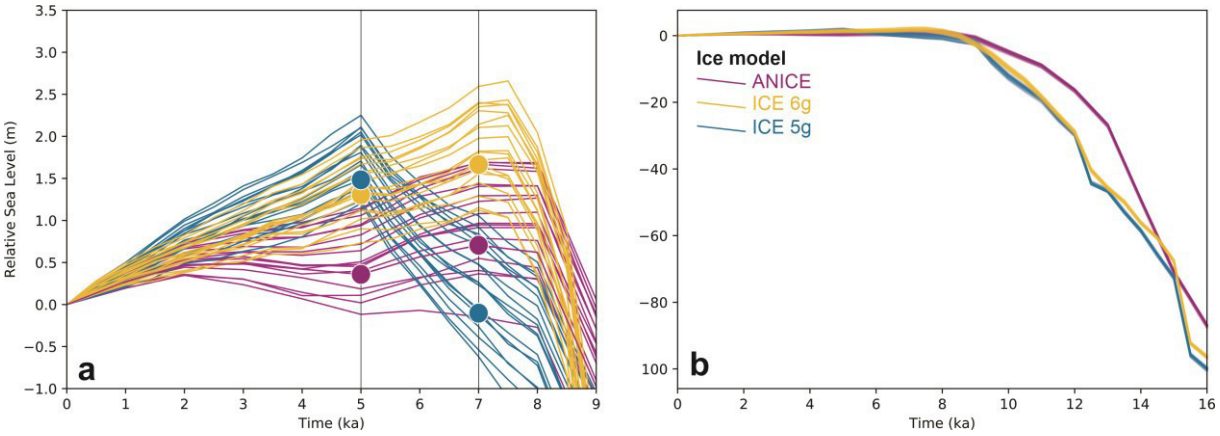

Figure 31: Results of the 54 GIA model runs for an island located in the center of the Spermonde Archipelago, a) last 9 ka. Dots indicate the points at which the maps in Figure 32 have been extracted. b) last 16 ka, representing the full time extent of the models. The eustatic sea level for each ice melting scenario is available in SM2. The Jupyter notebook used to create this graph is available as SM2.

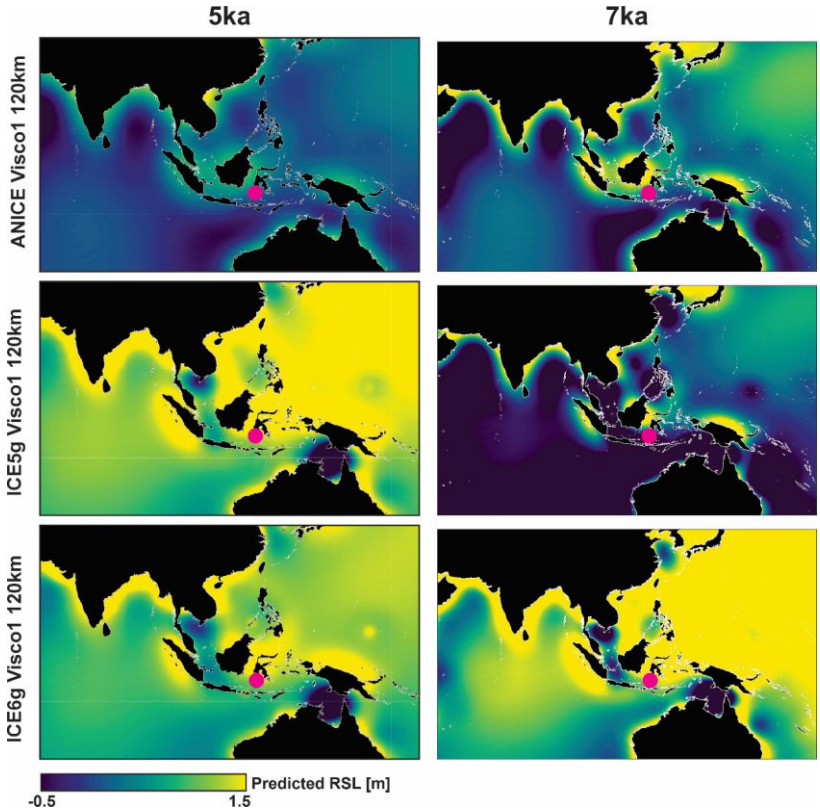

Figure 32: Relative sea level at 5 ka (left) and 7 ka (right) as predicted by three among the GIA models used in this study. See Table 4 for the definition of the mantle viscosity here labelled as "Visco1". The purple dot indicates the approximate position of the Spermonde Archipelago.

6.6 Discussion

The dataset presented in Table 5–Table 7 and shown in Figure 29a–c and Figure 30 allow discussing several relevant points that need to be taken into account as sea-level studies in the Makassar Strait and SE Asia progress.

6.6.1 Measuring living microatolls for paleo RSL calculations

As indicated by former studies (e.g. Mann et al., 2016; Smithers and Woodroffe, 2001; Woodroffe et al., 2012) the best practice to calculate paleo RSL from microatolls is, when possible, to measure the height of living coral microatolls (HLC) below MSL, to calculate their indicative meaning (Meltzner and Woodroffe, 2015).

Our results (Figure 30) show that, in the Spermonde Archipelago, HLC is subject to changes over short spatial scales. In fact, within similar reef contexts, we measured significant differences in HLC across the Spermonde Archipelago, which seem to conform to a geographic trend directed from nearshore towards the islands located on the outer shelf. The highest HLC (i.e., closer to mean sea level) was measured at the island closest to the mainland (Sanrobengi). The islands located in the middle of the archipelago (Panambungan, Sanane, and Barrang Lompo) differ slightly from each other but show comparable average HLC. At Tambakulu, located further away from the mainland (~70 km from Sanrobengi), the HLC is the lowest measured. On average, HLC at Tambakulu is ~0.4 m lower than that recorded at Sanrobengi. We highlight that this value is of the same magnitude (several decimeters) as the differences found by other studies reporting coral microatolls HLC measurements at different sites (Hallmann et al., 2018; Smithers and Woodroffe, 2001; Woodroffe, 2003; Woodroffe et al., 2012).

This pattern seems confirmed by the water level data we measured at the islands of Tambakulu and Barrang Lompo (Figure 30c). While our measurements are too short in time to extract well-constrained tidal datums, we remark that at Tambakulu (offshore) we measured a tidal range higher than at Barrang Lompo (mid-shelf), which in turn records a slightly higher tidal range than the Makassar tide gauge (onshore). The local tidal range is related to the bathymetry and can, therefore, differ even in relative proximity. We highlight that, while a complete analysis of the water level data we surveyed is beyond the scope of this work, SM1 contains all the water levels recorded during our surveys for further analysis.

The results discussed above stress the importance of measuring the HLC of living microatolls also at very small spatial scales. Had we only focused on the HLC published by Mann et al. (2016) for Panambungan, Sanane and Barrang Lompo (located in the center of the archipelago), our paleo RSL reconstructions would have been biased. Specifically, we would have overestimated paleo RSL at Tambakulu and underestimated it at Sanrobengi. Our reconstructions would have been similarly biased had we used, for our paleo RSL reconstructions, tidal datums derived from the tide gauge of Makassar.

6.6.2 Conflicting sea-level histories

Additionally to our new dataset and that of Mann et al. (2016) presenting index points, there are two studies reporting paleo sea-level observations for the Spermonde Archipelago: De Klerk (1982) and Tjia et al. (1972) (Figure 33). Mann et al. (2019b) re-analyzed data from these studies and recognized that most of the data originally interpreted as index points were instead better described as marine or terrestrial limiting indicators (Figure 29c). Our new data agree with those from Mann et al. (2016), but show relevant differences with Tjia et al. (1972) and De Klerk (1982) studies, that place RSL at 6–4 ka conspicuously higher than what is calculated using the microatoll record (Figure 29c).

This mismatch was recently pointed out by Mann et al. (2019b), who wrote: *"site-specific discrepancies between […] Tjia et al. (1972) […] and De Klerk (1982) and Mann et al. (2016) […] must be resolved with additional high-accuracy RSL data before the existing datasets can be used to decipher regional driving processes of Holocene RSL change within SE Asia".*

While the study by Mann et al. (2016) was based only on two islands, the data presented in this study provide definitive evidence to call for a reconsideration of the data reported by Tjia et al. (1972) and De Klerk (1982). Notwithstanding the importance of these datasets, we highlight that the higher late

Holocene RSL histories reported by these two authors are largely at odds with more precise RSL indicators reported here. Hence, the question arises: what is the possible reason for Tjia et al. (1972) and De Klerk (1982) data to be higher than the data reported by this study and Mann et al. (2016)?

One possible source of mismatch could reside in regional GIA differences. We suggest rejecting this hypothesis comparing the location of the areas surveyed in the Spermonde Archipelago with the outputs of our GIA models. Using the GIA models producing the most extreme differences within our region, we show that the discrepancy between the data cannot be explained by regional differences in the GIA signal. GIA differences remain within one meter among our sites (Figure 33a, b).

Similarly to GIA, another possible hypothesis is that the differences among sites in the Spermonde Archipelago are caused by differential tectonic histories between sites. While this is a possibility that would need further paleo RSL data to be explored (expanding the search of RSL indicators beyond the islands of the Spermonde Archipelago), we argue that there are several inconsistencies between the microatoll data and other sea-level data points surveyed within short geographic distances. For example, a fossil coral (not specified if in growth position) surveyed at Tanah Keke (GrN-9883, Table 7) by De Klerk (1982) would indicate that at 4237±180 a BP, RSL was above 1.03 m. At the same time, microatoll data from Sanrobengi (SB_FMA25, Table 5, ~20 km North of Tanah Keke) show that RSL was 0.46±0.23 m above present sea level. Similarly, at the site of Sarappo, De Klerk (1982) surveyed coral and shell accumulations that would propose the sea level was above 0.7 m at 3837±267 a BP (GrN-10978). This data point is at odds with microatoll data from the nearby islands of Panambungan, Bone Batang and Sanrobengi where, at the same time RSL is recorded by microatolls at elevations between -0.02±0.11 m and 0.46±0.23 m (BB_FMA13, SB_FMA26, Table 5 and FMA14 (PP), Table 6). We argue that invoking significant differential tectonic shifts between islands located so closely in space would require the presence of tectonic structures on the shelf of the Spermonde Archipelago that are, at present, unknown.

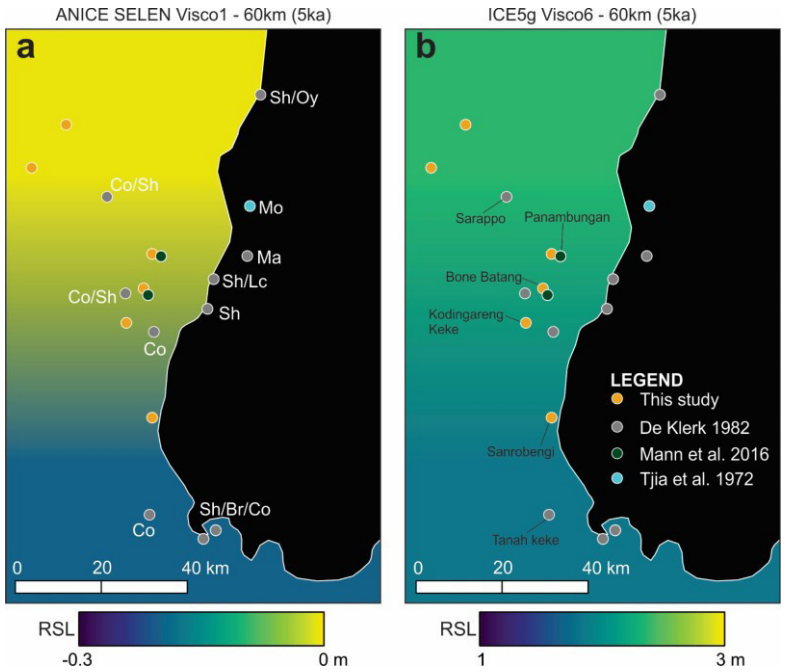

*Figure 33: Location of the RSL data presented in this study, Mann et al. (2016), De Klerk (1982) and Tjia et al. (1972) compared with RSL as predicted by GIA models. Land areas are filled in black. Here we show the models predicting, respectively, the lowest (a) and highest (b) RSL in the Spermonde Archipelago. Labels in a) represent the type of indicator reported by De Klerk (1982) and Tjia et al. (1972). Island names in b) refer to the islands mentioned in the discussion. Legend: **Sh** – shell accumulations; **Oy** – Oysters (no further details available); **Mo** – mollusks fixed on Eocene bedrock; **Ma** – Mangrove swamp; **Lc** – Loamy clays; **Br** – Beachrock; **Co** – Corals (in situ?). In b) we report the names of the islands discussed in the main text.*

Another possibility is that, while the original descriptions of Tjia et al. (1972) and De Klerk (1982) seem to indicate "marine limiting" points (i.e., indicating that sea level was above the measured elevation, Mann et al., 2019b), some of them may be instead representative of terrestrial environments, thus naturally above our paleo RSL index points. For example, it is not clear whether the "shell accumulations" reported at several sites and interpreted by Mann et al. (2019b) as marine limiting points may be instead representative of high-magnitude wave deposits by storms. The Spermonde Archipelago is subject to occasional strong storms that may explain the high emplacement of these deposits (see wave statistics in Figure 34).

Also, tsunamis are not unusual along the coasts of SE Asia (e.g. Rhodes et al., 2011) with the broader region in the Makassar Strait being one of the most tsunamigenic regions in Indonesia (Harris and Major, 2017; Prasetya et al., 2001). Nevertheless, the tsunamigenic earthquakes reported in this region are far north of our study area (Prasetya et al., 2001, see the left panel in Figure 34), and in general, they appear shallow and too small in magnitude to produce significant tsunamis propagating towards the Spermonde Archipelago. The earthquakes in this area are all generated along the Paternoster transform fault, which would point to tsunamis generated mostly by earthquake-triggered landslides rather than earthquakes themselves. Nevertheless, a tsunamigenic source for marine sediment deposition significantly above MSL cannot be ruled out until the deposits reported by Tjia et al. (1972) and De Klerk (1982) are re-investigated with respect to their precise elevations above MSL and their sediment facies.

Only further field data at the locations reported by Tjia et al. (1972) and De Klerk (1982) might help clarify the stratigraphy of these deposits and the processes that led to their deposition (i.e., paleo sea-level changes *versus* high-energy events).

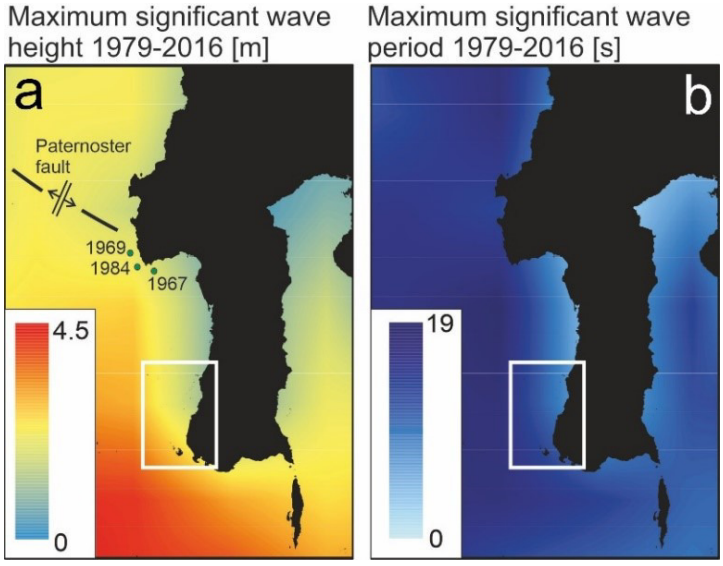

Figure 34: Maximum significant wave height (a) and period (b) extracted from the CAWCR wave hindcast (Durrant et al., 2013; Durrant et al., 2015). The left panel shows the approximate location and year of the three historical tsunami records reported by Prasetya et al. (2001), their Figure 1. Faultline and axis of spreading of the Paternoster fault are derived from Prasetya et al. (2001), their Figure 5. The box delimited by the white line indicates the approximate location of Figure 33 within this figure. CAWCR source: Bureau of Meteorology and CSIRO Copyright 2013.

6.6.3 Subsidence at a highly populated island?

As shown in Figure 29a, the data presented in this study together with the data from Mann et al. (2016), confirm a sea-level history with a higher-than-present RSL at 6–3.5 ka BP. The only exception to this pattern is the island of Barrang Lompo, where microatolls of roughly the same age are consistently lower (light blue crosses in Figure 29a). We compare the data at Barrang Lompo to the other RSL data points

in the Spermonde Archipelago using a Monte-Carlo simulation (see SM2 for details and methods) to highlight spatio-temporal clustering in these two datasets. We calculate that, on average, at ~5100 a BP, RSL at Barrang Lompo is 0.8±0.3 m lower than all the other islands where we surveyed microatolls of the same age (Figure 35).

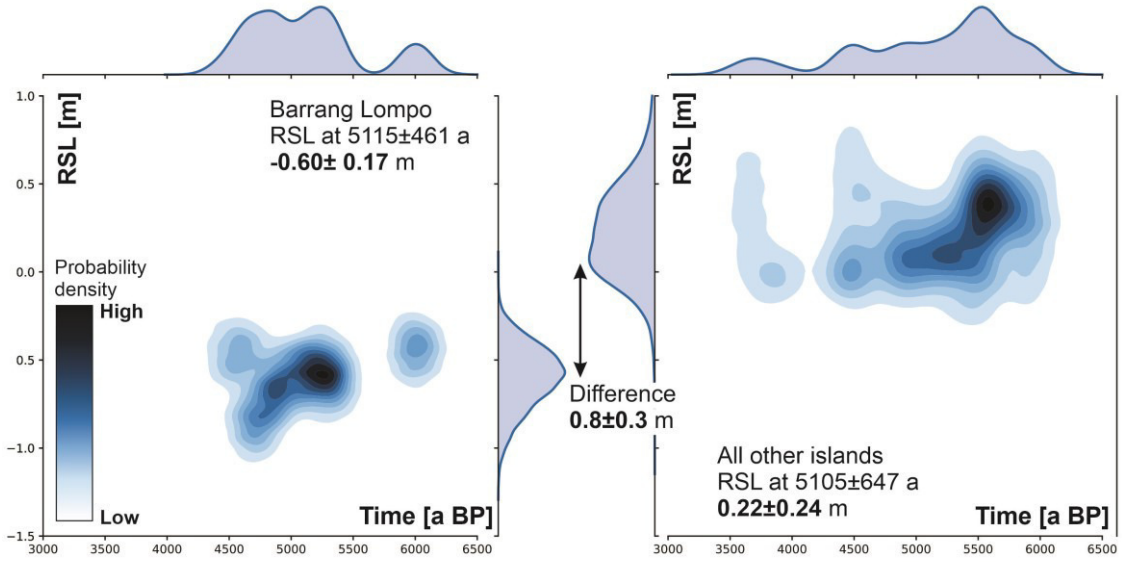

Figure 35: Joint plot showing bivariate (central plot) and univariate (marginal axes) distribution of RSL data points at Barrang Lompo (left) and all the other islands surveyed in this study and in Mann et al. (2016) (right). Darker blue areas in the central plots indicate a higher density of RSL point therefore darker colors indicate a higher probability of RSL at the given time. The Jupyter notebook used to create this graph is available as SM2.

The mismatch in RSL histories shown above can hardly be reconciled by differential crustal movements due to either tectonics or GIA over such short spatial scales (Figure 27b). For example, Bone Batang (where fossil microatolls were surveyed slightly above present sea level) and Barrang Lompo (where microatolls of roughly the same age were surveyed ca. 0.8 m below those of Bone Batang) are separated by less than 5 km and is, hence, highly unlikely that they were subject to very different tectonic or isostatic histories. The only geographic characteristic that separates Barrang Lompo from the other islands we surveyed is that it is heavily populated (~4.5 thousand people living on an island of 0.26 km²) (Syamsir et al., 2019). As such, it is characterized by a very dense network of buildings and concrete docks. The island is also subject to groundwater extraction (at least 8 wells were reported on Barrang Lompo, Syamsir et al., 2019).

The island of Barrang Lompo was populated since at least the 1720s (Clark, 2010; de Radermacher, 1786 as cited in Schwerdtner Manez and Ferse, 2010) when Barrang Lompo was (as it is today) a hub for sea cucumber fisheries (Schwerdtner Manez and Ferse, 2010). Assuming that the localized subsidence is anthropogenic, we cannot exclude that it started since the early colonization, but it seems appropriate to date it back to, at least, 100–150 years ago. At this time, the island population likely started to grow and to extract more groundwater for its sustenance. Using these inferences, our microatoll data show that Barrang Lompo might be affected by a subsidence rate in the order of ~3–11 mm/a (depending on the adopted subsidence amount and time of colonization) compared to the non-populated islands in the archipelago. Notwithstanding the obvious differences in patterns and causes of subsidence, we note that this rate is at least one order of magnitude smaller than what is observed in Indonesian mega-cities due to anthropogenic influences (Alimuddin et al., 2013). As this subsidence rate is a relative rate among different islands, any other regional subsidence or uplift rate (i.e., tectonic uplift or GIA-induced vertical land motions) should be added to this estimate.

As the fossil microatolls surveyed at anomalous positions were all located near the coast, one possibility is that they might have been affected by local subsidence due to the combined effect of groundwater extraction and construction load on the coral island. One point worth highlighting is that the depth of living microatolls, surveyed on the modern reef flat few hundred meters away from the island, does not show significant differences when compared to other islands nearby (Figure 30b). If the island is indeed subsiding, this observation could be interpreted in two ways. One is that the subsidence might be limited to the portions closer to the shoreline, and not to the distal parts (i.e., the reef flat) where modern microatolls are growing. The second is that the island has been subsiding fast in the recent past, but is now subsiding at roughly the same rate of upward growth of the living microatolls (Simons et al., 2007). Meltzner and Woodroffe (2015) report that microatolls are in general characterized by growth rates of ~10 mm/a, with extremes between 5 to 25 mm/a for those belonging to the genus *Porites*. These rates would allow modern microatolls to keep up with sea-level rise. We remark that, on average, living microatolls at Barrang Lompo are slightly thicker than those of islands nearby (Mann et al., 2016, Figure 30a).

A partial hint of a possible subsidence pattern at Barrang Lompo is given by the intense erosion problems that this island is reported to experience, which may be the consequence of high rates of land subsidence. Relatively recent reports indicate that coastal erosion is a particularly striking problem at Barrang Lompo (Williams, 2013; Tahir et al., 2012). Interviews of the local community led by Tahir et al. (2009) indicate that large parts of the island suffer from severe erosion problems, and that "*coastline retreat has occurred with a rate of change of 0.5 m/yr*". Williams (2013) reported that "*local people had constructed a double seawall of dead coral to mitigate erosion*".

We recognize that the mechanism of subsidence for Barrang Lompo proposed above should be regarded as merely hypothetical and needs confirmation through independent datasets. For example, the RSL change rates we propose for Barrang Lompo would be observable by instrumental means. For example, a comparative study using GPS measurements for a few days per year for 3–5 years would provide enough information to inform on vertical land motion rates in Barrang Lompo. Another approach would be the use of tide gauges to investigate multi-yearly patterns of land and sea-level changes in Barrang Lompo and at other populated and non-populated nearby islands. This would surely help to understand the reasons for the mismatch highlighted by our data.

Another way to detect recent vertical land movements between the island of Barrang Lompo and other uninhabited islands nearby would be to investigate whether there are differences in the morphology and growth patterns of living microatolls. If Barrang Lompo rapid subsidence is affecting also the distal part of the reef, this may be detectable through higher annual growth rates of the microatolls at this island compared to that measured at other islands.

To our knowledge, there is only one instrumental example of the kind of subsidence we infer here. At Funafuti Island (Tuvalu), Church et al. (2006) report that two closely located tide gauges (ca. 3 km apart) show a difference in RSL rise rates. In the search for an explanation to this pattern, they state that "*this tilting may be caused by tectonic movement or (most probably) local subsidence (for example, due to groundwater withdrawal) and demonstrates that even on a single island, the relative sea-level trend may differ by as much as 0.6 mm* yr^{-1}".

6.6.4 Common Era microatolls

Eight microatolls from the islands of Suranti and Tambakulu (located in the North of our study area, 12 km apart from each other) yielded ages spanning the last ~300 years (Figure 29b). This period represents the most recent part of the Common Era. Sea-level data from this period are relevant to assess rates of sea-level changes beyond the instrumental record (Kopp et al., 2016). Within Southeast Asia, the database of Mann et al. (2019b) (DOI: 10.17632/mr247yy42x.1 - Version 1) reports only one index point for this time frame (Singapore, Bird et al., 2010).

As the two islands of Suranti and Tambakulu are uninhabited and hence are not subject to the hypothetical anthropogenic subsidence discussed above for the island of Barrang Lompo, it is possible to use these data to calculate short-term vertical land motions. To do this, we first need to correct the paleo RSL as reported in Figure 29b to account for the 20th century sea-level rise and GIA land uplift since the microatolls were drowned (see SM2 for the complete calculation). We make this correction using the 20th-century global sea-level rise of 184.8±25.9 mm (Dangendorf et al., 2019) and GIA rates from our models (0.38±0.09 mm/a, see SM1 for details). We then iterate multiple linear fits through our data points by randomly selecting ages and CE RSL corrected as described above (full procedure and script available in SM2). After 10^4 iterations, we calculate that the average VLM rate indicated by our microatolls is -0.88±0.61 mm/a (Figure 36). While this range indicates that natural subsidence might be occurring at these islands, we cannot discard the possibility of a slight uplift, or stability.

We recognize that the calculation applied above to our data represents an approximation. Hence, the calculated rate is subject to several sources of uncertainty. First, five of eight Common Era microatolls were eroded, therefore the paleo RSL might be overestimated. Second, four of eight microatolls have large age error bars. Then, in our calculations, we use global mean sea-level rise rates instead of local ones, which are not available for this area due to the absence of a long-term tide gauge. The GIA models we employ are also limited, albeit they span a large range of possible mantle and ice configurations. Yet, our calculation is the best possible with the available data.

Notwithstanding the caveats above, we observe that the vertical land motion rates we calculate based on Common Era microatolls (-0.88±0.61 mm/a) are in agreement with the average vertical motion of -0.92±0.53 mm/a reported by Simons et al. (2007) (see their Supplementary Table 6) for the *PARE* GPS station (Lon: 119.650°, Lat: -3.978°, Height: 135 m). This station is located on the mainland, 78 km ENE of Tambakulu and Suranti. Nevertheless, the subsidence indicated by both our data and the *PARE* station appears at odds with another GPS station reported by Simons et al. (2007) in the proximity of Makassar (*UJPD,* Lon: 119.581°, Lat: -5.154°, Height: 153 m), that measures instead uplift rates at rates of 2.78±0.60 mm/a. While caution is needed when comparing long-term rates to the short-term ones measured by GNSS stations, these results provide important stepping stones for future studies in this area.

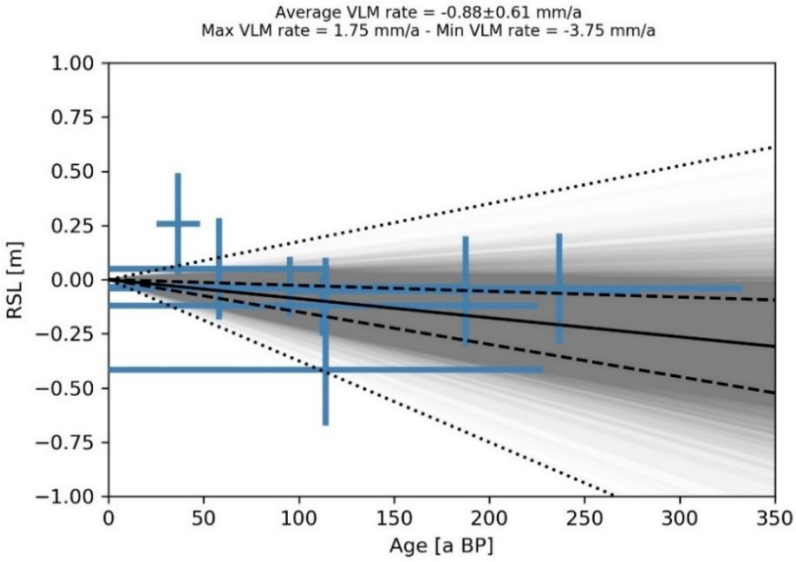

Figure 36: Common Era data points, corrected for 20th century sea-level rise and GIA uplift (blue crosses). Gray lines show the results of re-iterating a linear fit through random normal samples of the blue points. Dotted black lines show the linear fits with maximum and minimum slopes. Dashed black lines show average + standard deviation and average – standard deviation slopes. The solid black line shows the average slope. The Jupyter notebook used to create this graph is available as SM2.

6.6.5 Comparison with GIA models

Excluding the microatoll data from the island of Barrang Lompo (that, as per the discussion above, may have been subject to recent subsidence), 29 fossil microatolls in the Spermonde Archipelago (including also the data reported by Mann et al., 2016, Figure 29a) date between 3615 to 5970 a BP. This dataset can be compared with the predicted RSL from GIA models once vertical land movements due to causes different from GIA are considered. To estimate such movements in the Spermonde Archipelago, two options are available.

The first is to consider that the area has been tectonically stable during the Middle Holocene. This is plausible under the notion that, unlike the northern sector of Western Sulawesi (that is characterized by active lateral and thrust faults, (Bird, 2003), South Sulawesi is not characterized by strong tectonic movements (Sasajima et al., 1980; Hall, 1997; Walpersdorf et al., 1998; Prasetya et al., 2001). Considering the Spermonde Archipelago as tectonically stable (Figure 37a), our RSL data show the best fit with the RSL predicted by the ANICE model (VM2 – 60km, see Table 4 for details), in particular with those iterations predicting RSL at 6–4 ka few decimeters higher than present.

The second option is to interpret the rate of RSL change calculated from Common Era fossil microatolls (-0.88±0.61 mm/a), and make two assumptions: 1) that they were uniform through time and 2) that they can be applied to the entire Archipelago. Under these assumptions, we show in Figure 37b that, with subsidence rates below -0.5 mm/a, our data do not match any of our RSL predictions. Data start to match RSL predictions obtained using the ICE6g ice model with lower subsidence rates. For example, with a subsidence rate of -0.27 mm/a, representing the upper end of the 2-sigma range shown in Figure 36), the data show a good match with ICE6g (Figure 37c). As discussed above, based on both our Common Era data and GPS data from Simons et al. (2007) we cannot exclude that, instead of subsidence, the Archipelago is characterized by tectonic uplift. The maximum uplift compatible with our RSL data and models is 0.05 mm/a (Figure 37d). Regardless of the tectonic history chosen, we note that our data does not match the peak highstand predicted at 5 ka by the iterations of the ICE5g model.

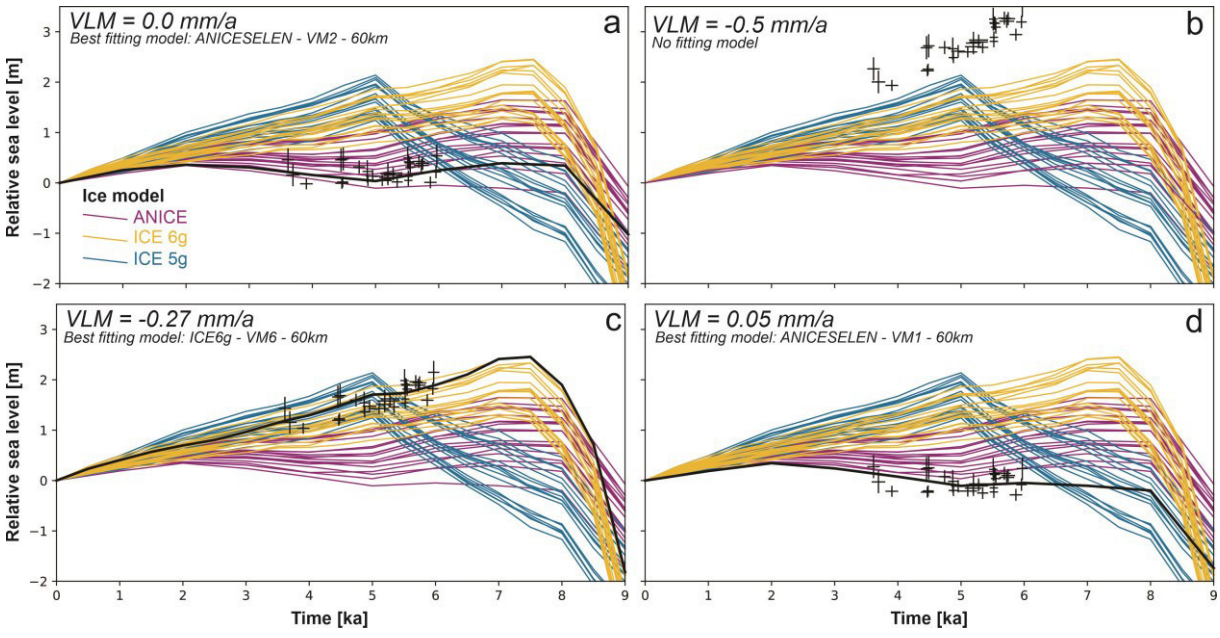

Figure 37: Comparison between RSL observations (except the island of Barrang Lompo) and predictions from GIA models (see Table 4 for model details). The model predictions were extracted by averaging latitude and longitude of all islands reported in this study, minus Barrang Lompo. Colored lines represent, respectively, ANICE, ICE5g and ICE6g models. Black thicker lines identify best fitting models. The different panels (a-d) show different tectonic corrections applied to the observed RSL data. The Jupyter notebook used to create this graph is available as SM2.

6.6.6 Paleo to modern RSL changes

Due to the existing uncertainties on vertical land motions discussed above, it is clear that the data in the Spermonde Archipelago cannot be used to infer global mean sea level. Yet, the matching exercise of our RSL data with GIA models under different vertical land motion scenarios shown in Figure 37 allows discussing the contribution of GIA to relative sea-level changes at broader spatial scales. GIA effects need to be taken into account in the analysis of both tide gauge and satellite altimetry data (see Rovere et al., 2016 for a review). One way to choose the GIA model(s) employed for this correction is to select those matching better with Late Holocene data.

To make an example of how different modeling choices (based on RSL data) propagate onto estimated modern GIA rates, in Figure 38a–c, we show the land motion rates caused by GIA as predicted by three models across Southern and Southeast Asia. These are the broad geographic results associated with the best-matching models under different assumptions on VLM (as shown in Figure 37). The difference between the two most extreme models matching with our data is within -0.3 and 0.5 mm/a (Figure 38d).

To give an example of the difference between these models, Figure 38d shows that ICE6g-VM6-60km predicts faster modern GIA rates than ANICESELEN-VM1-60km for India and Sri Lanka. As these rates would need to be subtracted from the data recorded by a tide gauge, this would affect any attempt of decoupling the magnitude of eustatic vs other land motions at tide gauges in that area.

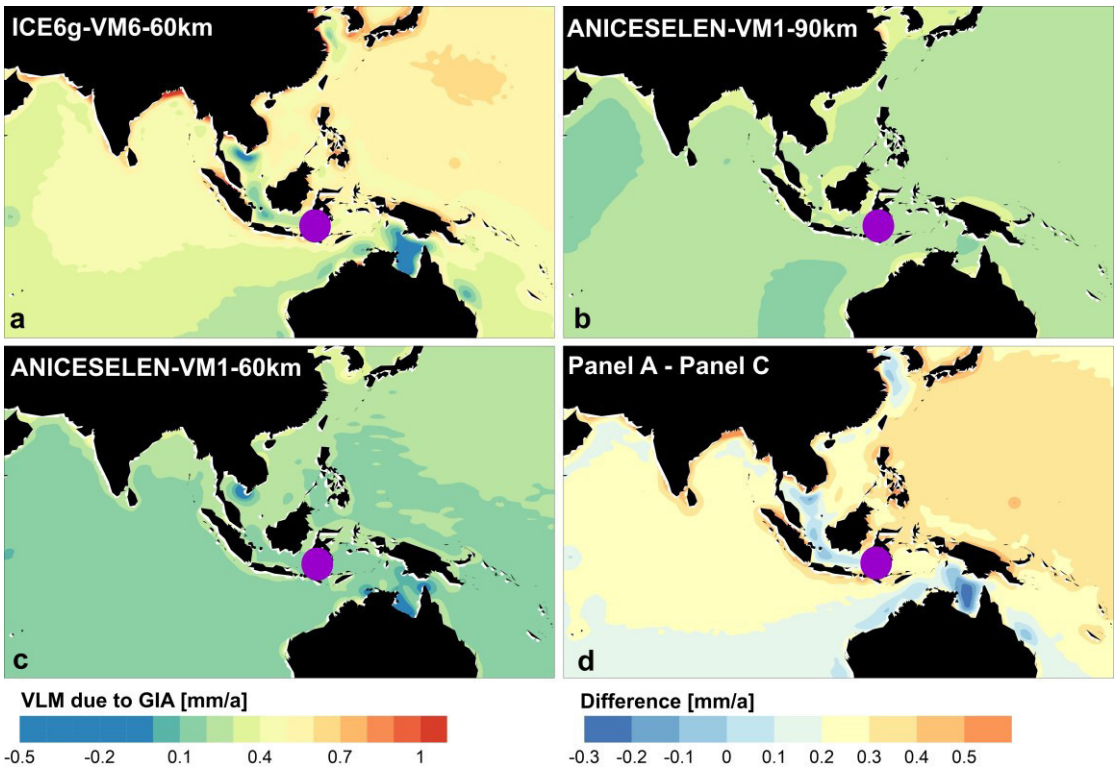

Figure 38 a-c) GIA-induced vertical land motion derived by linearly interpolating the last time step in our models (1 ka for ANICE, 0.5 ka for ICE6g) to present. d) Difference between the models with the most extreme predictions matching our Late Holocene sea-level index points under different vertical land motion scenarios (see Figure 37). The purple dot indicates the approximate position of the Spermonde Archipelago.

6.7 Conclusions

In this study, we report 25 new RSL index points (of which one was rejected due to evidence of reworking) and 75 living microatoll measurements from the Spermonde Archipelago. We also report 54 new GIA model iterations that span a large geographic region extending beyond Southeast Asia. Together with the data reported in Mann et al. (2016), these represent an accurate dataset against which paleo RSL changes in the Spermonde Archipelago and adjacent coasts (including the city of Makassar, the seventh-largest in Indonesia) can be benchmarked. Multiple implications are deriving from our discussions. We summarize these below.

Our measurements of living microatolls show that there is an elevation difference between the HLC results from the nearshore islands of the Archipelago (Sanrobengi, Figure 27) towards the outer shelf ones (Tambakulu and Suranti, Figure 27). The magnitude of this gradient or slope seems to be confirmed by water level data we measured at different islands and is ca. 0.4 m, with living microatolls deepening towards the offshore area. Recognizing the presence of this gradient was important to obtain coherent RSL reconstructions among different islands. This strengthens the notion that, when using microatolls as RSL indicators, living microatolls must be surveyed nearby of fossil ones to avoid biases in sea-level reconstructions.

The data surveyed in the Spermonde Archipelago by De Klerk (1982) and Tjia et al. (1972) are largely at odds with precisely measured and interpreted fossil microatolls presented in this study. We propose that, pending more accurate elevation measurements and reinterpretation of these data, they are excluded from sea-level compilations (i.e., Mann et al., 2019b in Khan et al., 2019). We also propose that there is the possibility that these deposits might represent storm (or tsunami) accumulations: this hypothesis needs further field investigations to be tested.

Data from the heavily populated island of Barrang Lompo are significantly lower (ca. 80 cm) than those at all the other islands. Here, we propose the hypothesis that groundwater extraction and loading of buildings on the island may be the cause of this discrepancy, which would result in local subsidence rates of Barrang Lompo in the order of ~3–11 mm/a. Due to the lack of instrumental data to support our hypothesis, we highlight the need for future studies acquiring both instrumental records and high-resolution RSL histories from fossil microatolls (e.g., reconstructing die-downs from microatoll slabs) across islands with different human population patterns. This mechanism of local subsidence needs to be verified with independent data. If confirmed, this would have wider implications for the resilience of low-lying, highly populated tropical islands to changes in sea level.

Besides the mechanism of local anthropogenic subsidence, we propose for the island of Barrang Lompo, eight microatolls dating to the last ca. 300–400 years allow us to calculate recent vertical land motion rates. We calculate that our data may indicate average vertical land motion rates of -0.88±0.61 mm/a. As these rates were calculated only for the two offshore islands in our dataset, we advise caution in extrapolating to broader areas. Nevertheless, we point out that this rate of subsidence is very consistent with that derived from a GPS station less than 100 km away (that recorded a rate of -0.92±0.53 mm/a Simons et al., 2007), but at odds with another GPS station in Makassar, for which uplift is reported.

Comparing the part of our dataset dated to 3–4 ka with the RSL predictions from a large set of GIA models, we show that the best matching ice model depends on the assumptions on vertical land movements. A generally better fit with models using the ICE6g ice history is obtained with moderate subsidence rates (-0.27 mm/a), while models using the ANICE ice history are more consistent with hypotheses of stability or slight tectonic uplift (0.05 mm/a). The ice model ICE5g shows a peak in RSL at ca. 5 ka that does not match our RSL observations at the same time.

In this study, we are not favoring one model over the others nor claim that our model ensemble is a complete representation of the possible variable space. We use the example of the Spermonde Archipelago to highlight how Holocene RSL data, coupled with GIA models, can inform on two aspects that are ultimately of interest to coastal populations.

First, they may help to benchmark subsidence rates obtained from GPS or tide gauges. It appears that, for the Spermonde Archipelago, long-term subsidence, tectonic stability or slight uplift are all possible. To settle this uncertainty, instrumental measures and more precise Common Era sea-level datasets should represent a focus of future sea-level research in this area.

Second, we showed here that matching GIA model predictions with Late-Holocene RSL data is useful to constrain which models might be a better choice to predict ongoing regional rates of GIA. While we do not have a definite "best match" for the Spermonde Archipelago, we suggest that iterations of ICE6g and ANICESELEN fit better with our data, and might produce more reliable GIA predictions than ICE5g, that seems not to match our data as well as the other two. To enable data/model comparisons such as the one performed in this study the supplementary material (SM2) contains all our model results at broad spatial scales for Southern and Southeast Asia.

6.8 Data availability

The supplementary material of SM1 and SM3 can be found on the DVD attached to this Email, while SM2 can be found at online at http://doi.org/10.5281/zenodo.3593965

SM1 – spreadsheet including 12 sheets containing the following information.

Sheet 1 – Site coordinates: Coordinates of the islands surveyed in this study and in Mann et al., 2016. The sheet includes the tidal model outputs calculated for each island and statistics on tidal levels.

Sheet 2 – Water level logger: raw data of the water level loggers positioned at each island, including date/time, depth and coordinates of deployment.

Sheet 3 – MSL calculations: details of the calculations done to reduce the water level at each island to MSL.

Sheet 4 – Complete table: spreadsheet version of the Tables 2, 3, 4 in the main text.

Sheets 5-9 – Data for each island: details on living and fossil microatolls surveyed at each island.

Sheet 10 – Modern GIA: current GIA rates for the Spermonde Archipelago extracted from the last time step of ANICE (1ka), ICE5g and ICE6g (0.5ka).

Sheet 11 – Results of XRD elemental analysis.

Sheet 12 – Living microatolls average and standard deviation elevation, and distance from the mainland.

SM2 – NetCDF files of GIA models and collection of Jupyter notebooks to reproduce the analyses in the paper. Available as: Rovere, A., Stocchi, P., Bender, M. 2020. Models, data and python tools for the analysis of sea level data in the Spermonde Archipelago. (Version v2.1). Zenodo. http://doi.org/10.5281/zenodo.3593965

SM3 – Laboratory data for Radiocarbon analyses.

6.9 Acknowledgments

We would like to thank SEASCHANGE (RO-5245/1-1) and HAnsea (MA-6967/2-1) from the Deutsche Forschungsgemeinschaft (DFG), which are part of the Special Priority Program (SPP)-1889 "Regional Sea Level Change and Society" for supporting this work. Thanks to Thomas Lorscheid and Deirdre Ryan for help and thoughtful comments. We acknowledge the help of the following Indonesian students and collaborators Andi Eka Puji Pratiwi “Wiwi”, Supardi and Veronica Lepong Purara, who provided support during fieldwork and sampling. We are grateful to the Indonesian Ministry for Research, Technology and Higher Education (RISTEKDIKTI) for assistance in obtaining research permits. The fieldwork for this study was conducted under Research Permit No. 311/SIP/FRP/E5/Dit.KI/IX/2017. We are also grateful to the Badan Informasi Geospasial (BIG), Indonesia, for sharing Makassar tide gauge data.

7 Probability difference analysis between geological sea-level indicators and GIA model predictions

7.1 Abstract

The Holocene sea level highstand differs spatially, temporally, and regionally. Glacial Isostatic Adjustment (GIA) models are constrained using geological field measurements to better understand local relative sea level (RSL) history. The comparison of predicted RSL histories from GIA models and paleo RSL observations are used to understand whether the RSL signal is mostly related to GIA, or if further post-depositional movements should be taken into account. In the region of South and Southeast Asia, the RSL results predicted by GIA models and indicated by geological field data in tectonically stable regions often differ. To evaluate the reason for these results, this study presents a statistical analysis to calculate the probabilities of mismatches between sea-level index points and 54 GIA models. We therefore utilize both an average probability calculation (APC) and a detailed probability calculation (DPC) to identify if the sample set and the individual index points show similar tendencies for agreement with each respective GIA model. The APD compares the dataset to the set of GIA models and the DPC individually compares each single index point within the sample set to the set of GIA models. The results are divided into three groups: 1.) high probability results, indicated by both analyses for the same mismatch (presented by eight of 16 regions). 2.) Low probability results in both analyses for the same mismatch (indicated in five of 16 regions). 3.) Deviating results, between both analyses, (indicated in three of 16 study sites). High probabilities indicate GIA as main driver for the RSL positions observed by the indicators, and low probability results imply tendencies of natural subsidence or indicate a RSL history significantly different from the RSL predicted by the models. Deviating results are very likely based on contrasting RSL predictions by the GIA models.

7.2 Introduction

After the Last Glacial Maximum (~21 ka BP) eustatic sea level rose quickly as a result of a changing climate, inducing polar land-ice melt (Lambeck et al., 2014; Lambeck et al., 2002). The thermosteric change and the influx of fresh-water from melting polar ice into the oceans caused changes in the total ocean water mass and affected local sea level through glacial isostatic adjustment (GIA) processes. As a consequence of GIA, ocean syphoning and continental levering were triggered (Milne and Mitrovica, 2008; Mitrovica and Milne, 2002; Mitrovica and Peltier, 1991), together with the redistribution of water masses due to changes in gravitational attraction and Earth rotation following ice mass loss (Kopp et al., 2015b).

Towards 7 ka before present (BP), meltwater input was greatly reduced. GIA processes caused a sea-level highstand in regions far from the poles (i.e., far-field, Khan et al., 2015). In several regions of South and Southeast Asia, models indicated that sea level reached its highstand in the Mid to Late Holocene between 6 ka BP in Indonesia and 2.5 ka BP in the Maldives (Mann et al., 2019b; Mann et al., 2019a). In general, the Holocene sea-level highstand was followed by a sea-level fall (Mitrovica and Milne, 2002) due to equatorial ocean syphoning (Mitrovica and Peltier, 1991). As ice-melt ceased, water masses migrated back to the poles to re-fill the space left by collapsing forebulges in the pole regions. These forebulges formed during the glaciation of the polar regions, when the increasing ice coverage caused a subsidence of the land masses below the ice and collapsed because of the induced uplift of the land when ice mases melted and the pressure on top of the land decreased (Mitrovica and Milne, 2002).

As the Holocene RSL highstand differs spatially and temporally, the occurrence of geological sea-level indicators deposited during the time of the local highstand and the comparison to adjusted GIA models are essential to analyze the local paleo RSL position and timing. However, GIA models and geological field samples often differ in the predicted RSL highstand and thus indicate deviating RSL histories. In

regions, such as Southeast (SE) Asia, that contain a high number of low-lying coastlines (e.g. the archipelago of Indonesia alone comprises of an 88,000 km long coastline; Marfai and King, 2007; Kench and Mann, 2017) and where land loss due to sea-level rise affects the inhabitants dramatically, detailed and well-studied local RSL histories are essential for future sea-level rise rate calculations.

In order to ascertain paleo RSL changes, precise RSL data and a wide range of GIA models are needed. This study aims to test the mismatch between observed RSL histories and those predicted by GIA models. The mismatch is the difference detected between RSL elevations predicted by GIA models and indicated by geological observations and explains if the deviation of both results is large or small i.e. comparable or completely at odds. We aim to detect mismatches among observations and predictions using two approaches: the average probability calculation (APC) and the detailed probability calculation (DPC). The APC tests the reliability of the indicated positive or negative mismatch between field data and GIA models. It calculates the average probability-range between all RSL elevations derived from index points of the sample set compared to the RSL predicted by GIA models over the entire distribution area. Therefore, the analysis shows higher or lower certainties depending on the quantity of index points and the related calculated probabilities within similar spatio-temporal distributions. The DPC derives the mismatch probabilities of the single RSL elevations obtained from individual observations. Both analyses are then compared in order to test whether the DPC agrees or disagrees with the APC results.

For our analysis, we used a set of 54 GIA models, forced by the ice models ICE5g, ICE6g (Peltier, 2009; Peltier et al., 2015) and ANICE (De Boer et al., 2015; De Boer et al., 2017). Each model was run with different assumptions on mantle viscosity properties. RSL observations are provided by 246 index points, divided into 16 locations #1 – #16 in Figure 39. All study areas are generally considered unaffected by major tectonic movements. However, post-depositional movements are always possible and can therefore not be excluded with certainty. We utilize field data that was previously compiled in the SEAMIS database by Mann et al. (2019a) and Mann et al. (2019b) along with two additional studies (Tam et al., 2018; Bender et al*., proof state*).

7.3 Regional setting

This study includes the central part of South to Southeast Asia (Figure 39) between the southern most Cocos Keeling Islands (Woodroffe et al., 1990), north to Song Hong (Red River) delta, Vietnam (Hori et al., 2004; Tanabe et al., 2003a; Tanabe et al., 2003b) and from the Maldives in the West (Kench et al., 2009) to Sulawesi in the east (De Klerk, 1982; Mann et al., 2016; Bender et al., *proof stage*).

In general, South and Southeast Asia are characterized by faulting and multiple plate motions (Simons et al., 2007; Hall and Spakman, 2015), that mainly affected the Indonesian archipelago in the Holocene due to its location between several colliding continental plates and the Java trench subduction zone (Horton et al., 2005). We therefore only include areas that are considered tectonically stable.

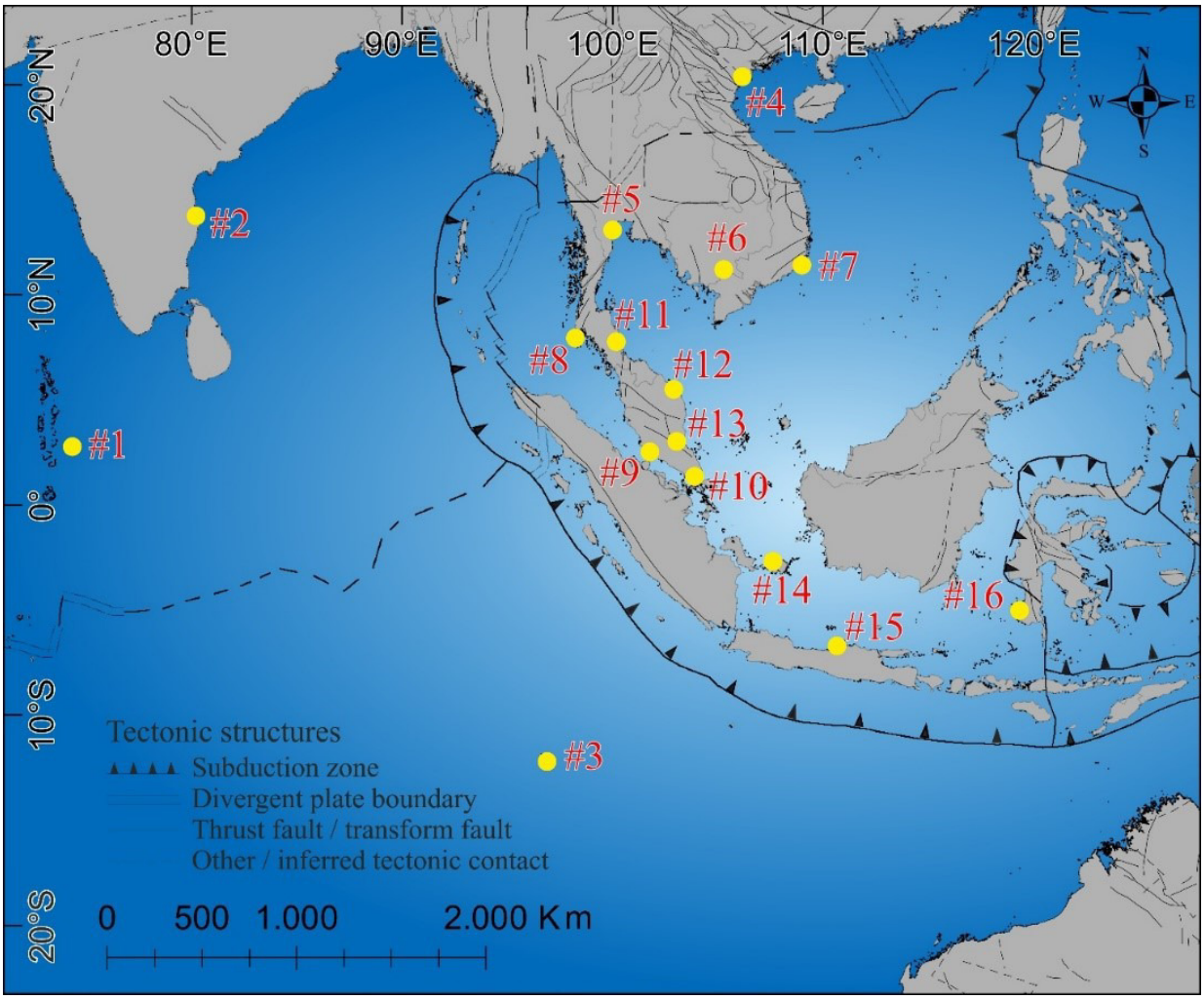

Figure 39: Overview map (modified from Mann et al., 2019b) of the different areas representing geological index points to indicate the Holocene sea-level history. For all locations (yellow dots) GIA predictions from the last 14 ka BP are extracted and compared to the index points to indicate, if the data matches or mismatches with the majority of the model predictions. In Figure 40Figure 53, the blue shades in the panels a) show the probability for the related mismatch between observed RSL elevations and predicted RSL results from GIA models for each region #1 to #16 (red numbers this figure). (Imagery source: Global Self-consistent Hierarchical High-resolution Shorelines from Wessel and Smith (2004).

7.4 Methods

We present 246 sea-level index points from 16 areas in South and Southeast Asia (Figure 39), compared to a set of 54 GIA model outputs from ICE5g, ICE6g (Peltier, 2009; Peltier et al., 2015) and ANICE (De Boer et al., 2015; De Boer et al., 2017). The GIA models are based on the solution of the Sea-Level Equation (Clark and Farrell, 1976; Spada and Stocchi, 2007) and a suite of ice-sheet and solid Earth model combinations. The solid earth models are characterized by a Maxwell viscoelastic rheology and are deformable, self-gravitating, rotating, and radially stratified. Further, the Earth's mantle is divided into two units: Upper (UM) and Lower Mantle (LM). Mantle viscosity profiles were combined with a perfectly elastic lithosphere with thicknesses of 60, 90, or 120 km.

In the first phase of our analysis, the difference between each model run and each observation point is calculated. Then, each percentile gets attributed a probability by a multivariate normal distribution. In order to show the mismatch between GIA models and field data, a discretized canvas is created. Each sea-level index point comprises of two dimensions: age and position of the paleo RSL. Here, each property has associated uncertainties, given in standard deviation of a normal distribution. While the

uncertainty for the RSL is assumed to be symmetric, age uncertainties can be asymmetric in nature. The probability of each percentile of each observation is evaluated for elevation and age, every 0.5 m and 0.25 ka respectively. For a better inter-comparability between the curves, and to take into account that some sites include more observations than others do, we do not re-normalize the graphs, but allow to add 100% of probability for each observation towards each plot. The first part of our analysis is the average probability calculation (APC), where the spread of all probabilities calculated for each index point involved in the related sample set is averaged within the distribution area. It means, probabilities are high, if many index points indicate RSL elevations at a similar level and age as predicted by the majority of the GIA models. For visualization, blue shadings indicate the different probability ranges. If the probabilities are high in a certain time frame, the blue color is limited to a small number of shades. In contrast, if the set of index points shows many different probability-ranges, due to a high variability in the spatio-temporal distribution of the index points, the graph shows a variety of blue shadings. A second step, the probabilities for each index point and the related mismatch for the location of the single index point was calculated, this analysis is called DPC, for detailed probability calculation. The DCP probability is low if the calculated values between sea-level data and models are close to 0% and high if it is close to 100%. Both analyses were compared to indicate if the results are similar or if deviations between the probabilities and indicated mismatches were detected (Figure 40Figure 53). The APC is provided in all figure panels a) and DCP is shown in the panels b).

7.5 Results and Discussion

In In this study, 16 locations (Table 8; Figure 39) provide sea-level index points that are statistically compared to 54 GIA model outputs. Of these 16 datasets, 10 regions (#1, #2, #3, #4, #7, #8, #11, #12, #13, and #15) are comprising of very small datasets (1 to 12 index points) and six locations (#5, #6, #9, #10, #14 and #16) consisting of large datasets with 20 to 45 index points. The probability calculations are based on the APC and DPC in relation to the set of GIA model outputs.

In the APC, the black crosses represent the average mismatch between index points and GIA model results. These were averaged and the spread of all probabilities is displayed in the APC. The average probability for the indicated mismatch between observations and models in the study location is indicated by a dark or light blue shading in the graphs of Figure 40a to 53a, while the scale bar on the right side of the figures presents the spread of all probabilities calculated for each index point within the distribution area. If the scaling number is high and the graph shows a small variety of blue shadings, the variance of included probability-ranges is small, thus index points provide either high or low probability-ranges. In contrast, if the number is small e.g. 0.05 and the graph shows a high variety of blue tones, the included probability-range in this sample set shows many deviations. Additionally, overlapping observations increase the probability at the related location, depending on the calculated probabilities of the points. This also intensifies the blue color at the overlapping position and results in a higher scaling maximum, especially if the remaining samples show significantly lower probabilities. To be clear in all points, we will explain the results of the APC by using the terms high and low certainties, i.e. dark blue or light blue shadings.

The DPC analyzes the probabilities for the related mismatch between each index point and the set of GIA models individually (Figure 40b to 53b). If an index point, including its error bars, is located at or close to the majority of GIA models, the calculated probability for the mismatch is high at the location of this point. The probability is smaller, if it deviates between the error bars. A comparison of the results between both analyses detects, if the APC result can be supported by the DPC or of deviations within the probabilities are detected.

We divide the results into three groups: (1) high probability (ranging from 67% to 100%, DPC) and a high certainty (APC) for the same direction of mismatch, (2) low probabilities (between 17% and 64.5%, DPC) and a low certainty (APC), and (3) divergent probabilities were calculated for the same type of mismatch between the APC and DPC. Divergent results show contrasting results for the same mismatch

direction between both analyses. In the case of significantly differing (average) probabilities for a mismatch derived from the APC and DPC the result implies that only the minority of the GIA models predicted a similar RSL history as the indicators.

The analysis of the APC shows 8 datasets having high certainties (#1, #3, #5, #6, #7, #8, #13 and #15) while the other 8 datasets (#2, #4, #9, #10, #11, #12, #14 and #16) have high uncertainty. In contrast, the DPC indicates 5 regions that show low to medium high probabilities (#4, #9, #10, #11 and #14,) and 11 locations (#1, #2, #3, #5, #6, #7, #8, #12, #13, #15 and #16) that show high probabilities. Comparing the results of both analyses, 8 regions (#1,#3, #5-8, #13 and #15) show high probabilities, 5 areas (#4, #9-11 and #14) show low probabilities and 3 locations (#2, #12 and #16) show divergent probability tendencies.

7. Probability difference analysis between geological sea-level indicators and GIA model predictions

Table 8: Data information of the regions #1 to #16. "Clear" indicates that the probability results between the APC and DPC are similar and unclear indicates deviating probability results between both analyses.

#	Name	Index Points n=	Max Age [a BP]	Min Age [a BP]	Clear	Unclear	Age [a BP]	Elevation [m]	Probability	Index Points per Probability n=	Mismatch positive (p) negative (n)
#1	**Maldives**	3	3445±124	2091±159	X		3445	0.061	100	1	p
							2112 to 2091	0.25	100	2	
#2	**east India**	1	7528±266			X		4.61	100	1	p
#3	**Cocos Keeling**	3	3174±256	2911±233	X		2940 to 2911	0.53	100	2	p
							3174	0.88	100	1	
#4	**Red River Delta (Vietnam)**	7	10376±128	5959±62	X		5959	-0.12	100	1	n
							7517 to 7471	-18.8 to -13	76	2	
							10376 to 9932	-42.07 to -31.57	17	4	
#5	**Chao Phraya delta in the Gulf of Thailand**	20	10554±1963	6635±1021	X		8517 to 6635	-3.38 to 0.65	80	14	n
							10554	-0.42	11	1	
							8497 to 6689	2.23 to 7.27	98	5	
#6	**Mekong River Delta, Vietnam**	45	10348±96	2870±84	X		4124 to 2870	-4.56 to -1.09	79	2	n
							8113 to 5749	-8.76 to -0.06	67	34	
							8354 to 8272	-10.26 to -9.46	18	3	
							10348 to 9113	-27.56 to -18.56	5	6	
#7	**SE Vietnam**	3	1157±100	600±69	X		1157	0.7	100	1	p

							689 to 600	0.7 to 0.68	100	2	
#8	**South Thailand at the Andaman Sea coast**	7	5726±118	1172±86	X		2454 to 1172	-0.4 to -0.1	92	3	fluctuating
							3731 to 2472	0.38 to 0.8	98	3	
							5726	1.5	100	1	
#9	**Strait of Malacca**	23	12348±586	996±265	X		5665 to 2200	1.38 to 5.39	89	6	n
							12348 to 6835; 1046 to 996	-54.37 to 0.51	58	17	
#10	**Singapore**	37	9142±603	132±131	X		6429 to 132	0.95 to 1.75	99.4	5	n
							9142 to 1807	14.49 to 0.7	64.5	32	
#11	**North-eastern area of the Malay-Thai Peninsula**	2	8316±262	7807±193	X		7807	-2.81	84.1	1	n
							8316	-5.52	25.7	1	
#12	**Malaysia east coast**	12	2299±45	845±7		X	913 to 845	-1.68 to -1.52	4.6	2	fluctuating
							2299 to 1218	-1.16 to -0.09	76.7	10	
#13	**Malaysia at the south-eastern coast**	7	6349±66	4408±120	X		4408	2.18	58.8	1	p
							6349 to 4532	3.06 to 3.8	96.5	6	
#14	**Belitung**	25	6772±0	6461±0	X		6772 to 6461	1.18 to 2.94	64.8	25	p
#15	**North Coast of Java**	6	6686±257	5727±222	X		6686 to 5727	1.2 to 1.6	99.7	6	p
#16	**South-west Sulawesi, Makassar**	45	6625±244	37±12		X	6625 to 58	-1.24 to -0.23	98.2	18	fluctuating
							5970 to 37	-0.6 to 0.31	100	27	

1.1 High probabilities

Regions #1, #3 and #7

The datasets from the **Maldives** (**#1**, microatolls, n=3, Kench et al., 2009), **Cocos Keeling (#3**, microatolls, n=3, Woodroffe et al., 1990) and **SE Vietnam** (**#7**, tidal beach and mangrove salt marshes, n=3, Stattegger et al., 2013) contain 3 index points each. Samples from the Maldives date between 3445±124 a BP and 2091±151 a BP and minimum/maximum elevations at 0.061±0.54 and 0.251±0.54 m above MSL, respectively. Index points from Cocos Keeling range in age from 3174±256 a BP to 2911±233 a BP and characterized by minimum/maximum elevations of 0.53±0.52 and 0.88±0.52 m above MSL, respectively. Indicators from SE Vietnam (#7)) have ages ranging from 600±69 a BP to 1157±100 a BP while the RSL is indicated in a range from 0.68±0.8 to 0.7±0.8 m above MSL (Table 8; Figure 40).

The comparison of the probabilities calculated for the entire datasets, shows in area #1 two index points at ~2 ka BP with a high certainty for a positive mismatch while the single index point at ~3.5 ka BP show a lower certainty indicated by light blue shading (Figure 40b). Thus, the probability is higher for a positive mismatch at ~ 2 ka BP, where samples indicate RSL 0.2 m above MSL. This result is similar at #3, where the entire dataset shows a high certainty for a positive mismatch one-thousand years later at ~3 ka BP. RSL in this region is indicated between ~0.5 m and ~0.9 m. These two results are comparable to the calculation of #7, where the comparison between the GIA models and the three index points shows high certainties for two observations indicating a positive mismatch at ~600 a BP and a lower certainty for the single point at ~1 ka BP at the same level. The DPC of all three regions show calculated probabilities of 100%. Therefore, all three areas clearly indicate a high probability that the RSL was 0.2 to ~1 m higher in the Late Holocene than MSL. Nevertheless, as these studies are based on only 3 index points per dataset, more data is needed to support this result and to detect the RSL history for the mid and early Holocene in these locations.

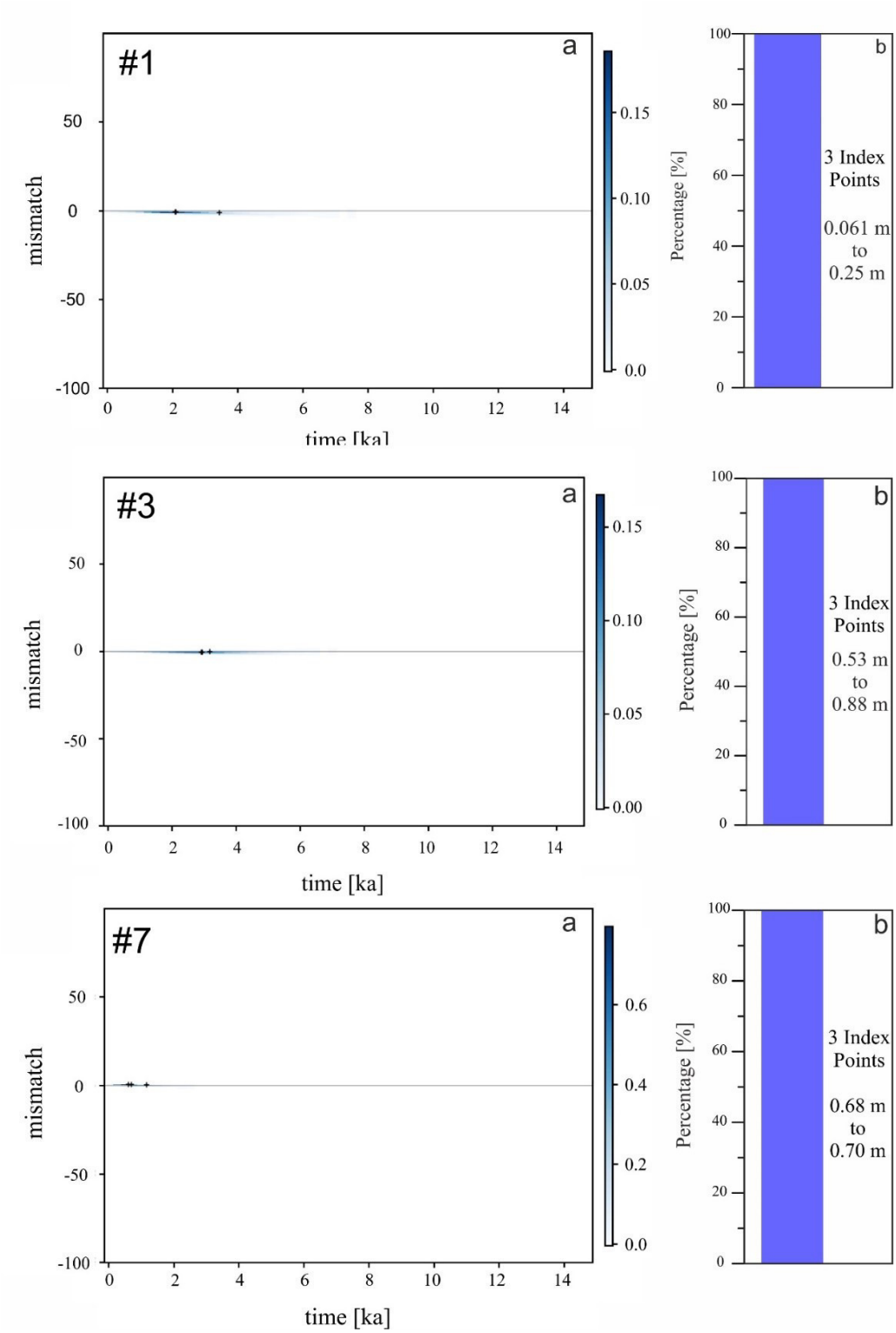

Figure 40: High probability results of the regions #1, #3 and #7 and each sample set includes 3 index points. a) The APC results display high certainties (blue shadings) for each region; black crosses are the average mismatch RSL elevation indicated by index points in relation to the RSL predicted by the set of GIA models. b) The DPC analysis shows, a 100% probability for all index points in each region, supporting the APC result. Right scale in a) and left scale in b) display both the percentage calculated of the involved index points in both analyses. The blue scale in a) shows the average variety in the probability-range [%] of all index points spread over the distribution area, and indicates high probabilities with a dark blue shading and lower probabilities with lighter blue shadings. The scale in b) shows the calculated probability-range for the included index points at its location. The number at the bar in b) indicates the elevation-range [m] of the index points and the number of included samples in the sample set.

Region #5

The **Chao Phraya delta in the Gulf of Thailand** (Figure 39#5) includes 20 index points based on peat from a mangrove salt marsh (Somboon and Thiramongkol, 1992) between 10554±1963 a BP and 6635±1021 a BP that indicate the paleo RSL range from 3.38±0.74 to 7.27±1.05 m (Table 8). The set of GIA models predict a slightly higher RSL than most of the field data.

Focusing on the APC, the certainty for a negative mismatch is high, indicated by 75% (15 of 20) of the index points. The remaining 25% of the observations show a positive mismatch, which is calculated to be less certain. In general, the probability for a mismatch is low between 6 ka BP and today as well as within the time frame from 14 ka BP to 9 ka BP. The DPC analysis shows that 70% (14 of 20 samples) of the index points show a negative mismatch with a probability of 80% between 8.5 ka BP and 6.6 ka BP. Within this time frame, RSL elevations are ranging from -3.38 to 0.65 m. However, five of 20 index points indicate a positive mismatch between 8.5 ka BP and 6.6 ka BP in a range from 2.23 to 7.27 m. The calculated average probability is 98%. One index point at 10.5 ka BP shows a positive mismatch with the models at an elevation of -0.42 m and is considered an outlier. The probability for this mismatch is 11%.

Based on the average probabilities calculated for the positive and negative mismatches, and on the number of samples indicating a related mismatch, both analyses show similar high probabilities for a negative mismatch (Figure 41). One reason for the data accumulation below MSL could be subsidence due to the sample originating from a delta.

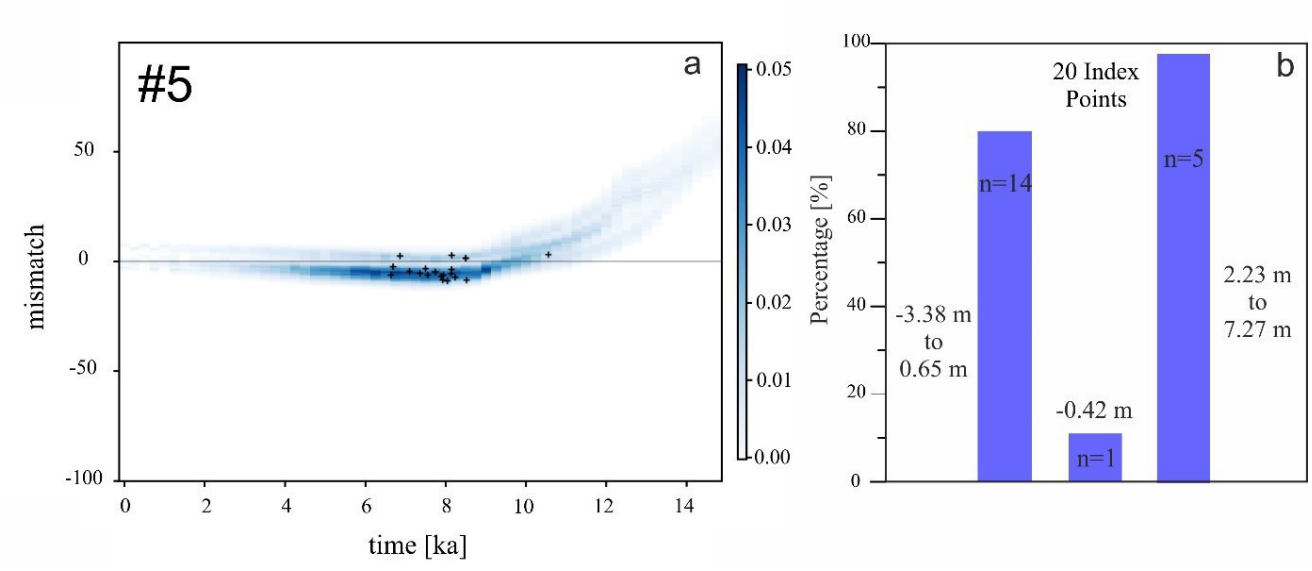

Figure 41: High probability results of region #5. The sample set includes 20 index points. a) The APC results display high certainties (blue shadings) and black crosses indicate the average mismatch of RSL elevations derived from index points in relation to the RSL predicted by the set of GIA models. b) The DPC analysis shows the probabilities for the 20 index points of the region, while the details are explained in the text. Right scale in a) and left scale in b) display the percentage calculated of the involved index points in both analyses. The blue scale in a) shows the average variety in the probability-range [%] of all index points spread over the distribution area, and indicates high certainties with a dark blue shading and lower certainties with lighter blue shadings (i.e. high uncertainties). The scale in b) shows the calculated average probabilities derived from each index point individually. The average was re-calculated to better show the probabilities for the indicated type of mismatch, derived from the index point positions. Numbers at the bars in b) indicate the elevation-ranges of the index points, while n= indicates the number of index points included in the elevation-range.

Region #6

The field data from the **Mekong River Delta, Vietnam (**Figure 39#6) contains 45 index points, derived from sediments, plant remains, charcoal, wood, oysters and diatom assemblages indicating a mangrove salt marsh, an intertidal mudflat, and a tidal beach (Tamura et al., 2007; Tamura et al., 2009; Hanebuth et al., 2012). Sample ages range from 10348±96 a BP to 2870±84 a BP indicating the RSL minimum/ maximum, at respectively, -27.6±0.47 and -0.06±0.31 m (Table 8). The GIA models indicate the RSL slightly higher than most of the field data.

Based on the APC, the calculated certainty for a negative mismatch is high, for 75.5% (34 of 45 samples) of the index points between 8.1 ka BP and 5.7 ka BP. In contrast, in the time frame from ~5 ka BP to 2.8 ka BP, (n=2; 4%) and between 8.3 ka BP and 8.2 ka BP (n=3; 6%) the negative mismatch is uncertain. However, 13.3% (6 of 45 index points) of the samples dating between 10.3 ka BP and 9.1 ka BP show the highest uncertainties for the negative mismatch. Thus, a negative mismatch in the Mid to Early Holocene is highly certain, while it is uncertain in the Mid to Late Holocene. Furthermore, the DPC shows an average probability of 67% for a negative mismatch indicated by 34 (75.5%) index points, locating RSL between -8.76 to -0.06 m (8.1 ka BP and 5.7 ka BP). In contrast, an average probability of 79% for a negative mismatch is calculated for two samples (4%) indicating RSL ranging from -4.56 to -1.09 m (2.8 ka BP and 4.1 ka BP). Low average probabilities, 18% and 5%, were calculated for an RSL range from -10.26 and -9.76 m (n=3, 18%) between 8.3 ka BP to 8.2 ka BP and for RSL elevations from -27.56 to -18.56 m below today (10.3 ka BP to 9.1 ka BP; n=6, 5%). Thus, the probability for an RSL below -9 m in the Early Holocene is unlikely (Figure 42) and, the DPC and APC show that more than 70% of the sample set indicate high certainties for the negative mismatch in the Mid to Late Holocene.

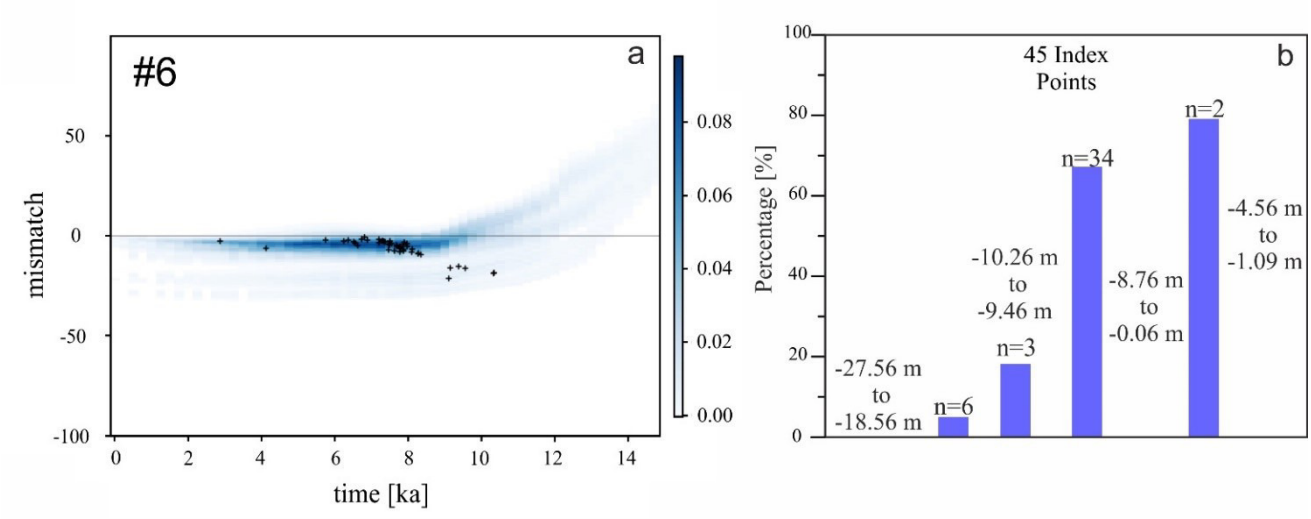

Figure 42: High probability results of region #6 and the sample set includes 45 index points. a) The APC results display high certainties (blue shadings) and black crosses indicate the average mismatch RSL elevation derived from index points in relation to the RSL predicted by the set of GIA models. b) The DPC analysis shows the probabilities for the 45 index points of the region, while the details are explained in the text. Right scale in a) and left scale in b) display the percentage calculated of the involved index points in both analyses. The blue scale in a) shows the average variety in the probability-range [%] of all index points spread over the distribution area, and indicates high certainties with a dark blue shading and lower certainties with lighter blue shadings (i.e. high uncertainties). The scale in b) shows the calculated average probabilities derived from each index point individually. The average was re-calculated to better show the probabilities for the indicated type of mismatch, derived from the index point positions. Numbers at the bars indicate the elevation-ranges of the index points, while n= indicates the number of included index points within the elevation-ranges.

Region #8

The region of the **South Thailand / Andaman Sea** coast contains 7 index points (oyster belts of *saccostrea cucullata*; Scheffers et al., 2012) with ages from 5726±118 a BP to 1172±86 a BP, and indicate RSL between -0.4±1.89 and 1.5±1.89 m above MSL (Table 8). The comparison of GIA models and the APC shows a high uncertainty for the time frame between 14 ka BP and ~5 ka BP, where one index point is located at 5.7 ka BP. Samples between 3731 a BP and 2472 a BP show higher certainties for slight a positive mismatch. The highest certainty for a slight negative mismatch within the error bars between 2454 a BP and 1172 a BP. Thus, based on the APC, a slight fluctuating mismatch within the error bars of ~±0.5 m is certain.

The DPC shows high probabilities for all indicators, while the outlier sample at 5726 a BP indicating RSL at 1.5 m above MSL shows the highest probability of 100%. The average probability of the three index points between 3731 a BP and 2472 a BP is 98% and indicates RSL between 0.38 and 0.8 m. For the three samples indicating RSL between -0.4 and -0.1 m (2.4 ka BP to 1 ka BP) the probability is 92% (Figure 43). Thus, derived from the DPC, a positive mismatch is slightly more probable than a negative one. Nevertheless, both types of mismatches indicated by the DPC, show probabilities close to 95%, and therefore match the result provided by the APC. Both analyses locate the RSL elevations within a range of ~± 0.5 m compared MSL. The only exception is the high probability calculated for the index point at ~5.7 ka BP that is at odds with the APC analysis. More data is needed to precisely locate RSL in the mid to early Holocene in this region and to clarify if the probability calculated for the index point at 5.7 ka BP is certain.

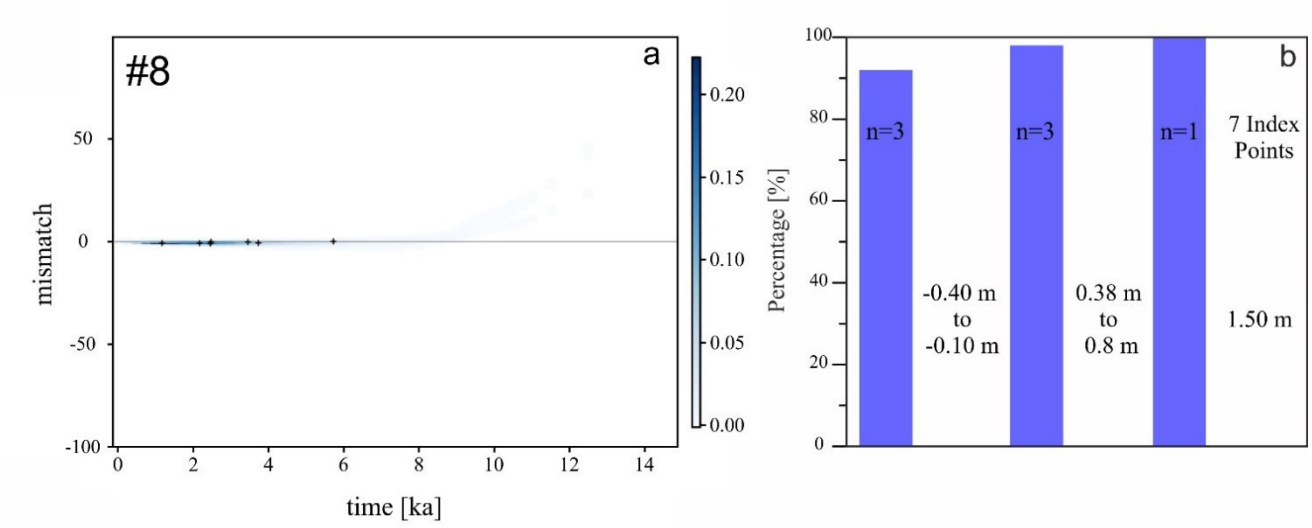

Figure 43: The sample set includes 7 index points. High probability results of region #8. a) The APC results display high certainties (blue shadings) and black crosses indicate the average mismatch RSL elevation derived from index points in relation to the RSL predicted by the set of GIA models. b) The DPC analysis shows the probabilities for the 7 index points of the region, while the details are explained in the text. Right scale in a) and left scale in b) display the percentage calculated of the involved index points in both analyses. The blue scale in a shows the average variety in the probability-range [%] of all index points spread over the distribution area, and indicates high certainties with a dark blue shading and lower certainties with lighter blue shadings (i.e. high uncertainties). The scale in b) shows the calculated average probabilities derived from each index point individually. The average was re-calculated to better show the probabilities for the indicated type of mismatch, derived from the index point positions. Numbers at the bars indicate the elevation-ranges of the index points and the number of the entirely included samples.

Region #13

Samples from pollen and diatoms indicating a mangrove salt marsh compiled along the south-eastern Malaysian coast, in Kelang and Kuantan (Figure 39#13) (n=7, Kamaludin, 2001) show ages between 4408±120 a BP and 6349±66 a BP and RSL elevations ranging from 2.18±1 to 3.8±1.23 m (Table 8). The APC in region #13 shows a high certainty for a positive mismatch between 7 ka BP to 2.5 ka BP. This mismatch is calculated to be uncertain between 14 ka BP and 7 ka BP as well as between 2.5 ka BP and today. The DPC shows for 6 of 7 samples similar results with RSL locations between 3.06 and 3.80 m in the time frame from 6349 a BP to 4532 a BP. The calculated probability for this positive mismatch is 96.5% on average. Only one sample (at 4408 a BP) locates the RSL ~1 m lower (2.18 m) than the rest of the data and has a calculated probability of 58.8%. Thus, apart from the sample at 4408 a BP, which is an outlier (Figure 44), the result from area #13, shows a high probability for a slight positive mismatch in both analyses.

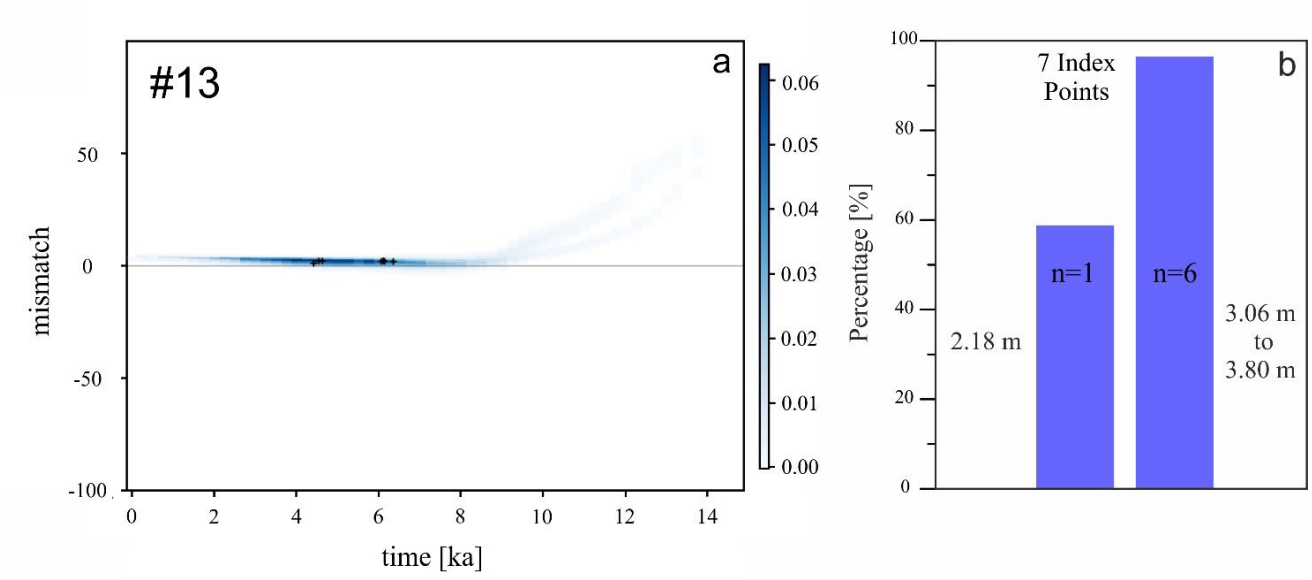

Figure 44: High probability results of region #13 and the sample set includes 7 index points. a) The APC results display high certainties (blue shadings) and black crosses indicate the average mismatch RSL elevation derived from index points in relation to the RSL predicted by the set of GIA models. b) The DPC analysis shows the probabilities for the 7 index points of the region, while the details are explained in the text. Right scale in a) and left scale in b) display the percentage calculated of the involved index points in both analyses. The blue scale in a) shows the average variety in the probability-range [%] of all index points spread over the distribution area, and indicates high certainties with a dark blue shading and lower certainties with lighter blue shadings (i.e. high uncertainties). The scale in b) shows the calculated average probabilities derived from each index point individually. The average was re-calculated to better show the probabilities for the indicated type of mismatch, derived from the index point positions. Numbers at the bars indicate the elevation-ranges of the index points and n= indicates the number of samples included in the elevation-ranges.

Region #15

The **north coast of Java** dataset (n=6, Azmy et al., 2010) contains microatoll ages between 5727±222 a BP and 6686±257 a BP and RSL elevations ranging from 1.2±0.52 to 1.6±0.52 m (Table 8). Both models and index points indicate the RSL higher than MSL, 1.2 and 1.6 m respectively. The calculated probability for this positive mismatch is high for both the APC and DPC. The APC shows a high certainty in the time frame from 8 ka BP to 4 ka BP. However, the uncertainty is high from 14 ka BP to 8 ka BP and between 4 ka BP to today as there is no field data available. Further, the DPC supports the clear result of the APC, and shows an average probability of 99.7% for the slight positive mismatch, in a range from 1.2 and 1.6 m, between 5.7 ka BP and 6.6 ka BP, respectively (Figure 45). Therefore, both probability calculations show a high probability for a positive mismatch in this region, with more data

needed for the late and early Holocene to widen the RSL history and support this agreement between GIA models and field data.

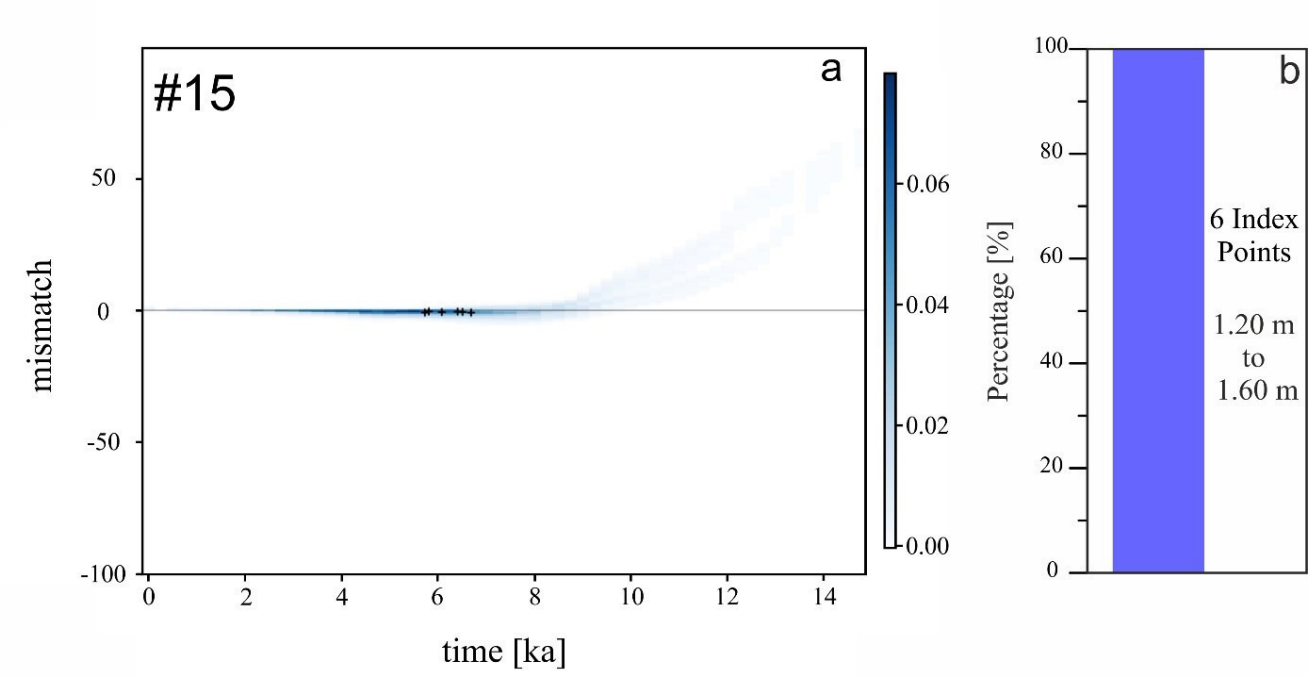

Figure 45: High probability results of region #15 and the sample set includes 6 index points. a) The APC results display high certainties (blue shadings) and black crosses indicate the average mismatch RSL elevation derived from index points in relation to the RSL predicted by the set of GIA models. b) The DPC analysis shows the probabilities for the 6 index points of the region, while the details are explained in the text. Right scale in a) and left scale in b) display the percentage calculated of the involved index points in both analyses. The blue scale in a) shows the average variety in the probability-range [%] of all index points spread over the distribution area, and indicates high certainties with a dark blue shading and lower certainties with lighter blue shadings (i.e. high uncertainties). The scale in b) shows the calculated average probability derived from each index point individually. The average was re-calculated to better show the probabilities for the indicated type of mismatch, derived from the index point positions. Numbers at the bar indicates the elevation-ranges of the index points and the number of the entirely included samples.

1.2 Low probabilities

Region #4

In In the **Red River Delta (Vietnam) (**Figure 39#4**)**, seven index points (Tanabe et al., 2003a; Tanabe et al., 2003b; Hori et al., 2004), sampled from sediment cores of peaty mangrove salt marshes and intertidal mudflats date ages between 10376±128 a BP and 5959±62 a BP. The samples indicate the RSL minimum/maximum at -42.07±1.05 and -0.12±1.05 m respectively (Table 8), with GIA models predicting a higher RSL than the index points.

The APC analysis shows that the negative mismatch is divided into three sections, where each section shows similar high uncertainties between 11 ka BP and 3 ka BP, which is the broader time frame of the data locations. Uncertainties are even higher between14 ka BP and 11 ka BP and between 3 ka BP and today. In contrast, the DPC analysis shows a calculated average probability of 17% for four samples indicating the RSL between -42.07 m (10.3 ka BP) and -31.57 m (9.9 ka BP), respectively. An average probability of 76% is calculated for two samples at ~7.5 ka BP that predict the RSL ranging from -18.8 to -13.0 m, while a probability of 100% is derived from the single sample at 5.9 ka BP locating the RSL at -0.12 m (Figure 44). Thus, in contrast to the APC, the DPC clearly indicates a higher average probability for the RSL to be located between -18.8 and -0.12 m in the Early to Mid-Holocene

and a significantly lower average probability of 17% for RSL elevations between 10.3 ka BP and 9.9 ka BP (Figure 46).

The majority of the GIA models show significantly different RSL histories than the field data, and therefore the probability for this negative mismatch between ~6 ka BP and ~11 ka BP is consistently low. As the data points were extracted from drill cores in a delta, subsidence or sediment compaction due to continuous sediment loading could be the reason for these elevations however the sample set is too small to fully explain this result. Nevertheless, based on the DPC, the RSL elevations between -0.12 and -18.8 m are more certain than a lower RSL position. To detect if the deviating sample elevations are based on subsidence or compaction, a detailed study of the samples is necessary.

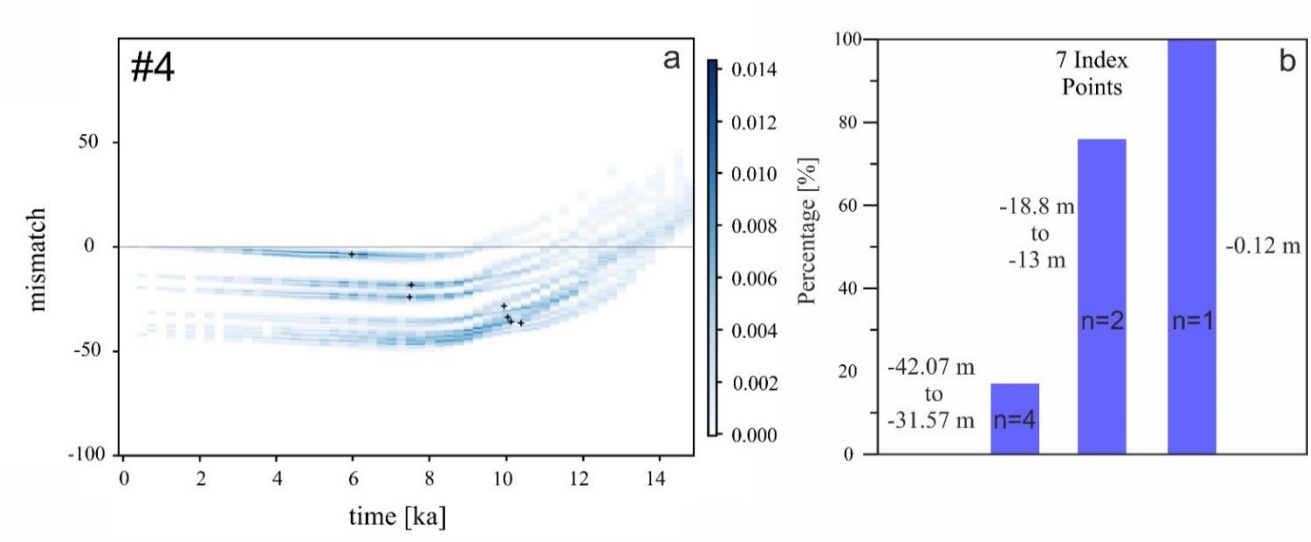

Figure 46: Low probability results of region #4 and the sample set includes 7 index points. a) The APC results display high uncertainties (light blue shadings) and black crosses indicate the average mismatch RSL elevation derived from index points in relation to the RSL predicted by the set of GIA models. b) The DPC analysis shows the probabilities for the 7 index points of the region, while the details are explained in the text. Right scale in a) and left scale in b) display the percentage calculated of the involved index points in both analyses. The blue scale in a) shows the average variety in the probability-range [%] of all index points spread over the distribution area, and indicates high certainties with a dark blue shading and lower certainties with lighter blue shadings (i.e. high uncertainties). The scale in b) shows the calculated average probabilities derived from each index point individually. The average was re-calculated to better show the probabilities for the indicated type of mismatch, derived from the index point positions. Numbers at the bars indicate the elevation-ranges of the index points and n= indicates the number of included samples within the elevation-rang.

Region #9

Area 9 (Figure 39 #9) is located in the **Strait of Malacca** and contains 23 index points (peat from a mangrove salt marsh; Geyh et al., 1979) with ages ranging from 12348±586 a BP to 996±265 a BP. RSL elevations are indicated between -54.37±0.94 m and 5.39±0.73 m (Table 8) and the set of GIA models indicate RSL between the minimum and maximum elevations of the samples set. The APC of the dataset (Geyh et al., 1979) shows high uncertainties for all elevations and ages, with two index points at ~1 ka BP showing a slightly higher certainty for this very small negative mismatch. The DPC shows a positive mismatch with an average probability of 89%, which is supported by 26% of the index points (n=6). These samples indicate the RSL between 1.38 m and 5.39 m above MSL (5.6 ka BP to 2.2 ka BP). In contrast, 74% of the index points (n=17) dated from 12348 a BP to 6835 a BP and from 1046 to 996 a BP, show an average probability of 58% for a negative mismatch between -54.7 m and 0.61 m (Figure 47).

Thus, due to the range of calculated probabilities for the negative mismatch, the result is less probable. Here, the negative mismatch and the low probability result could be attributed to the samples being

mangrove wood and peat, which could be affected by compaction. However, the positive mismatch is more certain but indicated by a smaller probability variability. This alternating mismatch pattern combined with low probabilities indicates that post-depositional movements may have affected this study site. Another aspect, as mentioned by Kamaludin (2002), could be a misinterpretation of the data due to missing an analysis of the biostratigraphy of the sample area. Apart from this, deviations between predicted and observed RSL are also possible. This is indicated in the very Late Holocene, where two index points at ~1 ka BP show slightly higher results in the APC and significantly higher results in the DPC for the mismatch in elevations between -1.67 and -1.52 m below MSL. Furthermore, samples in the Mid to Early Holocene indicating RSL more than 2 to 5 m above MSL also show high probabilities in the DPC. Consequently, at limited number of the set of GIA models seems to agree with these samples, while the majority of the models seems to predict higher RSL elevations.

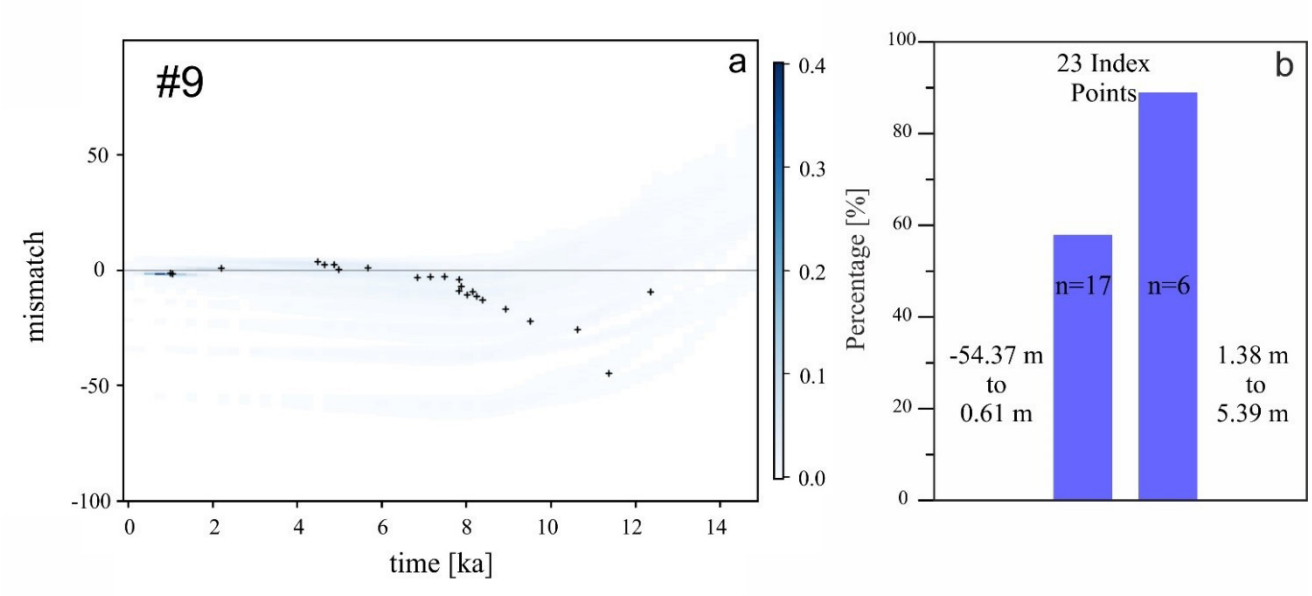

Figure 47: Low probability results of region #9 and the sample set includes 23 index points. a) The APC results display high uncertainties (light blue shadings) and black crosses indicate the average mismatch RSL elevation derived from index points in relation to the RSL predicted by the set of GIA models. b) The DPC analysis shows the probabilities for the 23 index points of the region, while the details are explained in the text. Right scale in a) and left scale in b) display the percentage calculated of the involved index points in both analyses. The blue scale in a) shows the average variety in the probability-range [%] of all index points spread over the distribution area, and indicates high certainties with a dark blue shading and lower certainties with lighter blue shadings (i.e. high uncertainties). The scale in b) shows the calculated average probabilities derived from each index point individually. The average was re-calculated to better show the probabilities for the indicated type of mismatch, derived from the index point positions. Numbers at the bars indicate the elevation-ranges of the index points and n= indicates the number of included samples in the elevation-range.

Region #10

This study from **Singapore** (Figure 39#10) contains 37 index points based on oysters, wood, peat from *Nypa fruticans,* and shells collected from different sediments cores (Hesp et al., 1998; Bird et al., 2007; Bird et al., 2010). The field data shows dated ages from 9142±603 a BP to 132±131 a BP and indicates RSL elevations ranging from -14.49±1.17 to 1.75±0.66 m (Table 8). Here, the GIA models consistently predict higher RSL values than the field data.

The APC provides a high uncertainty range for all ages and elevations. Based on this analysis the certainty for a negative or a positive mismatch is equally low. In contrast, the DPC provides an average probability of 99.4% for a slightly positive mismatch between 6429 a BP and 132 a BP (13.5% samples of the data set) locating RSL between 0.95 and 1.75 m above MSL. Contrary to the positive mismatch, 86.5% of the data points (n=32) dated between 2.4 ka BP and 1.8 ka BP and from 9.1 ka BP to 6.1 ka BP

show a negative mismatch in elevations from -14.49 to 0.70 m below and above MSL. The resulting probability is 64.5% (Figure 48).

However, a high probability on average of 92.6 % was calculated for RSL elevations between -2.5 and 2 m (n=21, 56.7%). This result is probably caused by the dated material originating from mangrove salt marshes and intertidal mudflats as in fact, 94% of the samples indicating the RSL significantly lower than the GIA models are derived from wood and shells from an intertidal mudflat (15 of 16 samples), with one sample coming from a mangrove salt marsh (wood). In contrast, 86% (18 of 21 samples) of the samples indicating the RSL between -2.5 and 2 m are mangrove wood and peat from *Nypa fructicans* (a mangrove species). The remaining 14% (3 samples) are derived from wood with tidal mudflat origin. Therefore, the reason for the negative mismatch could be explained by natural subsidence due to sediment compaction.

However, due to the high uncertainties detected by the APC and high probabilities calculated in the DPC for a mismatch, this sample set needs further analysis to properly elucidate the cause of this high uncertainty. Both regions #10 and #9 show similar probability results for a negative mismatch and high uncertainties in the APC. It is less probable that both datasets have interpretation inconsistencies even though mangrove peat is part of both sample sets. Therefore, both results are probably based on significantly different GIA model predictions, where the majority of the models mismatching with the data, fall within a large range. The medium probabilities calculated in the DPC for some field data RSL elevations seem to be comparable with only a limited number of the RSL predictions from the models. Thus, the GIA models predict a higher RSL than the field data and as detected by the DPC, particularly within the elevation range of -2.5 to 2 m. Therefore, it can be argued that the low probabilities are more strongly influenced by the higher RSL elevations predicted by GIA, than supposed by field RSL data.

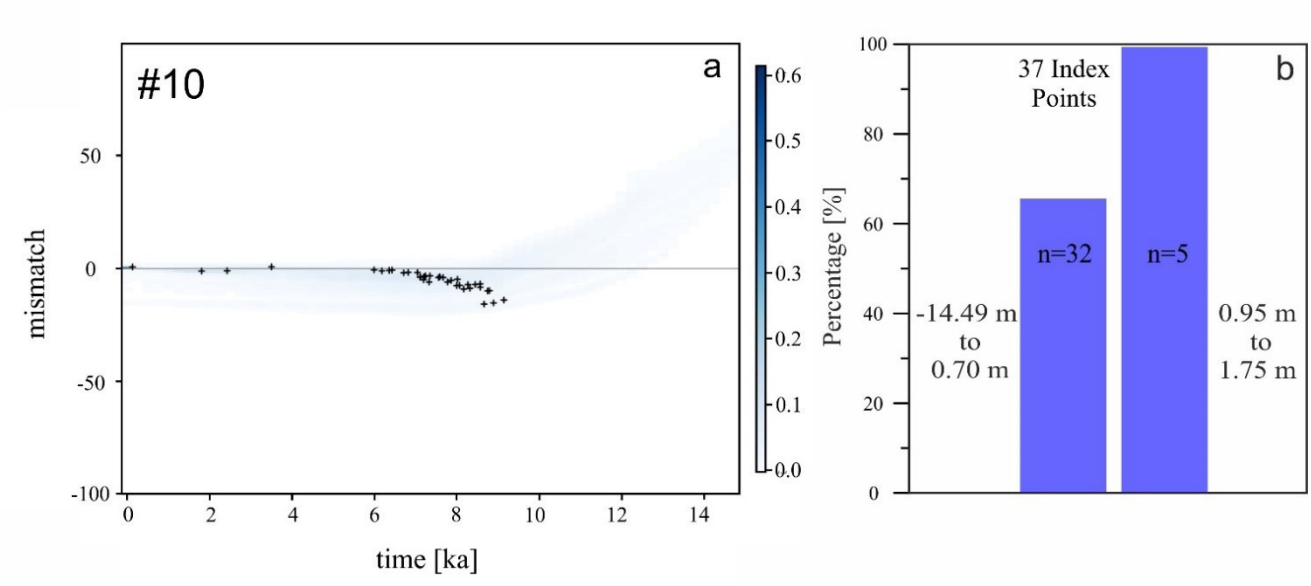

Figure 48: Low probability results of region #10, and the sample set includes 37 index points. a) The APC results display high uncertainties (light blue shadings) and black crosses indicate the average mismatch RSL elevation derived from index points in relation to the RSL predicted by the set of GIA models. b) The DPC analysis shows the probabilities for the 37 index points of the region, while the details are explained in the text. Right scale in a) and left scale in b) display the percentage calculated of the involved index points in both analyses. The blue scale in a) shows the average variety in the probability-range [%] of all index points spread over the distribution area, and indicates high certainties with a dark blue shading and lower certainties with lighter blue shadings (i.e. high uncertainties). The scale in b) shows the calculated average probabilities derived from each index point individually. The average was re-calculated to better show the probabilities for the indicated type of mismatch, derived from the index point positions. Numbers at the bars indicate the elevation-ranges of the index points and n= indicates the number of included samples within the elevation-range.

Region #11

Thale Noi (Figure 39#11) is located in the **north-eastern area of the Malay-Thai Peninsula.** The sample set consists of two index points derived from clay and macrofossils characteristic of a high salt marsh environment (peat and organic mud; Horton et al., 2005). Related ages are 7807±193 a BP and 8316±262 a BP with RSL is indicated between -2.80±0.52 and -5.52±0.52 m (Table 8). The set of GIA models predict a higher RSL for this time frame than the samples.

The results of the APC analysis are medium high for a slight negative mismatch, indicated by a fluctuation between lower and higher uncertainties between 8.5 ka BP and 6 ka BP, while the index points are located at around 8 ka BP. The uncertainty for this result is higher between 14 ka BP and ~9 ka BP and from ~3.5 ka BP to present. In contrast, the DPC analysis for the index point at 7807 a BP with an elevation of 2.81 m shows a probability of 84.1% for the negative mismatch. This is higher than the probability of 25.7% calculated for the second data point at 5.52 m (8316 a BP) (Figure 49). Therefore, both analyses show a medium high result.

The reason for the different probabilities between the two samples is probably based on the sample origin as the RSL position at -2.81 m is derived from peat while the second RSL location is derived from organic mud. However, to detect if one of the samples or both were affected by compaction that could have affected the sample elevations, more data is needed to compare the result.

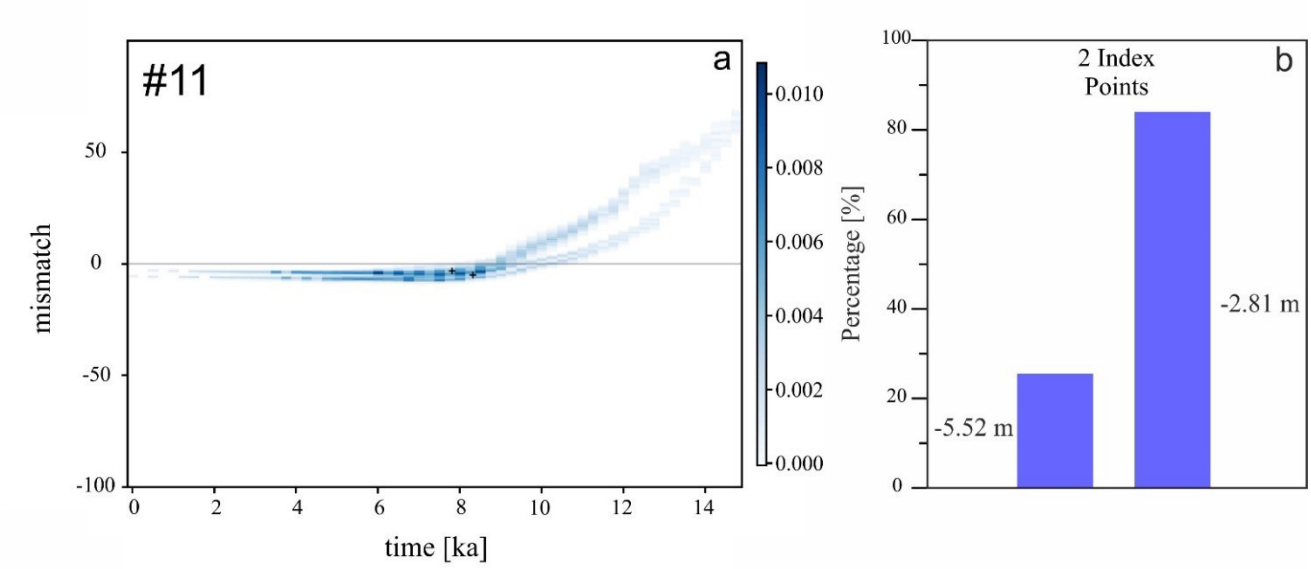

Figure 49: Low probability results of region #11 and the sample set includes 2 index points. a) The APC results display high uncertainties (light blue shadings) and black crosses indicate the average mismatch RSL elevation derived from index points in relation to the RSL predicted by the set of GIA models. b) The DPC analysis shows the probabilities for the 2 index points of the region, while the details are explained in the text. Right scale in a) and left scale in b) display the percentage calculated of the involved index points in both analyses. The blue scale in a) shows the average variety in the probability-range [%] of all index points spread over the distribution area, and indicates high certainties with a dark blue shading and lower certainties with lighter blue shadings (i.e. high uncertainties). The scale in b) shows the calculated average probabilities derived from each index point individually. The average was re-calculated to better show the probabilities for the indicated type of mismatch, derived from the index point positions. Numbers at the bars indicate the elevation-ranges of the index points.

Region #14

Belitung (Figure 39#14) contains 25 index points derived from microatoll die-downs (Meltzner et al., 2017) with ages dated between 6461±0 a BP and 6772±0 a BP and RSL elevations ranging from 1.18±0.56 to 2.94±0.64 m (Table 8). The sample set shows a positive mismatch with the GIA models.

The APC analysis shows medium high certainties, and the DPC result for this positive mismatch is 64.8% at average. Thus, the result of both analyses is medium well (Figure 50). As the spatially and

temporally distribution of the samples is very limited more data is needed to expand the range of RSL index points, to widen the RSL history for all other time steps apart ~6.5 ka BP in this region.

.

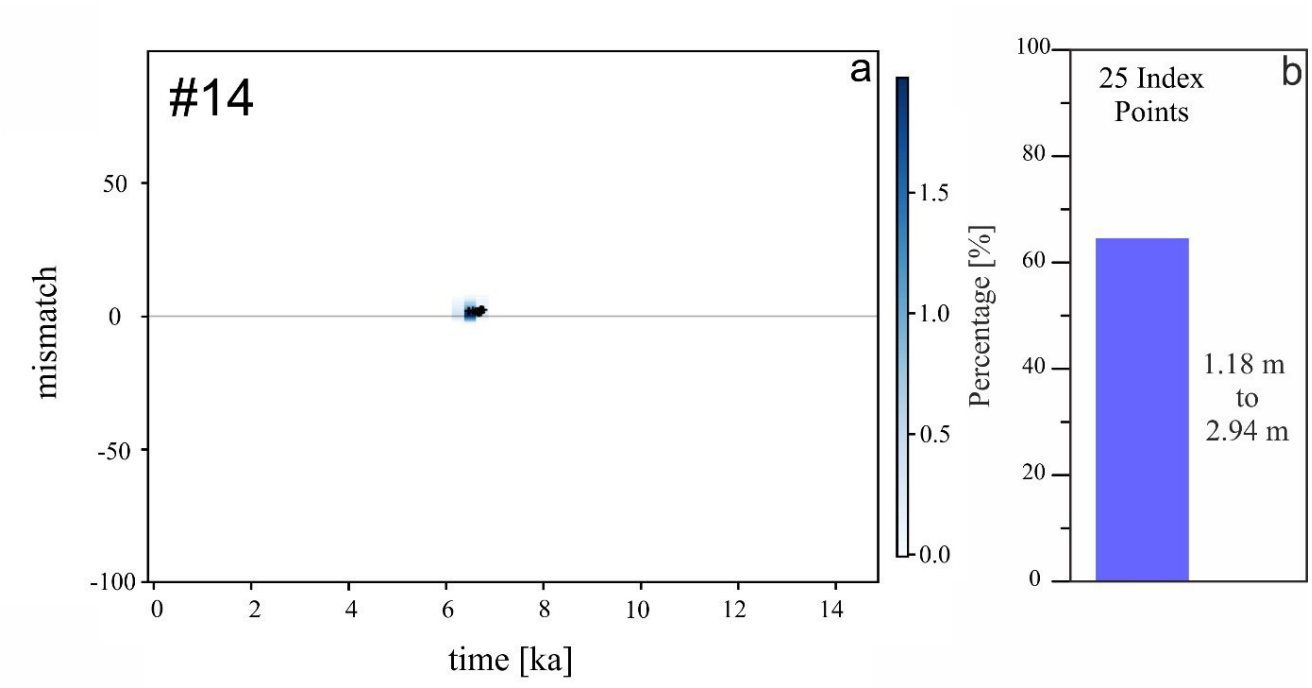

Figure 50: Low probability results of region #14 and the sample set includes 25 index points. a) The APC results display high uncertainties (light blue shadings) and black crosses indicate the average mismatch RSL elevation derived from index points in relation to the RSL predicted by the set of GIA models. b) The DPC analysis shows the probabilities for the 25 index points of the region, while the details are explained in the text. Right scale in a) and left scale in b) display the percentage calculated of the involved index points in both analyses. The blue scale in a) shows the average variety in the probability-range [%] of all index points spread over the distribution area, and indicates high certainties with a dark blue shading and lower certainties with lighter blue shadings (i.e. high uncertainties). The scale in b) shows the calculated average probabilities derived from each index point individually. The average was re-calculated to better show the probabilities for the indicated type of mismatch, derived from the index point positions. Numbers at the bar indicates the elevation-range of the index points.

1.3 Deviating results between APC and DPC

Region #2

The area of **East India** (Figure 39#2) (Vaz and Banerjee, 1997) contains only one index point at 7528±266 ka BP from mangrove peat, that indicates the RSL at 4.61±0.63 m above MSL (Table 8) and the GIA model outputs predict a slightly lower RSL than the index point.

The positive mismatch derived from the APC for the time frame from 14 ka BP to ~9.5 ka BP and from 6 ka BP to present is considered to be uncertain, while there is a less uncertainty calculated for frame the broader time frame from ~9 ka BP to 6 ka BP, in which the index point is located. In contrast, the DPC result is 100% for a positive mismatch (Figure 51). Thus, the APC and DPC show a medium reliability and high probability, respectively. To demonstrate whether this calculation is reliable, more sea-level data is needed to further elaborate on this result. Nevertheless, due to the medium well result of the APC and the high probability calculated in the DPC, at least a limited number of models seem to predict a comparable RSL to that of the index point.

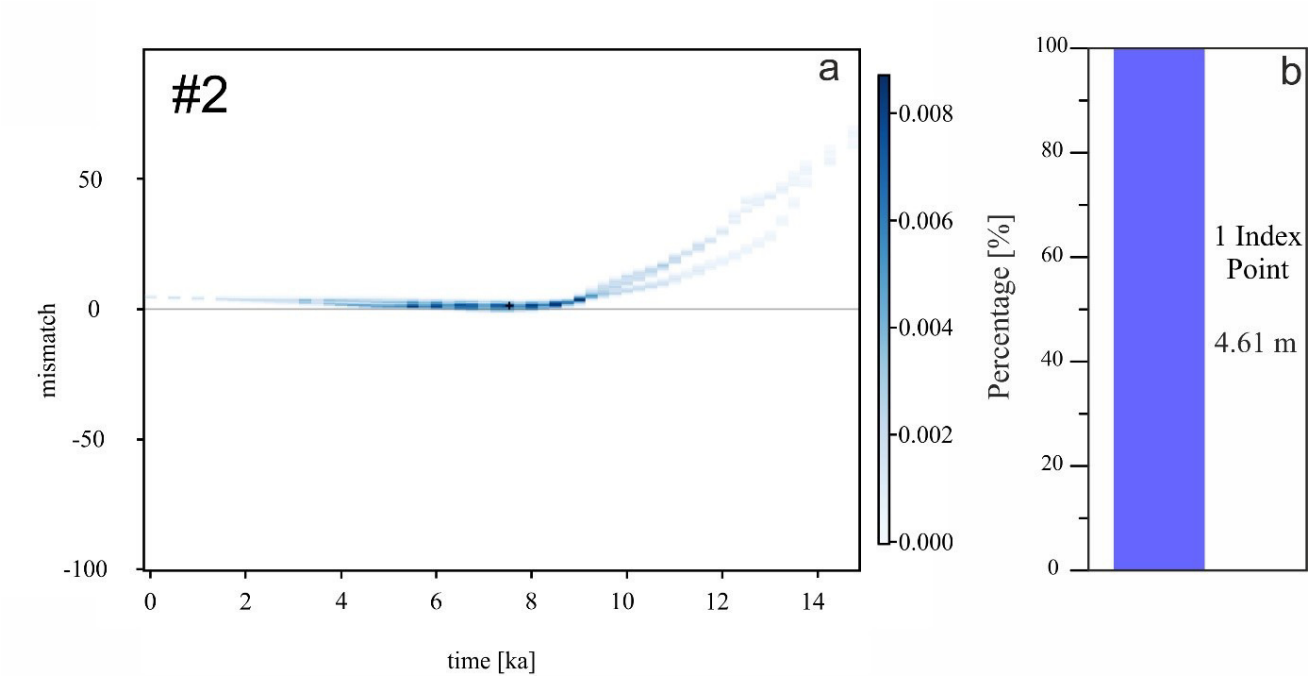

Figure 51: The sample set includes 1 index points and a deviating probability result of region #2. a) The APC results display high uncertainties (light blue shadings) and black crosses indicate the average mismatch RSL elevation derived from index points in relation to the RSL predicted by the set of GIA models. b) The DPC analysis shows the probability for 1 index point in the region. Right scale in a) and left scale in b) display the percentage calculated of the involved index points in both analyses. The blue scale in a) shows the average variety in the probability-range [%] of all index points spread over the distribution area, and indicates high certainties with a dark blue shading and lower certainties with lighter blue shadings. The scale in b) shows the calculated probability of the single index point. Numbers at the bar indicate the elevation of the index point and the number of the entirely included samples.

Region #12

The dataset collected along the **Malaysia east coast** (Figure 39#12) consists of 12 index points from pollen within mangrove peat, *Nypa* swamp and Lagoon swamp (Tam et al., 2018). Dated ages vary from 2299±45 a BP to 845±7 a BP. The RSL within this time frame is indicated between -1.68±0.87 and -0.09±0.87 m (Table 8). The set of model outputs show slightly higher elevations between 1000 a BP and 800 a BP and between 2299 a BP and 1218 a BP.

Samples located between 2299 a BP and 1218 a BP (n=10) have high uncertainties in the APC for a slight fluctuation from a consensus to a very slight negative mismatch for. In contrast, the uncertainty is low between ~1.2 ka BP and 845 a BP. Contrary to the APC the DPC shows an average probability of 76.7 % for 10 of 12 index points between 2299 a BP and 1218 a BP indicating the RSL between -1.16 m and -0.09 m below MSL. The remaining two of 12 samples indicate the RSL lower than -1.52 m, and show an average probability of 4.6 % (Figure 52).

Thus, the APC shows a 100% contrasting result compared to the DPC. Due to similar elevations at different ages but within a close time frame, the deviation between GIA models and field data cannot be explained by tectonic movement or subsidence/uplift alone. The low APC probabilities indicates the possibility that the majority of GIA models predict completely deviating RSL elevations from that of the field data. At least one model prediction appears to predict comparable RSL elevations to the samples at the individually observed RSL location, based on the high probabilities of the DPC.

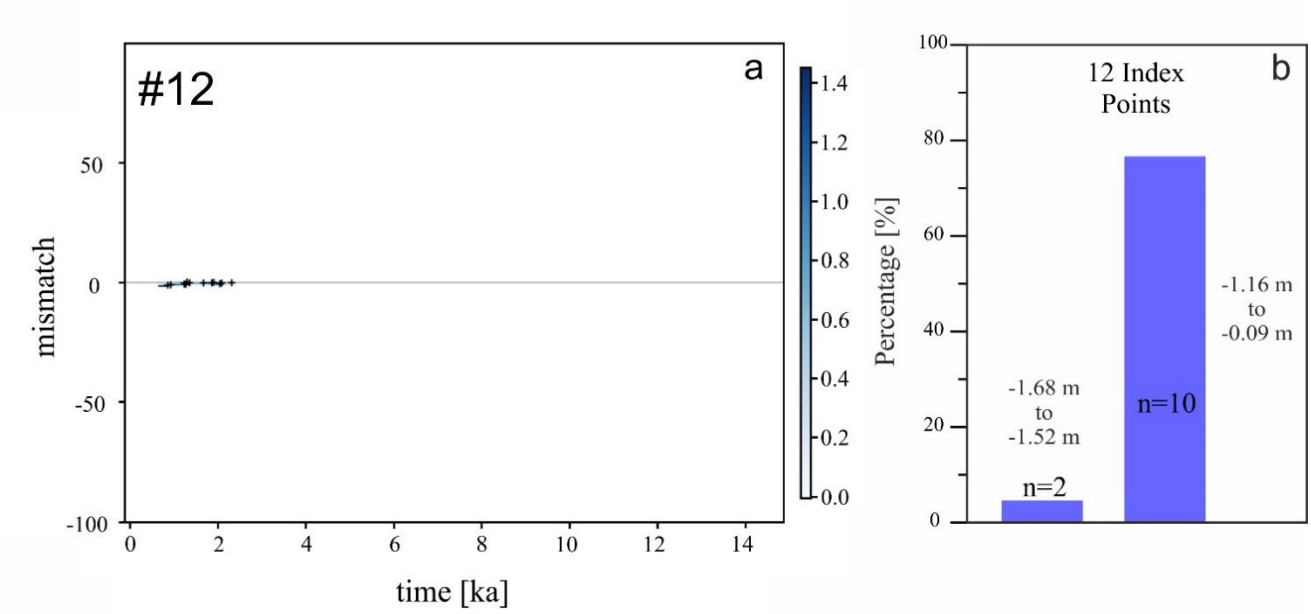

Figure 52: The sample set includes 12 index points and shows deviating probability results of region #12. a) The APC results display high uncertainties (light blue shadings) and black crosses indicate the average mismatch RSL elevation derived from index points in relation to the RSL predicted by the set of GIA models. b) The DPC analysis shows the probabilities for the 12 index points of the region, while the details are explained in the text. Right scale in a) and left scale in b) display the percentage calculated of the involved index points in both analyses. The blue scale in a) shows the average variety in the probability-range [%] of all index points spread over the distribution area, and indicates high certainties with a dark blue shading and lower certainties with lighter blue shadings. The scale in b) shows the calculated average probabilities derived from each index point individually. The average was re-calculated to better show the probabilities for the indicated type of mismatch, derived from the index point positions. Numbers at the bars indicate the elevation-ranges of the index points and n= indicates the number of samples included in the elevation-ranges.

Region #16

Area 16 (Figure 39 #16) consists of a dataset from different islands in the Spermonde Archipelago that is located in **south-west Sulawesi, Makassar**. This region presents 45 index points derived from microatolls and one peat sample from a mangrove salt marsh (De Klerk, 1982; Mann et al., 2016; Bender et al., *proof stage*) with ages dated between 6625±244 a BP and 37±12 a BP and RSL elevations ranging from -1.25±0.31 to 0.31±0.11 m (Table 8). The samples show a fluctuating RSL from a slightly negative to a slightly positive mismatch with the models.

The APC analysis produces very high uncertainties for this slightly fluctuating mismatch. In contrast, the probability for this mismatch derived from the DPC varies between 98.2% for elevations between -1.24 to -0.23 m (n= 18 index points) and 100% for -0.6 m to 0.31 m (n=27 index points) (Figure 53). The variable results can be attributed to the set of GIA models, where only a very limited number of models seem to predict a comparable RSL to the observed RSL by field data. The DPC analysis shows high probabilities of the field data agreeing with the model predictions.

.

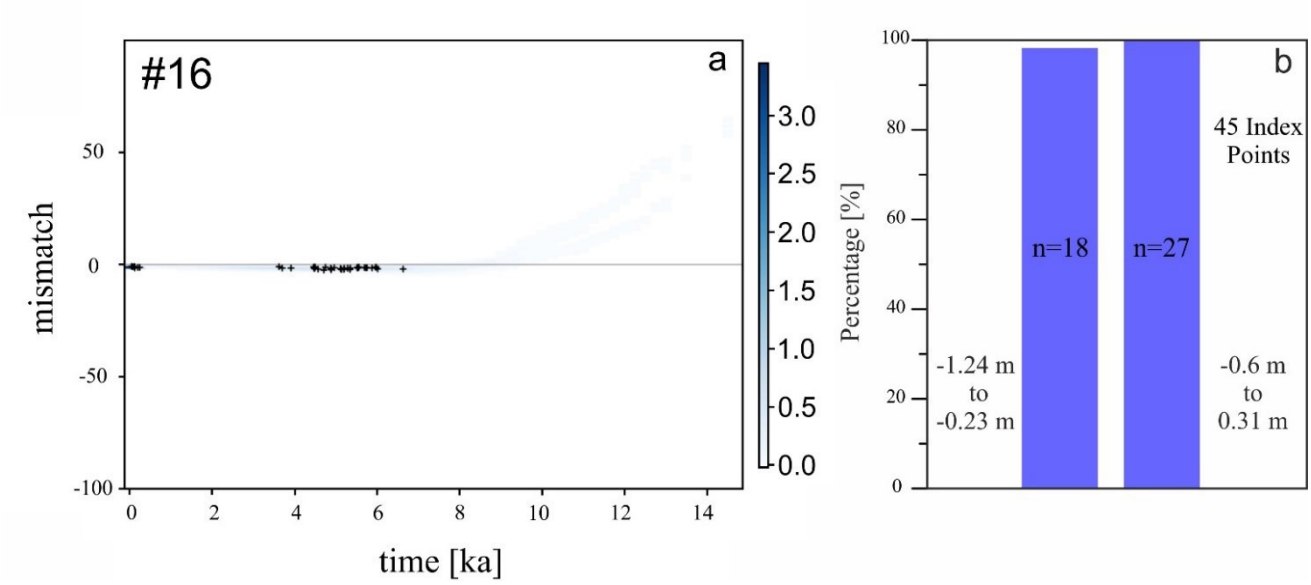

Figure 53: The sample set includes 45 index points and shows deviating probability results between the APC and DPC in region #16. a) The APC results display high uncertainties (light blue shadings) and black crosses indicate the average mismatch RSL elevation derived from index points in relation to the RSL predicted by the set of GIA models. b) The DPC analysis shows the probabilities for the 45 index points of the region, while the details are explained in the text. Right scale in a) and left scale in b) display the percentage calculated of the involved index points in both analyses. The blue scale in a) shows the average variety in the probability-range [%] of all index points spread over the distribution area, and indicates high certainties with a dark blue shading and lower certainties with lighter blue shadings. The scale in b) shows the calculated average probabilities derived from each index point individually. The average was re-calculated to better show the probabilities for the indicated type of mismatch, derived from the index point positions. Numbers at the bars indicate the elevation-ranges of the index points and n= indicates the number of samples included in the elevation-ranges.

7.6 Conclusion

Here, we tested a statistical probability analysis between RSL data and GIA models from South and Southeast Asia. We analyzed the sample sets in two ways. The first analysis focused on the average probability calculated for the entire dataset (APC). In this analysis, the probability for mismatching elevations between the RSL positions indicated by sea-level index points and the RSL predictions from 54 GIA models were calculated and averaged over the distribution area. In a second step, the probability for a positive or negative mismatch of each individual index point in relation to the set of GIA models was calculated (DCP).

Both analysis results were evaluated and the results are divided into three groups: *high probability*, *low probability*, and *completely deviating* between the two analyses. Sample sets that show high probability results for the same type of mismatch were identified in 8 regions. The results of these studies are reliable and mean that RSL observations from field data and RSL predictions from models provide comparable elevations. In contrast, for low probabilities indicated by both analyses, extraneous influences that could affect the sample elevations are assumed. The final group shows deviating results, where the reason for the low APC and high DPC results is most likely based on significantly different RSL elevations predicted by the majority of the GIA models. Therefore, further analyses are required for the sample sets, indicating low probability and deviating probability results to indicate a reason for the low or unclear mismatch tendencies. Nevertheless, the majority of the studies are characterized by high probabilities and therefore this study provides a good initial framework for GIA model and index point probability analyses.

8 Extended discussion and conclusions

Future sea-level rise and ongoing global warming are among the greatest threats of modern society in the 21st century and yet our understanding surrounding the causes of sea-level change is still incomplete. For that reason, studies on Holocene RSL variability need to be improved. The chapters of this thesis contribute to the understanding of this problem. In the following chapter, three scientific questions, introduced in the motivation part at the beginning of this work, will cover the main subjects of the four manuscripts presented in this thesis.

- *Why is a standardized analysis of sea-level data indispensable for the compilation of a database and how does this improve data handling?*

According to Hijma et al. (2015), to step forward in sea-level studies, a standardized analysis of geological field data is essential. Following their statement and explanations, the use of different sampling techniques requires standardized sampling errors to allow and support the comparison of index points (Shennan et al., 1983; Van de Plassche, 1986) from different studies. This comparison of standardized datasets is essential for the compilation of a database and the study of the resulting RSL curves. However, a sea-level index point needs to report four standardized criteria as defined by Shennan et al. (2015).

Standardizing sea-level index points, results in the possibility to compare all RSL curves to each other, enabling one to complete the global Holocene sea-level history puzzle piece by piece. This is especially essential for regions where sea-level studies are rare and field data is limited or missing. During the compilation of the SEAMIS database (see section 4) some studies provided information about marine and terrestrial limiting indicators instead of sea-level index points for their RSL analysis (Shennan and Horton, 2002). Marine and terrestrial limiting points include corals, shells, wood and leaves or pollen (e.g. De Klerk, 1982; Tjia et al., 1972; Geyh et al., 1979; Kayanne et al., 2002; Chappell and Polach, 1991), which provide enough information, only to conclude that measured feature was either above or below paleo sea level. While these indicators cannot provide precise spatio-temporal RSL position, they are still important to constrain RSL histories. Compiled in the database, these indicator types help to complete the global RSL information and increase local RSL information availability, especially when index points from other studies are provided for the region.

Obstacles for the expansion of global RSL information include standardized sampling errors, publications leaving important information unreported, spatial and temporal gaps in sample availability, as well as inconsistencies between parts of datasets within the same study regions. For example, some papers do not report how the age of their sample was calculated, whether or not the reservoir age was taken into account, which sampling method was used, or how the errors were calculated (e.g. Somboon, 1988; Somboon and Thiramongkol, 1992; Tjia et al., 1972; De Klerk, 1982). These data sets needed to be carefully re-analyzed. In this thesis individual samples were re-interpreted as limiting indicators or index points taking into account the four criteria from Shennan et al. (2015), the given sample description, and (if necessary) by correcting the age for the reservoir age. Further, if a sampling method was mentioned, related errors had to be corrected after Hijma et al. (2015) to avoid biased RSL results due to insufficient consideration of the different sampling errors. Therefore, without the standardization work done in this thesis, inter-regional comparisons would have been impossible.

- *Can the database and new data collected in this thesis help to highlight critical areas in S and SE Asia for which concerns flooding risk?*

In fact, a standardization of sample sets compiled in a database allows a much better handling of the data and possible related sampling errors. This in turn, improves local and global RSL reconstructions and provides more reliable results. Following the compilation of standardized datasets to compare the

RSL history within South and Southeast Asia from the Mid to Late Holocene, it is possible to indirectly indicate critical areas at risk to flooding. The comparison of different sea-level studies presented in the database or with newly studied sample sets, dated to similar ages and investigated in study sites in close proximity to one another, can help not only to detect where study results support each other, but also identify where there are disagreements between datasets and elucidate possible causes for this deviation.

In a study conducted within the framework of this thesis, (Bender et al., *in proofs*), new field data from different islands within the Spermonde Archipelago were compared to a previous study by Mann et al. (2016) from the same study area. Mann et al. identified index points on an uninhabited island that indicated an RSL slightly higher than MSL, while they further showed deviating RSL results for the densely populated island of Barrang Lompo located nearby. Bender et al. (*in proof stage)* further studied surrounding islands and was able to support the deviating result for Barrang Lompo. The RSL indicated on this island is 0.8 m lower than that found on the remaining islands within this study. After indicating different environmental aspects including, anthropogenic activity, erosion patterns and protection features (Williams, 2013; Tahir et al., 2012), it appears that this lower RSL result is triggered by local subsidence of the island. Therefore, a rise in sea level is not the only risk factor contributing to flooding. Local specialties, like an overload of the area due to a dense population, or environmental changes triggered by anthropogenic activity that might affect the local coastal environment and natural protection of the area, such as beach ridges or coral reef flats, are aspects that might increase the risk to flooding. Those aspects should be further analyzed since contradicting results were detected in this region.

Therefore, as explained on this example, the comparison of different sea-level studies can help to indicate deviating RSL results within a study region, prompting further analysis which can show that this region might be prone to vertical land motion and is therefore at risk of additional flooding. Further, as vertical land motions change the paleo RSL considerations and modern GIA rates for the affected area, this needs to be taken into account for modern sea-level studies as these movements affect regional tide gauges as well as satellite altimetry data. The comparison of sample sets from Common Era or the late Holocene using "matching" GIA models can help to constrain which models predict ongoing GIA rates and thus can be adapted for use in modern regional sea-level studies. Due to highlighting and indicating critical areas and further analysis that might indicate vertical land motion, modern sea-level rate estimates can be improved and therefore the database and new field data can help to detect regions at risk of flooding.

To indicate how future sea level might propagate constrained GIA predictions are essential. This is especially true for regions where sea-level index points or limiting indicators are missing or are inconsistent GIA models need to predict a reliable RSL. However, in many cases GIA models and RSL data provide different sea-level histories, which makes it difficult to decide if there are discrepancies in the geological field data or in the model adjustments. Therefore, as there were many discrepancies or lack of RSL data detected within the study areas in the database, we use a statistical analysis calculating the probability of a mismatch or match between models and sea-level index points in order to mitigate these discrepancies.

- *Does a statistical probability calculation help to constrain GIA model predictions for all study sites in S and SE Asia and can the models be applied for locations without field data?*

A set of 54 GIA model predictions was compared to the datasets of 16 locations in South and Southeast Asia. An average probability calculation (APC) of each sample set in relation to each model was calculated to identify whether an indicated positive or negative mismatch between the models and the data is reliable and if it indicates possible influences of post-depositional processes. Further, in a second analysis based on the same GIA model outputs the probability for each index point was calculated individually (DPC), and compared to the APC to examine whether the APC results can be supported.

The results show that 8 out of 16 study sites present high probabilities for the related mismatches ranging from 67% to 100% indicated by both analyses, while 5 regions present only low probabilities of 17% to 64.5% for the predicted mismatch. However, in three regions deviating results between the APC and DPC show contrasting probabilities. Derived from the high probability results, it is obvious that GIA model predictions and index points show comparable RSL histories, while the reason for the low and deviating probability results are based on assumptions. However, sample sets indicating lower probabilities are mainly derived from peat and organic mud or wood and leaves, sampled partly on deltas or inter tidal mudflats implying that post-depositional processes cannot be excluded as driving factors that affected the sample elevation. Further, significantly deviating RSL predictions of GIA models and field data is possible in locations indicated by low probabilities, where sample set information seem to exclude post-deposition of the indicators due to small variabilities in sample elevations and ages. Following this, deviating probability results can be explained by significantly different RSL predictions presented by the majority of GIA models. In all three regions, the DPC analysis shows a medium to high probability that the predicted and observed RSL matches at the location of the index points. This shows, that at least one model prediction is comparable to the observed RSL location while the low probability calculated in the APC indicates that RSL predicted by the majority of the models is at odds with the observed RSL position.

Based on high probability results of 50% of the tested regions, so far, for areas where GIA was the major driving process in Holocene, this analysis is a good start to calculate the probability of a mismatch between predicted and observed RSL histories. Nevertheless, due to the 50% of the tested areas that provide low or deviating probabilities, this statistical probability analysis cannot be applied to study sites where no sea-level data is reported nor to regions where mainly post-depositional affected the forming of RSL indicators in Holocene. This method needs some improvements to better understand and explain the reasons for low probability as well as identification of discrepancies within the sample sets. The first step to improve this method is to use a more accurate and more in-depth statistical analysis and to either re-analyze the related sample sets (low and deviating probability results) in a very detailed way or to expand the sample set with more and new sea-level data from the same region. This would help to indicate if the problem of unclear mismatch tendencies is derived from the sample types or sample analysis to finally exclude low probability results while deviating results help to indicate that most likely the RSL predictions from GIA models are at odds with the samples.

9 Outlook and future work

In this thesis, I show the following contributions to science that were developed within my PhD in the last three years:

- A new standardized Holocene sea-level database
- Newly surveyed field data from 5 islands in the Spermonde Archipelago, measured and dated with standardized methods
- New ideas on possible land subsidence patterns and vertical land movements in the Spermonde
- A novel suite of GIA models for the entire SE Asia that is open access
- An attempt to develop a probabilistic framework to compare systematically standardized RSL observations and GIA for SE Asia.

The new standardized Holocene sea-level database consists of a high number of paleo sea-level studies of South and Southeast Asia. While many sample sets were re-analyzed and standardized, there are still unsolved problems that complicate the study of Holocene relative sea-level changes. Inconsistencies within datasets or between samples of different studies conducted in the same study site are a significant issue especially when the study region (in general) is rarely studied. In those locations, limited data availability is not the main problem as shown in chapters 4, 5 and 6. The example of the Spermonde Archipelago, where new field data from five islands was investigated to expand and support existing RSL results, to solve data inconsistencies, and fill the gaps in information, shows, that adding data to existing sample sets, does not automatically solve the problem. Even though the results support one of the previous studies, it further opens more questions that need to be answered to detect the local RSL history. However due to the comparison of the previously published sample set by Mann et al. (2016) with the new surveys, it was possible to constrain the idea that the densely inhabited island of Barrang Lompo is affected by local subsidence due to anthropogenic activities and to develop the idea of possible vertical land movements in the Spermonde Archipelago. For this study a whole suite of GIA models was run to predict which model best fits the sea-level data from the Spermonde Archipelago. The vertical land movements within this region needs to be further analyzed by independent datasets. For Barrang Lompo subsidence, GPS measurements for a defined time frame in a period of a few years could prove that the island is indeed subsiding and the related rates can be calculated. Further, growth patterns and morphological differences between living microatolls on Barrang Lompo and on other islands nearby can be analyzed to see if the ones on Barrang Lompo different in growth rate.

Here, the study in the Spermonde Archipelago shows that data inconsistencies are not only due to a small dataset, and further analysis is indispensable to identify the problem in each study region where inconsistencies within the sample sets were detected. This would also help highlight regions that are prone to local subsidence, which might be a serious problem with ongoing sea-level rise. Thus, the lack of data in some regions in South and Southeast Asia, where many coastlines are low-lying but densely inhabited, is a big issue. The analysis of local paleo sea-level changes and the comparison between the studies in similar areas is important not only to complete the RSL history of the broader region but also to help to detect critical locations at risk of flooding, to constrain GIA models to the data for the study sites and to improve GIA models in general. A better knowledge of local sea-level variability and the processes affecting it, whether GIA or post-depositional processes is the main driver, are essential to improve local, regional, and ultimately global RSL studies. Thus, in the future, re-analyzing datasets providing inconsistencies not only by the original literature but also by studying the environment and comparing it to similar regional sea-level studies to indicate elevation differences in the RSL to indicate potential post-depositional processes in detail is the first approach. Further, more data is needed in unstudied areas especially in regions that are at risk to flooding or drowning. Detected changes in RSL due to post-depositional processed as in the Spermonde archipelago need to be further analyzed and taken into account for modern sea-level studies as well as modern GIA rates need to also be constrained to changing RSL considerations.

However, in some study sites (chapters 4, 5 and 6) GIA models and index points show contradicting or strongly deviating RSL histories. To solve this discrepancy, in chapter 7, I showed a statistical analysis approach based on probability calculations to indicate whether these RSL mismatches between GIA models and samples are small and comparable or if the predicted and the observed RSL are at odds with each other. It turned out that this method works partly very well for some regions, where model predicts and observations show comparable RSL results, while for some regions deviating RLS histories were predicted. These are influenced either by post-depositional processes that might have affected the samples elevations after forming or on the differing GIA model results. To improve this approach, a refined in-depth statistical analysis is needed to better analyze the problematic sea-level data more detailed. Further, more newly surveyed data for the study regions is required to exclude large sampling or analysis uncertainties due to the use of unstandardized methods. In future this approach should be used to identify whether GIA models and samples show a matching RSL result to improve GIA models intensively, to (eventually) take them to the next level, where they can be applied to regions indicating data inconsistencies or a lack of data. This would improve global sea-level studies and help to better forecast critical regions at risk of flooding that are yet undetected and unprotected.

In conclusion, this thesis improved our understanding of RSL in South and Southeast Asia due to the standardized revision of published data, new field data investigations, a large new suite of GIA models for the broader region of South and Southeast Asia and a probability-based comparison between field data and GIA models. Several questions and possibilities for future research arising from my results still exists, while opening the chance for further research in this important region. The work in this thesis and the data available on open access will set a milestone for future research.

10 References

Alimuddin, I., Bayuaji, L., Langkoke, R., Sumantyo, J. T. S., and Kuze, H.: Evaluating Land Surface Changes of Makassar City Using DInSAR and Landsat Thematic Mapper Images, David Publishing Company www. davidpublishing. com, 1287, 2013.

Allison, I., Bindoff, N. L., Bindschadler, R. A., Cox, P. M., de Noblet, N., England, M. H., Gruber, F., J.E. , de Noblet, N., Haywood, A. M., Karoly, D. J., Kaser, G., Le Quéré, C., Lenton, T. M., Mann, M. E., McNeil, B. I., Pitman, A. J., Rahmstorf, S., Rignot, E., Schellnhuber, H. J., Schneider, S. H., Sherwood, S. C., Somerville, R. C. J., Steffen, K., Steig, E. J., Visbeck, M., and Weaver, A. J.: The Copenhagen Diagnosis : Updating the World on the Latest Climate Science, The University of New South Wales Climate Change Research Centre (CCRC), Sydney, Australia., 60pp, 2009.

Armitage, S. J., Jasim, S. A., Marks, A. E., Parker, A. G., Usik, V. I., and Uerpmann, H.-P.: The Southern Route "Out of Africa": Evidence for an Early Expansion of Modern Humans into Arabia, Science, 331, 453 LP-456, 2011.

Austermann, J., Mitrovica, J. X., Huybers, P., and Rovere, A.: Detection of a dynamic topography signal in last interglacial sea-level records, 1-9, 10.1126/sciadv.1700457, 2017.

Azmy, K., Edinger, E., Lundberg, J., and Diegor, W.: Sea level and paleotemperature records from a mid-Holocene reef on the North coast of Java, Indonesia, International Journal of Earth Sciences, 99, 231-244, 10.1007/s00531-008-0383-3, 2010.

Baden-Powell, D. F. W.: On a Marine Holocene Fauna in North-Western Scotland, Journal of Animal Ecology, 6, 273-283, 1937.

Banerjee, P. K.: Holocene and Late Pleistocene relative sea level fluctuations along the east coast of India, Marine Geology, 167, 243-260, 10.1016/S0025-3227(00)00028-1, 2000.

Bird, M. I., Fifield, L. K., Teh, T. S., Chang, C. H., Shirlaw, N., and Lambeck, K.: An inflection in the rate of early mid-Holocene eustatic sea-level rise: A new sea-level curve from Singapore, Estuarine, Coastal and Shelf Science, 71, 523-536, 2007.

Bird, M. I., Austin, W. E. N., Wurster, C. M., Fifield, L. K., Mojtahid, M., and Sargeant, C.: Punctuated eustatic sea-level rise in the early mid-Holocene, Geology, 38, 803-806, 10.1130/G31066.1, 2010.

Bird, P.: An updated digital model of plate boundaries, Geochemistry, Geophysics, Geosystems, 4, 1-52, 10.1029/2001GC000252, 2003.

Bloom, A. L.: Atlas of sea level curves. International Geological Correlation Program, Project 16. Ithaca, NY: Cornell University, Geology Department, 1977.

Bradley, S. L., Milne, G. A., Horton, B. P., and Zong, Y.: Modelling sea level data from China and Malay-Thailand to estimate Holocene ice-volume equivalent sea level change, Quaternary Science Reviews, 137, 54-68, 10.1016/j.quascirev.2016.02.002, 2016.

Brain, M. J., Long, A. J., Woodroffe, S. A., Petley, D. N., Milledge, D. G., and Parnell, A. C.: Modelling the effects of sediment compaction on salt marsh reconstructions of recent sea-level rise, Earth and Planetary Science Letters, 180-193, http://dx.doi.org/10.1016/j.epsl.2012.06.045, 2012.

Brain, M. J., Kemp, A. C., Horton, B. P., Culver, S. J., Parnell, A. C., and Cahill, N.: Quantifying the contribution of sediment compaction to late Holocene salt-marsh sea-level reconstructions, North Carolina, USA, Journal of experimental psychology. General, 144, 744-763, 2015.

Carto, S. L., Weaver, A. J., Hetherington, R. e., Lam, Y., and Wiebe, E. C.: Out of Africa and into an ice age: on the role of global climate change in the late Pleistocene migration of early modern humans out of Africa, Journal of Human Evolution, 56, 139-151, 10.1016/j.jhevol.2008.09.004, 2009.

Cazenave, A., Dominh, K., Guinehut, S., Berthier, E., Llovel, W., Ramillien, G., Ablain, M., and Larnicol, G.: Sea level budget over 2003-2008: A reevaluation from GRACE space gravimetry, satellite altimetry and Argo, Global and Planetary Change, 65, 83-88, 10.1016/j.gloplacha.2008.10.004, 2009.

Cazenave, A., and Cozannet, G. L.: Sea level rise and its coastal impacts, Earth's Future, 2, 15-34, 10.1002/2013EF000188.Received, 2013.

Chappell, J., and Polach, H.: Post-glacial sea-level rise from a coral record at Huon Peninsula, Papua New Guinea, Nature, 349, 147-149, 10.1038/349147a0, 1991.

Chaussard, E., Amelung, F., Abidin, H., and Hong, S. H.: Sinking cities in Indonesia: ALOS PALSAR detects rapid subsidence due to groundwater and gas extraction, Remote Sensing of Environment, 128, 150-161, 10.1016/j.rse.2012.10.015, 2013.

Church, J. A., Gregory, J. M., Huybrechts, P., Kuhn, M., Lambeck, K., Nhuan, M. T., Qin, D., and Woodworth, P. L.: Changes in Sea Level, in: J.T Houghton, Y. Ding, D.J. Griggs, M. Noguer, P.J. Van der Linden, X. Dai, K. Maskell, and C.A. Johnson (eds.): Climate Change 2001: The Scientific Basis: Contribution of Working Group I to the Third Assessment Report of the Intergovernmental Panel, 57, 287-295, 10.1256/004316502320517380, 2001.

Church, J. A., White, N. J., and Hunter, J. R.: Sea-level rise at tropical Pacific and Indian Ocean islands, Global and Planetary Change, 53, 155-168, 10.1016/j.gloplacha.2006.04.001, 2006.

Church, J. A., and White, N. J.: Sea-Level Rise from the Late 19th to the Early 21st Century, 585-602, 10.1007/s10712-011-9119-1, 2011.

Clark, J. A., and Farrell, W. E.: On Postglacial Sea Level, 647-667, 1976.

Clark, M.: Tangible heritage of the Macassan–Aboriginal encounter in contemporary South Sulawesi. (2013), Journeys, Encounters and Influences. ANU Press. , In Clark M. & May S. (Eds.), Macassan History and Heritage:, pp. 159-182, 2010.

Daly, R. A.: A Recent Worldwide Sinking of Ocean-level, Geological Magazine, 57, 246-261, 10.1017/S0016756800101670, 1920a.

Daly, R. A.: A general sinking of sea-level in recent time, Geology, 246-250, 1920b.

Daly, R. A.: The changing world of the ice age, Yale University Press, 1934.

Dangendorf, S., Marcos, M., Woppelmann, G., Conrad, C. P., Frederikse, T., and Riva, R.: Reassessment of 20th century global mean sea level rise, Proc Natl Acad Sci U S A, 114, 5946-5951, 10.1073/pnas.1616007114, 2017.

Dangendorf, S., Hay, C., Calafat, F. M., Marcos, M., Piecuch, C. G., Berk, K., and Jensen, J.: Persistent acceleration in global sea-level rise since the 1960s, Nature Climate Change, 9, 705-710, 10.1038/s41558-019-0531-8, 2019.

Darman, H., and Sidi, F. H.: An outline of the geology of Indonesia, Indonesian Association of Geologists, Jakarta, 192, 2000.

Davies, P. J., and Montaggioni, L.: Reef growth and sea-level change: The environmental signature, In: Proceedings 5th International Coral Reef Congress, Tahiti, 1985, 477-511,

10. References

De Boer, B., Dolan, A. M., Bernales, J., Gasson, E., Goelzer, H., Golledge, N. R., Sutter, J., and Huybrechts, P.: Simulating the Antarctic ice sheet in the late-Pliocene warm period : PLISMIP-ANT , an ice-sheet model intercomparison project, 881-903, 10.5194/tc-9-881-2015, 2015.

De Boer, B., Stocchi, P., Whitehouse, P. L., and Wal, R. S. W. V. D.: Current state and future perspectives on coupled ice-sheet e sea-level modelling, Quaternary Science Reviews, 169, 13-28, 10.1016/j.quascirev.2017.05.013, 2017.

De Klerk, L. G.: Zeespiegel Riffen en Kustflakten in zuitwest Sulawesi, Indonesia, Utrecht, 172-172 pp., 1982.

de Radermacher, J. C. M.: Korte beschrijving van het eiland Celebes, en de eilanden Floris, Sumbauwa, Lombok, en Baly, Reinier Arrenberg, 1786.

Durrant, T., Hemer, M., Trenham, C., and Greenslade, D.: CAWCR Wave Hindcast 1979–2010, Data Collection, 2013.

Durrant, T., Hemer, M., Smith, G., Trenham, C., and Greenslade, D.: CAWCR Wave Hindcast extension June 2013 - July 2014. v2. CSIRO., Service Collection. https://doi.org/10.4225/08/55C99193B3A63, 2015.

Dutton, A., and Lambeck, K.: Ice Volume and Sea Level During the Last Interglacial, 337, 216-220, 2012.

Dutton, A., Carlson, A. E., Long, A. J., Milne, G. A., Clark, P. U., DeConto, R., Horton, B. P., Rahmstorf, S., and Raymo, M. E.: Sea-level rise due to polar ice-sheet mass loss during past warm periods, Science, 349, 10.1126/science.aaa4019, 2015.

Egbert, G. D., and Erofeeva, S. Y.: Efficient Inverse Modeling of Barotropic Ocean Tides, Journal of Atmospheric and Oceanic Technology, 19, 183-204, 10.1175/1520-0426(2002)019<0183:EIMOBO>2.0.CO;2, 2002.

Engelhart, S. E.: Mangrove Pollen of Indonesia and its Suitability as a Sea-Level Indicator Simon Edward Engelhart Thesis submitted for the degree of Master of Science Department of Geography, 2007.

Engelhart, S. E., Horton, B. P., Roberts, D. H., Bryant, C. L., and Corbett, D. R.: Mangrove pollen of Indonesia and its suitability as a sea-level indicator, Marine Geology, 242, 65-81, 10.1016/j.margeo.2007.02.020, 2007.

Engelhart, S. E., Peltier, W. R., and Horton, B. P.: Holocene relative sea-level changes and glacial isostatic adjustment of the U.S. Atlantic coast, Geology, 39, 751-754, 10.1130/G31857.1, 2011.

Engelhart, S. E., and Horton, B. P.: Holocene sea level database for the Atlantic coast of the United States, Quaternary Science Reviews, 54, 12-25, 10.1016/j.quascirev.2011.09.013, 2012.

Engelhart, S. E., Vacchi, M., Horton, B. P., Nelson, A. R., and Kopp, R. E.: A sea-level database for the Pacific coast of central North America, Quaternary Science Reviews, 113, 78-92, 10.1016/j.quascirev.2014.12.001, 2015.

Fieux, M., Andri, C., Charriaud, E., Ilahude, A. G., Metzl, N., Molcard, R., and Swallow, J. C.: Hydrological and chloroflouromethane measuremtens of the Indonesian throughflow entering the Indian Ocean, 101, 1996.

Fontana, A., Vinci, G., Tasca, G., Mozzi, P., Vacchi, M., Bivi, G., Salvador, S., Rossato, S., Antonioli, F., and Asioli, A.: Lagoonal settlements and relative sea level during Bronze Age in Northern Adriatic: Geoarchaeological evidence and paleogeographic constraints, Quaternary International, 439, 17-36, 2017.

Gehrels, R., and Long, A.: Sea level is not level, Geography, 93, 2008.

Gehrels, W. R., Horton, B. P., Kemp, A. C., and Sivan, D.: Two millennia of sea level data: The key to predicting change, EOS, Transactions American Geophysical Union, 92, 289-290, 2011.

Grossman, E. E., Fletcher, C. H., and Richmond, B. M.: The Holocene sea-level highstand in the equatorial Pacific: Analysis of the insular paleosea-level database, Coral Reefs, 17, 309-327, 10.1007/s003380050132, 1998.

Hall, R.: Cenozoic plate tectonic reconstructions of SE Asia SE Asia Research Group , Department of Geology , Royal Holloway University of London, Geological Society, London, Special Publications, 11-23, 1997.

Hall, R., and Spakman, W.: Mantle structure and tectonic history of SE Asia, Tectonophysics, 658, 14-45, 2015.

Hallmann, N., Camoin, G., Eisenhauer, A., Botella, A., Milne, G. A., Vella, C., Samankassou, E., Pothin, V., Dussouillez, P., Fleury, J., and Fietzke, J.: Ice volume and climate changes from a 6000 year sea-level record in French Polynesia, Nature Communications, 9, 1-12, 10.1038/s41467-017-02695-7, 2018.

Hanebuth, T., Stattegger, K., and G, P. M.: Rapid Flooding of the Sunda shelf: a late glacial sea level record, Science, 288, 1033-1035, 10.1126/science.288.5468.1033, 2000.

Hanebuth, T. J. J., Voris, H. K., Yokoyama, Y., Saito, Y., and Okuno, J. i.: Formation and fate of sedimentary depocentres on Southeast Asia's Sunda Shelf over the past sea-level cycle and biogeographic implications, Earth-Science Reviews, 104, 92-110, 10.1016/j.earscirev.2010.09.006, 2011.

Hanebuth, T. J. J., Proske, U., Saito, Y., Nguyen, V. L., and Ta, T. K. O.: Early growth stage of a large delta—Transformation from estuarine-platform to deltaic-progradational conditions (the northeastern Mekong River Delta, Vietnam), Sedimentary Geology, 261, 108-119, 2012.

Hanson, S., Nicholls, R., Ranger, N., Hallegatte, S., Corfee-Morlot, J., Herweijer, C., and Chateau, J.: A global ranking of port cities with high exposure to climate extremes, Climatic Change, 104, 89-111, 10.1007/s10584-010-9977-4, 2011.

Harris, R. O. N., and Major, J.: Waves of destruction in the East Indies : the Wichmann catalogue of earthquakes and tsunami in the Indonesian region from 1538 to 1877, 9-46, 2017.

Hesp, P. A., Hung, C. C., Hilton, M., Ming, C. L., and Turner, I. M.: A first tentative Holocene sea-level curve for Singapore, Journal of Coastal Research, 14, 308-314, Available from: http://www.jstor.org/stable/4298779., 1998.

Hibbert, F. D., Rohling, E. J., Dutton, A., Williams, F. H., Chutcharavan, P. M., Zhao, C., and Tamisiea, M. E.: Coral indicators of past sea-level change: A global repository of U-series dated benchmarks, Quaternary Science Reviews, 145, 1-56, 10.1016/j.quascirev.2016.04.019, 2016.

Hijma, M. P., and Cohen, K. M.: Timing and magnitude of the sea-level jump preluding the 8200 yr event, Geology, 38, 275-278, 2010.

Hijma, M. P., Engelhart, S. E., Törnqvist, T. E., Horton, B. P., Hu, P., and Hill, D. F.: A protocol for a geological sea-level database, Handbook of Sea-Level Research, 536-553, 10.1002/9781118452547.ch34, 2015.

Hopley, D., and Gehrels, R.: Holocene sea-level research and IGCP – The last 40 years, 1986, 2007.

Hori, K., Tanabe, S., Saito, Y., Haruyama, S., Nguyen, V., and Kitamura, A.: Delta initiation and Holocene sea-level change: Example from the Song Hong (Red River) delta, Vietnam, Sedimentary Geology, 164, 237-249, 10.1016/j.sedgeo.2003.10.008, 2004.

Horton, B. P., Gibbard, P. L., Mine, G. M., Morley, R. J., Purintavaragul, C., and Stargardt, J. M.: Holocene sea levels and palaeoenvironments, Malay-Thai Peninsula, southeast Asia, The Holocene, 158, 1199-1213, 2005.

Horton, B. P., Zong, Y., Hillier, C., and Engelhart, S.: Diatoms from Indonesian mangroves and their suitability as sea-level indicators for tropical environments, Marine Micropaleontology, 63, 155-168, 10.1016/j.marmicro.2006.11.005, 2007.

Horton, B. P., Peltier, W. R., Culver, S. J., Drummond, R., Engelhart, S. E., Kemp, A. C., Mallinson, D., Thieler, E. R., Riggs, S. R., and Ames, D. V.: Holocene sea-level changes along the North Carolina Coastline and their implications for glacial isostatic adjustment models, Quaternary Science Reviews, 28, 1725-1736, 2009.

Horton, B. P., Engelhart, S. E., Hill, D. F., Kemp, A. C., Nikitina, D., Miller, K. G., and Peltier, W. R.: Influence of tidal-range change and sediment compaction on Holocene relative sea-level change in New Jersey, USA, Journal of Quaternary Science, 28, 403-411, 2013.

Houghton, E.: Climate change 1995: The science of climate change: contribution of working group I to the second assessment report of the Intergovernmental Panel on Climate Change, Cambridge University Press, 1996.

IPCC: Climate change 2001: impacts, adaptation and vulnerability. J. J. McCarthy, O. F. Canziani, N. A. Leary, D. J. Dokken and K. S. White (eds). Third assessment report of the intergovernmental panel on climate change. Cambridge University Press, Cambridge, Forbes, 343-379, 2001.

Janßen, A., Wizemann, A., Klicpera, A., and Satari, D. Y.: Sediment Composition and Facies of Coral Reef Islands in the Spermonde Archipelago , Indonesia, 4, 1-13, 10.3389/fmars.2017.00144, 2017.

Kamaludin, B. H.: Holocene sea level changes in Kelang and Kuantan , Peninsular Malaysia, 309-309, 2002.

Kamaludin, H. B.: Holocene sea level changes in Kelang and Kuantan, Peninsular Malaysia, Durham University, 309-309 pp., 2001.

Kayanne, H., Yamamo, H., and Randall, R. H.: Holocene sea-level changes and barrier reef formation on an oceanic island, Palau Islands, western pacific, Sedimentary Geology, 150, 47-60, 2002.

Kench, P. S., Smithers, S. G., McLean, R. F., and Nichol, S. L.: Holocene reef growth in the Maldives: Evidence of a mid-Holocene sea-level highstand in the central Indian Ocean, Geology, 37, 455-458, 10.1130/G25590A.1, 2009.

Kench, P. S., and Mann, T.: Reef Island Evolution and Dynamics: Insights from the Indian and Pacific Oceans and Perspectives for the Spermonde Archipelago, Frontiers in Marine Science, 4, 10.3389/fmars.2017.00145, 2017.

Kench, P. S., McLean, R. F., Owen, S. D., Ryan, E., Morgan, K. M., Ke, L., Wang, X., and Roy, K.: Climate-forced sea-level lowstands in the Indian Ocean during the last two millennia, Nature Geoscience, 10.1038/s41561-019-0503-7, 2019.

Khan, N. S., Ashe, E., Shaw, T. A., Vacchi, M., Walker, J., Peltier, W. R., Kopp, R. E., and Horton, B. P.: Holocene Relative Sea-Level Changes from Near-, Intermediate-, and Far-Field Locations, Current Climate Change Reports, 1, 247-262, 10.1007/s40641-015-0029-z, 2015.

Khan, N. S., Hibbert, F., and Rovere, A.: Sea-level databases, Past Global Changes Magazine, 27, 10.22498/pages.27.1.10, 2019.

Kopp, R. E., Hay, C. C., Little, C. M., and Mitrovica, J. X.: Geographic Variability of Sea-Level Change, Current Climate Change Reports, 1, 192-204, 10.1007/s40641-015-0015-5, 2015a.

Kopp, R. E., Horton, B. P., Kemp, A. C., and Tebaldi, C.: Past and future sea-level rise along the coast of North Carolina, USA, Climatic Change, 132, 693-707, 10.1007/s10584-015-1451-x, 2015b.

Kopp, R. E., Kemp, A. C., Bittermann, K., Horton, B. P., Donnelly, J. P., Gehrels, W. R., Hay, C. C., Mitrovica, J. X., Morrow, E. D., and Rahmstorf, S.: Temperature-driven global sea-level variability in the Common Era, Proceedings of the National Academy of Sciences, 113, E1434 LP-E1441, 10.1073/pnas.1517056113, 2016.

Lambeck, K.: Sea-level change, flacial rebound and mantle viscosity for northen Europe, Geophys, 134, 102-144, 1998.

Lambeck, K., and Chappell, J.: Sea level change through the last glacial cycle, 292, 679-686, 10.1126/science.1059549, 2001.

Lambeck, K., Chappell, J., Smith, J., and Uppenbrink, J.: Sea level change through the last glacial cycle Paleoclimate; Earth's variable climatic past, Science, 292, 679-686, 2001.

Lambeck, K., Esat, T. M., and Potter, E.-K.: Links between climate and sea levels for the past three million years, Nature, 419, 199-206, 2002.

Lambeck, K., Woodroffe, C. D., Antonioli, F., Anzidei, M., Gehrels, W. R., Laborel, J., and Wright, A. J.: Paleoenvironmental records, geophysical modeling, and reconstruction of sea-level trends and variability on centennial and longer timescales, in, edited by: Church, J. A., Woodworth, P. L., Aarup, T., and Wilson, W. S., Wiley-Blackwell, 61-121, 2010.

Lambeck, K., Rouby, H., Purcell, A., Sun, Y., and Sambridge, M.: Sea level and global ice volumes from the Last Glacial Maximum to the Holocene, Proceedings of the National Academy of Sciences, 111, 15296-15303, 10.1073/pnas.1411762111, 2014.

Long, A. J., Roberts, D. H., and Dawson, S.: Early Holocene history of the west Greenland Ice Sheet and the GH-8.2 event, Quaternary Science Reviews, 25, 904-922, 2006.

Love, R., Milne, G. A., Tarasov, L., Engelhart, S. E., Hijma, M. P., Latychev, K., Horton, B. P., and Törnqvist, T. E.: The contribution of glacial isostatic adjustment to projections of sea-level change along the Atlantic and Gulf coasts of North America, Earth's Future, 4, 440-464, 10.1002/2016EF000363, 2016.

Mann, T., Rovere, A., Schöne, T., Klicpera, A., Stocchi, P., Lukman, M., and Westphal, H.: The magnitude of a mid-Holocene sea-level highstand in the Strait of Makassar, Geomorphology, 257, 155-163, 10.1016/j.geomorph.2015.12.023, 2016.

Mann, T., Bender, M., Lorscheid, T., Stocchi, P., Vacchi, M., Switzer, A., and Rovere, A.: Relative sea-level data from the SEAMIS database compared to ICE-5G model predictions of glacial isostatic adjustment, Data Brief, 27, 104600, 10.1016/j.dib.2019.104600, 2019a.

Mann, T., Bender, M., Lorscheid, T., Stocchi, P., Vacchi, M., Switzer, A. D., and Rovere, A.: Holocene sea levels in Southeast Asia, Maldives, India and Sri Lanka: The SEAMIS database, Quaternary Science Reviews, 219, 112-125, 10.1016/j.quascirev.2019.07.007, 2019b.

Marfai, M. A., and King, L.: Potential vulnerability implications of coastal inundation due to sea level rise for the coastal zone of Semarang city, Indonesia, Environmental Geology, 54, 1235-1245, 10.1007/s00254-007-0906-4, 2007.

Mauz, B., Vacchi, M., Green, A., Hoffmann, G., and Cooper, A.: Beachrock: A tool for reconstructing relative sea level in the far-field, Marine Geology, 362, 1-16, 10.1016/j.margeo.2015.01.009, 2015.

McCaffrey, R.: Slip partitioning at convergent plate boundaries of SE Asia, Geological Society, London, Special Publications, 106, 3-18, 1996.

Melis, R. T., Di Rita, F., French, C., Marriner, N., Montis, F., Serreli, G., Sulas, F., and Vacchi, M.: 8000 years of coastal changes on a western Mediterranean island: A multiproxy approach from the Posada plain of Sardinia, Marine Geology, 403, 93-108, 2018.

Meltzner, A. J., and Woodroffe, C. D.: Coral microatolls, Handbook of Sea-Level Research, 125-145, 2015.

Meltzner, A. J., Switzer, A. D., Horton, B. P., Ashe, E., Qiu, Q., Hill, D. F., Bradley, S. L., Kopp, R. E., Hill, E. M., Majewski, J. M., Natawidjaja, D. H., and Suwargadi, B. W.: Half-metre sea-level fluctuations on centennial timescales from mid-Holocene corals of Southeast Asia, Nature Communications, 8, 14387-14387, 10.1038/ncomms14387, 2017.

Michelli, M.: Sea-level changes, coastal evolution and paleoceanography of coastal waters in SE-Vietnam since the mid-Holocene, 2008.

Millard, A. R.: Conventions for Reporting Radiocarbon Determinations, Radiocarbon, 56, 555-559, 10.2458/56.17455, 2014.

Milne, G. A., Mitrovica, J. X., and Schrag, D. P.: Estimating past continental ice volume from sea-level data, Quaternary Science Reviews, 21, 361-376, 10.1016/S0277-3791(01)00108-1, 2002.

Milne, G. A., Long, A. J., and Bassett, S. E.: Modelling Holocene relative sea-level observations from the Caribbean and South America, Quaternary Science Reviews, 24, 1183-1202, 2005.

Milne, G. A., and Mitrovica, J. X.: Searching for eustasy in deglacial sea-level histories, Quaternary Science Reviews, 27, 2292-2302, 10.1016/j.quascirev.2008.08.018, 2008.

Milne, G. A., Gehrels, W. R., Hughes, C. W., and Tamisiea, M. E.: Identifying the causes of sea-level change, Nature Geoscience, 2, 471-478, 10.1038/ngeo544, 2009.

Milne, G. A., and Peros, M.: Data-model comparison of Holocene sea-level change in the circum-Caribbean region, Global and Planetary Change, 107, 119-131, 10.1016/j.gloplacha.2013.04.014, 2013.

Mitrovica, J. X., and Peltier, W. R.: On Postglacial Geoid Subsidence Over the Equatorial Oceans, 96, 53-71, 1991.

Mitrovica, J. X., and Milne, G. A.: On the origin of late Holocene sea-level highstands within equatorial ocean basins, Quaternary Science Reviews, 21, 2179-2190, 10.1016/S0277-3791(02)00080-X, 2002.

Murray-Wallace, C. V., and Scott, D. B.: Late quaternary coastal records of rapid change: Application to present and future conditions (IGCP Project 367)-Preface, Quaternary International, 1999.

Nakada, M., and Lambeck, K.: Late Pleistocene and Holocene sea-level change in the Australian region and mantle rheology, Geophysical Journal International, 96, 497-517, 10.1111/j.1365-246X.1989.tb06010.x, 1989.

Neumann, A. C., and Macintyre, I.: Reef response to sea level rise: Keep-up, catch-up or give up, In: Proceedings 5th International Coral Reef Congress, Tahiti, 1985, 105-110,

Neumann, B., Vafeidis, A. T., Zimmermann, J., and Nicholls, R. J.: Future coastal population growth and exposure to sea-level rise and coastal flooding--a global assessment, PLoS One, 10, e0118571, 10.1371/journal.pone.0118571, 2015.

Nicholls, R., and Cazenave, A.: Sea-Level Rise and Its Impact on Coastal Zones, Science (New York, N.Y.), 328, 10.1126/science.1185782, 2003.

Nicholls, R. J.: Coastal megacities and climate change, GeoJournal\, 37, 369-379, 1995.

Nicholls, R. J., and Mimura, N.: Regional issues raised by sea-level rise and their policy implications, Climate Research, 11, 5–18, 1998.

Nicholls, R. J., Hoozemans, F. M. J., and Marchand, M.: Increasing flood risk and wetland losses due to global sea-level rise: Regional and global analyses, Global Environmental Change, 9, 10.1016/S0959-3780(99)00019-9, 1999.

Nicholls, R. J.: Coastal flooding and wetland loss in the 21st century: Changes under the SRES climate and socio-economic scenarios, Global Environmental Change, 14, 69-86, 10.1016/j.gloenvcha.2003.10.007, 2004.

Overpeck, J. T., Otto-Bliesner, B. L., Miller, G. H., Muhs, D. R., Alley, R. B., and Kiehl, J. T.: Paleoclimatic Evidence for Future Rapid Sea-Level Rise, Science, 2934, 1747-1750, 10.1126/science.1115159, 2006.

Parham, P. R., Saito, Y., Sapon, N., Suriadi, R., and Mohtar, N. A.: Evidence for ca. 7-ka maximum Holocene transgression on the Peninsular Malaysia east coast, Journal of Quaternary Science, 29, 414-422, 10.1002/jqs.2714, 2014.

Peltier, W. R., Farrell, W. E., and Clark, J. A.: Glacial isostasy element model, Materials Science, 50, 81-110, 1978.

Peltier, W. R.: Ice Age Paleotopography, 265, 195-202, 1994.

Peltier, W. R.: IMPLICATIONS VARIATIONS FOR CLIMATE IN THE LEVEL OF THE SEA ' DYNAMICS AN D SOLI D-EARTH, 603-689, 1998.

Peltier, W. R.: Global sea level rise and glacial isostatic adjustment, Global and Planetary Change, 20, 93-123, http://dx.doi.org/10.1016/S0921-8181(98)00066-6, 1999.

Peltier, W. R.: GLOBAL GLACIAL ISOSTASY AND THE SURFACE OF THE ICE-AGE EARTH: The ICE-5G (VM2) Model and GRACE, Annual Review of Earth and Planetary Sciences, 32, 111-149, 10.1146/annurev.earth.32.082503.144359, 2004.

Peltier, W. R., and Fairbanks, R. G.: Global glacial ice volume and Last Glacial Maximum duration from an extended Barbados sea level record, Quaternary Science Reviews, 25, 3322-3337, 10.1016/j.quascirev.2006.04.010, 2006.

Peltier, W. R.: Closure of the budget of global sea level rise over the GRACE era: the importance and magnitudes of the required corrections for global glacial isostatic adjustment, Quaternary Science Reviews, 28, 1658-1674, 10.1016/j.quascirev.2009.04.004, 2009.

Peltier, W. R., Argus, D. F., and Drummond, R.: Space geodesy constrains ice age terminal deglaciation: The global ICE-6G_C (VM5a) model, Journal of Geophysical Research: Solid Earth, 120, 450-487, 10.1002/2014jb011176, 2015.

Pirazzoli, P. A., and Pluet, J.: World atlas of Holocene sea-level changes, Elsevier, 1991.

Prasetya, G. S., De Lange, W. P., and Healy, T. R.: The Makassar Strait Tsunamigenic region, Indonesia, Natural Hazards, 24, 295-307, 10.1023/A:1012297413280, 2001.

Preuss, H.: Progress in computer evaluation of sea level data within the IGCP Project no. 61, 1979, 104-134,

Reimer, P. J., Bard, E., Bayliss, A., Beck, J. W., Blackwell, P. G., Bronk Ramsey, C., Buck, C. E., Cheng, H., Edwards, R. L., Friedrich, M., Grootes, P. M., Guilderson, T. P., Haflidason, H., Hajdas, I., Hatté, C., Heaton, T. J., Hoffmann, D. L., Hogg, A. G., Hughen, K. A., Kaiser, K. F., Kromer, B., Manning, S. W., Niu, M., Reimer, R. W., Richards, D. A., Scott, E. M., Southon, J. R., Staff, R. A., Turney, C. S. M., and van der Plicht, J.: IntCal13 and Marine13 Radiocarbon Age Calibration Curves 0–50,000 Years cal BP, Radiocarbon, 55, 1869-1887, 10.2458/azu_js_rc.55.16947, 2013.

Rhodes, B. P., Kirby, M. E., Jankaew, K., and Choowong, M.: Evidence for a mid-Holocene tsunami deposit along the Andaman coast of Thailand preserved in a mangrove environment, Marine Geology, 282, 255-267, 10.1016/j.margeo.2011.03.003, 2011.

Rignot, E., Velicogna, I., van den Broeke, M. R., Monaghan, A., and Lenaerts, J. T. M.: Acceleration of the contribution of the Greenland and Antarctic ice sheets to sea level rise, Geophysical Research Letters, 38, n/a-n/a, 10.1029/2011gl046583, 2011.

Rohling, E. J., Grant, K., Hemleben, C., Siddall, M., Hoogakker, B. A. A., Bolshaw, M., and Kucera, M.: High rates of sea-level rise during the last interglacial period, Nature Geoscience, 1, 38-42, 10.1038/ngeo.2007.28, 2008.

Rovere, A., Antonioli, F., and Bianchi, C. N.: Chapter 18 Fixed biological indicators, Handbook of Sea-Level Research, 268-280, 2015.

Rovere, A., Stocchi, P., and Vacchi, M.: Eustatic and Relative Sea Level Changes, Current Climate Change Reports, 1-11, 10.1007/s40641-016-0045-7, 2016.

Roy, K., and Peltier, W. R.: Glacial isostatic adjustment, relative sea level history and mantle viscosity: reconciling relative sea level model predictions for the US East coast with geological constraints, Geophysical Journal International, 201, 1156-1181, 2015.

Sasajima, S., Nishimura, S., Hirooka, K., Otofuji, Y., Leeuwen, T. V., and Hehuwat, F.: Paleomagnetic studies combined with fission-track datings on the western arc of Sulawesi, east Indonesia, Tectonophysics, 64, 163-172, https://doi.org/10.1016/0040-1951(80)90267-X, 1980.

Sawall, Y., Teichberg, M. C., Seemann, J., Litaay, M., Jompa, J., and Richter, C.: Nutritional status and metabolism of the coral Stylophora subseriata along a eutrophication gradient in Spermonde Archipelago (Indonesia), Coral Reefs, 30, 841-853, 10.1007/s00338-011-0764-0, 2011.

Scheffers, A., Brill, D., Kelletat, D., Bruckner, H., Scheffers, S., and Fox, K.: Holocene sea levels along the Andaman Sea coast of Thailand, The Holocene, 22, 1169-1180, 10.1177/0959683612441803, 2012.

Schwerdtner Manez, K., and Ferse, S. C.: The history of Makassan trepang fishing and trade, PLoS One, 5, e11346, 10.1371/journal.pone.0011346, 2010.

Schwerdtner Máñez, K., Husain, S., Ferse, S. C. A., and Máñez Costa, M.: Water scarcity in the Spermonde Archipelago, Sulawesi, Indonesia: Past, present and future, Environmental Science and Policy, 23, 74-84, 10.1016/j.envsci.2012.07.004, 2012.

Scoffin, T. P., and Stoddart, D. R.: The Nature and Significance of microatolls, JSTOR, 284, 23-23, 10.1093/oxfordhb/9780199557257.013.0023, 1978.

Scoffin, T. P., and Le Tissier, M. D. A.: Late Holocene sea level and reef-flat progradation, Phuket, South Thailand, Coral Reefs, 17, 273-276, 10.1007/s003380050128, 1998.

Shennan, I.: Interpretation of Flandrian sea-level data from the Fenland, England, Proceedings of the Geologists' Association, 93, 53-63, 10.1016/S0016-7878(82)80032-1, 1982.

Shennan, I., Tooley, M. J., Davis, M. J., and Haggart, B. A.: Analysis and interpretation of Holocene sea-level data, Nature, 302, 130404-130406, 1983.

Shennan, I.: Flandrian sea-level changes in the Fenland . II : Tendencies of sea-level movement , altitudinal changes , and local and regional factors, 1, 1986.

Shennan, I.: Quaternary coastal evolution: case studies, models and regional patterns, 1992,

Shennan, I., and Horton, B.: Holocene land-and sea-level changes in Great Britain, Journal of Quaternary science, 17, 511-526, 2002.

Shennan, I., Long, A. J., and Horton, B. P.: Handbook of sea-level research, John Wiley & Sons, 2015.

Sieh, K., Natawidjaja, D. H., Meltzner, A. J., Shen, C.-C., Cheng, H., Li, K.-S., Suwargadi, B. W., Galetzka, J., Philibosian, B., and Edwards, R. L.: Earthquake supercycles inferred from sea-level changes recorded in the corals of west Sumatra, Science, 322, 1674-1678, 2008.

Simandjuntak, T. O., and Barber, A. J.: Contrasting tectonic styles in the Neogene orogenic belts of Indonesia, Geological Society, London, Special Publications, 106, 185-201, 1996.

Simons, W. J. F., Socquet, A., Vigny, C., Ambrosius, B. A. C., Haji Abu, S., Promthong, C., Subarya, C., Sarsito, D. A., Matheussen, S., Morgan, P., and Spakman, W.: A decade of GPS in Southeast Asia: Resolving Sundaland motion and boundaries, Journal of Geophysical Research, 112, B06420-B06420, 10.1029/2005JB003868, 2007.

Smithers, S. G., and Woodroffe, C. D.: Microatolls as sea-level indicators on a mid-ocean atoll, Marine Geology, 168, 61-78, 10.1016/S0025-3227(00)00043-8, 2000.

Smithers, S. G., and Woodroffe, C. D.: Coral microatolls and 20th century sea level in the eastern Indian Ocean, Earth and Planetary Science Letters, 191, 173-184, 10.1016/S0012-821X(01)00417-4, 2001.

Somboon, J. R. P., and Thiramongkol, N.: Holocene highstand shoreline of the Chao Phraya delta, Thailand, Journal of Southeast Asian Earth Sciences, 7, 53-60, 10.1016/0743-9547(92)90014-3, 1992.

Southon, J., Kashgarian, M., Fontugne, M., Metivier, B., and Yim, W. W. S.: Marine reservoir corrections for the Indian Ocean and Southeast Asia, Radiocarbon, 44, 167-180, 2002.

Spada, G. Ã., and Stocchi, P.: SELEN : A Fortran 90 program for solving the ‘‘ sea-level equation ’’ Computers & Geosciences, 33, 538-562, 10.1016/j.cageo.2006.08.006, 2007.

Stattegger, K., Tjallingii, R., Saito, Y., Michelli, M., Trung Thanh, N., and Wetzel, A.: Mid to late Holocene sea-level reconstruction of Southeast Vietnam using beachrock and beach-ridge deposits, Global and Planetary Change, 110, 214-222, 10.1016/j.gloplacha.2013.08.014, 2013.

Stuiver, M., and Polach, H. A.: Discussion reporting of 14 C data, Radiocarbon, 19, 355-363, 1977.

Stuiver, M., Reimer, P., and Reimer, R.: CALIB 7.1 [WWW program] at http://calib. org, Last accessed, 8-24, 2017.

Suess, E.: Das Satilitz der Ende, Band l., Wien, Leipzig, 1885.

Switzer, A. D., Sloss, C. R., Horton, B. P., and Zong, Y.: Preparing for coastal change, Quaternary Science Reviews, 54, 1-3, 10.1016/j.quascirev.2012.09.005, 2012.

Syamsir, Birawida, A. B., and Faisal, A.: Development of Water Quality Index of Island Wells in Makassar City, Journal of Physics, 10.1088/1742-6596/1155/1/012106, 2019.

Tahir, A., Boer, M., Susilo, S. B., and Jaya, d. I.: Indeks Kerentanan Pulau-Pulau Kecil: Kasus Pulau Barrang Lompo-Makasar, ILMU KElautan, 14, 183-188, 2009.

Tahir, A., Boer, M., Susilo, S. B., and Jaya, I.: Indeks Kerentanan Pulau-Pulau Kecil: Kasus Pulau Barrang Lompo-Makasar, Ilmu Kelautan: Indonesian Journal of Marine Sciences, 14, 183-188, 2012.

Tam, C.-y., Zong, Y., Xiong, H., Wu, P., Sun, Y., and Huang, G.: A below-the-present late Holocene relative sea level and the glacial isostatic adjustment during the Holocene in the Malay Peninsula, Quaternary Science Reviews, 201, 206-222, 10.1016/j.quascirev.2018.10.009, 2018.

Tamura, T., Saito, Y., Sieng, S., Ben, B., and Kong, M.: Depositional facies and radiocarbon ages of a drill core from the Mekong River lowland near Phnom Penh , Cambodia : Evidence for tidal sedimentation at the time of Holocene maximum X ooding, 29, 585-592, 10.1016/j.jseaes.2006.03.009, 2007.

Tamura, T., Saito, Y., Sieng, S., Ben, B., Kong, M., Sim, I., Choup, S., and Akiba, F.: Initiation of the Mekong River delta at 8 ka: evidence from the sedimentary succession in the Cambodian lowland, Quaternary Science Reviews, 28, 327-344, 10.1016/j.quascirev.2008.10.010, 2009.

Tanabe, S., Hori, K., Saito, Y., Haruyama, S., Doanh, L. Q., Sato, Y., and Hiraide, S.: Sedimentary facies and radiocarbon dates of the Nam Dinh-1 core from the Song Hong (Red River) delta, Vietnam, Journal of Asian Earth Sciences, 21, 503-513, 10.1016/S1367-9120(02)00082-2, 2003a.

Tanabe, S., Hori, K., Saito, Y., Haruyama, S., Vu, P. V., and Kitamura, A.: Song Hong (Red River) delta evolution related to millennium-scale Holocene sea-level changes, Quaternary Science Reviews, 22, 2345-2361, 10.1016/S0277-3791(03)00138-0, 2003b.

Thomson, W.: Polar Ice-Caps and their Influence in changing Sea Levels, in, 322-340, 1888.

Tibbetts, J.: Coastal Cities - Living on the Edge, Environmental Health Perspectives, 11, 2002.

Tjia, H. D., Fujii, S., Kigoshi, K., Sugimura, A., and Zakaria, T.: Radiocarbon dates of elevated shorelines, Indonesia and Malaysia. Part 1, Quaternary Research, 2, 487-495, 10.1016/0033-5894(72)90087-7, 1972.

Tjia, H. D., Fujii, S., and Kigoshi, K.: Holocene shorelines of Tioman island in the South China sea, in J.H.,J. Terwindt, H. Van Steijn (Eds.), Developments in Physical Geogrqphy - a Tribute to J. I. S. Zonneveld. Geologie en Mijnbouw, 599-604, 1983.

Tjia, H. D., and Fujii, S.: Late Quaternary Shorelines in Peninsular Malaysia, The Coastal Zone of Peninsular Malaysia, 2, 28-41, 1992.

Tjia, H. D.: Sea-level changes in the tectonically stable Malay-Thai Peninsula, Quaternary International, 31, 95-101, 10.1016/1040-6182(95)00025-E, 1996.

Tjia, H. D., and Liew, K. K.: Changes in tectonic stress field in northern Sunda Shelf basins, Geological Society, London, Special Publications, 106, 291-306, 1996.

Törnqvist, T. E., González, J. L., Newsom, L. A., van der Borg, K., de Jong, A. F. M., and Kurnik, C. W.: Deciphering Holocene sea-level history on the US Gulf Coast: A high-resolution record from the Mississippi Delta, Geological Society of America Bulletin, 116, 1026-1039, 2004.

Törnqvist, T. E., Rosenheim, B. E., Hu, P., and Fernandez, A. B.: Radiocarbon dating and calibration, Handbook of Sea-Level Research, edited by: Shennan, I., Long, AJ, and Horton, BP, 349-360, 2015.

Toscano, M. A., Peltier, W. R., and Drummond, R.: ICE-5G and ICE-6G models of postglacial relative sea-level history applied to the Holocene coral reef record of northeastern St Croix, U.S.V.I.: Investigating the influence of rotational feedback on GIA processes at tropical latitudes, Quaternary Science Reviews, 30, 3032-3042, 10.1016/j.quascirev.2011.07.018, 2011.

Vacchi, M., Marriner, N., Morhange, C., Spada, G., Fontana, A., and Rovere, A.: Multiproxy assessment of Holocene relative sea-level changes in the western Mediterranean: Sea-level variability and improvements in the definition of the isostatic signal, Earth-Science Reviews, 155, 172-197, 10.1016/j.earscirev.2016.02.002, 2016.

van de Plassche, O.: Sea-level change and water-level movements in the Netherlands during the Holocene, [Geological Survey of the Netherlands], [Amsterdam], 1982.

Van de Plassche, O.: Sea-level research: a manual for the collection and evaluation of data, Springer, 1986.

Van Veen, J.: TIDE-GAUGES , SUBSIDENCE-GAUGES AND FLOOD-STONES IN THE NETHERLANDS, Geologie en mijnbouw, 16e, 214-219, 1954.

Vaz, G. G., and Banerjee, P. K.: Middle and late Holocene sea level changes in and around Pulicat Lagoon, Bay of Bengal, India, Marine Geology, 138, 261-271, 10.1016/S0025-3227(97)00008-X, 1997.

Vitousek, S., Barnard, P. L., Fletcher, C. H., Frazer, N., Erikson, L., and Storlazzi, C. D.: Doubling of coastal flooding frequency within decades due to sea-level rise, Scientific Reports, 7, 1-9, 10.1038/s41598-017-01362-7, 2017.

Walpersdorf, A., Vigny, C., Manurung, P., Subarya, C., and Sutisna, S.: Determining the Sula block kinematics in the triple junction area in Indonesia by GPS, 1998.

Warrick, R., Kenny, G., Sims, G., Ericksen, N., Ahmad, Q., and Mirza, M.: Integrated model systems for national assessments of the effects of climate change: applications in New Zealand and Bangladesh, in: Climate Change Vulnerability and Adaptation in Asia and the Pacific, Springer, 215-227, 1996.

Watson, C. S., White, N. J., Church, J. A., King, M. A., Burgette, R. J., and Legresy, B.: Unabated global mean sea-level rise over the satellite altimeter era, Nature Climate Change, 5, 565-568, 10.1038/nclimate2635, 2015.

Wessel, P., and Smith, W. H. F.: A global, self-consistent, hierarchical, high-resolution shoreline database, Journal of Geophysical Research: Solid Earth, 101, 8741-8743, 10.1029/96jb00104, 2004.

Williams, S. L.: A new collaboration for Indonesia's small islands, Frontiers in Ecology and the Environment, 11, 274-275, 2013.

Woodroffe, C., McLean, R., Polach, H., and Wallensky, E.: Sea level and coral atolls: Late Holocene emergence in the Indian Ocean, Geology, 18, 62-66, 10.1130/0091-7613(1990)018<0062:SLACAL>2.3.CO;2, 1990.

Woodroffe, C. D.: Mid-late Holocene El Niño variability in the equatorial Pacific from coral microatolls, Geophysical Research Letters, 30, 1-4, 10.1029/2002GL015868, 2003.

Woodroffe, C. D., McGregor, H. V., Lambeck, K., Smithers, S. G., and Fink, D.: Mid-Pacific microatolls record sea-level stability over the past 5000 yr, Geology, 40, 951-954, 10.1130/G33344.1, 2012.

Woodroffe, C. D., and Webster, J. M.: Coral reefs and sea-level change, Marine Geology, 352, 248-267, 10.1016/j.margeo.2013.12.006, 2014.

Woodroffe, S. A., and Horton, B. P.: Holocene sea-level changes in the Indo-Pacific, Journal of Asian Earth Sciences, 10.1016/j.jseaes.2004.01.009, 2005.

Woodroffe, S. A., Long, A. J., Lecavalier, B. S., Milne, G. A., and Bryant, C. L.: Using relative sea-level data to constrain the deglacial and Holocene history of southern Greenland, Quaternary Science Reviews, 92, 345-356, 10.1016/j.quascirev.2013.09.008, 2014.

Yi, S., Sun, W., Heki, K., and Qian, A.: An increase in the rate of global mean sea level rise since 2010, Geophysical Research Letters, 42, 3998-4006, 10.1002/2015gl063902, 2015.

Yokoyama, Y., and Esat, T. M.: Coral reefs, in, Wiley Online Books, John Wiley & Sons, Ltd, Chichester, 104-124, 2015.

Yokoyama, Y., Esat, T. M., Thompson, W. G., Thomas, A. L., Webster, J. M., Miyairi, Y., Sawada, C., Aze, T., Matsuzaki, H., Okuno, J. i., Fallon, S., Braga, J.-C., Humblet, M., Iryu, Y., Potts, D. C., Fujita, K., Suzuki, A., and Kan, H.: Rapid glaciation and a two-step sea level plunge into the Last Glacial Maximum, Nature, 559, 603-607, 10.1038/s41586-018-0335-4, 2018.

Yousefi, M., Milne, G. A., Love, R., and Tarasov, L.: Glacial isostatic adjustment along the Pacific coast of central North America, Quaternary Science Reviews, 193, 288-311, 10.1016/J.QUASCIREV.2018.06.017, 2018.

Yusuf, A. A., and Francisco, H.: Climate Change Vulnerability Mapping for Southeast Asia, 2009.

Zachariasen, J.: Paleoseismology and Paleogeodesy of the Sumatra Subduction Zone: A Study of Vertical Deformation Using Coral Micoatolls, 1998.

11 Appendix

Within the three years of my PhD, I had the chance to participate in several conferences, which are listed below together with the related abstracts. I additionally listed one further publication that was completed and published in the second year of my PhD even though it was related to my master thesis.

11.1 Conference contributions

11.1.1 European Geosciences Union, EGU, 2017, Vienna, Austria

A Holocene sea-level database for Southeast Asia

M. Bender, T. Mann, P. Stocchi, A. D. Switzer, B. P. Horton, M. Lukman, J. Jompa, and A. Rovere

The study of former relative sea-level (RSL) changes is essential to disentangle changes in sea level due to vertical land motion (e.g. tectonics, Glacial Isostatic Adjustment - GIA) and eustatic (e.g. ice equivalent sea level) causes. To study RSL changes at a regional scale it is essential that databases of sea-level indicators are produced following standardized protocols (Hijma et al., 2015). This has been already done in several regions (e.g. the US Atlantic coast, the Caribbean, or the Mediterranean (Engelhart and Horton, 2002) A database has been compiled for Southeast Asia but was limited in geographical extent and didn't include the influence of local process such as tidal range changes and compaction. Southeast Asia is highly vulnerable to relative sea level changes, as it is characterized by low-lying, densely populated islands and subsiding deltas. We present a database of Holocene sea-level histories in Southeast Asia and part of the Indo-Pacific from published and unpublished data, which has been evaluated and using a standardized protocol. We analyzed 526 sea level index points, defining their locations the height of former sea level and the age with their associated uncertainty. Radiocarbon ages were re-calibrated using Calib 7.0.0 / 7.1 (Stuiver et al., 2017) and the calibration curves Intcal13 or Marine13. In our database, we also indicated possible tectonic vertical land motion, and we present the results of GIA modelling for different areas in SE Asia. We also show regions of South East Asia and parts of the Indo-Pacific where there is an absence of data and where the collection of new RSL data is mostly needed.

11.1.2 SPP-1889 "Regional Sea Level Change and Society" Kick-Off meeting

Holocene sea-level changes in Southeast Asia

M. Bender; PIs: A. Rovere, T. Mann, H. Westphal, T. Schöne

– No abstract –

11.1.3 Regional Sea Level Changes and Coastal Impacts 2017, New York, USA

A Holocene Sea-Level Database For Southeast Asia

M. Bender, T. Mann, P. Stocchi, A. D. Switzer, B. P. Horton, M. Lukman, J. Jompa, A. Rovere

A Change in relative-sea-level (RSL) is a reaction based on vertical land motion, effected by tectonics or Glacial Isostasy Adjustment (GIA) and eustatic causes (e.g. ice equivalent sea level). Therefore, to unravel those post depositional effects it is essential to study former RSL changes especially on a regional scale. For that reason, databases of sea-level indicators are produced following standardized protocols (Hijma et al., 2015). By this time, this was been done in numerous regions (e.g. the US Atlantic coast, the Caribbean, or the Mediterranean (Engelhart and Horton, 2012). For Southeast Asia a database has been compiled but was limited in geographical extent and didn't include the influence of local process caused by tidal range changes and compaction. Southeast Asia is highly vulnerable to relative sea level changes, as it is characterized by low-lying, densely populated islands and subsiding deltas. Based on this, we present a database of Holocene sea-level histories in Southeast Asia and part of the Indo-Pacific from published and unpublished data, which is evaluated and uses a standardized protocol.

We analyzed 680 sea level index points, defined each location, the height of former sea level and the age with its associated uncertainty. Radiocarbon ages were re-calibrated using Calib 7.1 (Stuiver et al., 2017) and the calibration curves Intcal13 for terrestrial material or Marine13 for the marine samples. In our database, we indicated possible vertical land motion caused by tectonic, and we present the results of GIA modelling for different areas in SE Asia. Further, we show regions of SE Asia and parts of the Indo-Pacific where an absence of data was detected and where the collection of new RSL data is mostly needed.

11.1.4 European Geosciences Union, EGU, 2018, Vienna, Austria

Holocene sea-level changes in SE Asia – Fieldwork in Indonesia and first results

Maren Bender, Thomas Mann, Dominik Kneer, Paolo Stocchi, Jamaluddin Jompa, Alessio Rovere

Changes in sea level are endangering global settlements and are making coastal populations more vulnerable to flooding. In order to understand which processes are contributing to local sea level changes, it is necessary to investigate paleo sea-level proxies and compare them to different glacio-isostatic adjustment models (GIA). Within the framework of the project "Holocene sea-level changes in SE Asia", part of Spp. 1889 "Regional Sea Level and Society", we measured Holocene sea-level proxies in October 2017 in Indonesia, on small islands of the Spermonde Archipelago, South Sulawesi. The fieldwork focused on fossil and living microatolls, which grow as high as the lowest astronomical tide and modify their growth behavior following changes in local sea level. In total, 26 fossil microatolls were sampled and will be dated with radiocarbon. Their elevation was measured above MSL, and compared with that of living microatolls, which were treated as modern analogues. The results will be used to improve the current knowledge of Holocene sea-level changes in the Spermonde Archipelago. We intend to compare this data with a new sea-level database for the Indo-Pacific and with different GIA models to disentangle which processes are driving Holocene sea level changes in the broader region, and identify best-performing ice and earth models.

11.1.5 International Scientific Advisory Board meeting at ZMT

Holocene sea-level changes in SE Asia, Database and Fieldwork

M. Bender, T. Mann, J. Jompa, D. Kneer, T. Schöne, A. Rovere

The first phase of the project "Holocene sea-level changes in Southeast Asia" was the compilation of a Holocene sea-level database. All existing literature was reviewed and re-analyzed following a standardized protocol and aiming on the classification of each data point into one of three different data types. These types are sea level index points, which describe samples indicating the position of the paleo sea level directly, or marine and terrestrial limiting, if the sea level position is roughly describes as, above or below the indicator. The second phase of this project was a fieldwork period of three weeks in the Spermonde Archipelago, Indonesia, aiming on the collection of new sea-level data and enlarging the database. The sampling of 26 fossil microatolls, resulted in 16 radiocarbon dated ages, ranging from modern ages to 5550.5 a BP. Combined with the measured elevations this project will lead to a new sea-level curve of the Spermonde Archipelago and the larger area of SE Asia.

11.2 Further publications

11.2.1 Thousands of cold-water coral mounds along the Moroccan Atlantic continental margin: Distribution and morphometry

D. Hebbeln, M. Bender, S. Gaide, J. Titschack, T. Vandorpe, D. Van Rooij, P. Wintersteller, C. Wienberg

Published in Marine Geology

Coral mounds formed by framework-forming cold-water corals pierce the seabed along most continental margins of the Atlantic Ocean and new sites are continuously being discovered. Here, we describe an extremely high accumulation of coral mounds at the NW Moroccan Atlantic margin between 35°N and

35.5°N. Within an area of only 1440 km^2, >3400 mounds were found exposed at the seabed. The coral mounds are nowadays characterized by an almost complete lack of living cold-water corals. In addition, numerous buried mounds were identified in hydroacoustic sub-bottom profiles, and are estimated to be ~3.7 times more frequent than the exposed mounds. Consequently, a total of ~16.000 buried and exposed mounds is estimated for the entire study area. The exposed mounds are rather small with a mean height of 18 m and show a conspicuous arrangement in two slope-parallel belts that centre in water depths between 720 and 870 m and 890–980 m, respectively, putting them among the deepest mound occurrences discovered so far in the Atlantic. The mostly elongated mounds largely stretch downslope pointing to a significant influence of internal waves in the mound formation process. Moreover, based on their average dimensions, the entire coral mound volume can be estimated as 1.3 km^3, which means the mounds store a considerable amount of coral carbonate highlighting their potentially important role as regional carbonate factories. In combination with further occurrences of coral mounds along the Moroccan margin, both in the Mediterranean and in the Atlantic Ocean, these new findings underline Morocco's role as a hotspot for the occurrence of cold-water coral mounds.